Phase-locked, multiple ridge waveguide, semiconductor laser arrays

Buckley, David

Award date:
1992

Awarding institution:
University of Bath

PHASE-LOCKED, MULTIPLE RIDGE WAVEGUIDE, SEMICONDUCTOR LASER ARRAYS

submitted by David Buckley
for the degree of PhD
of the University of Bath
December 1992

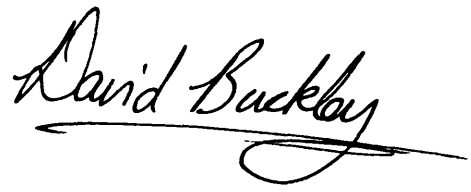

ProQuest LLC
789 East Eisenhower Parkway
P.O. Box 1346
Ann Arbor, MI 48106-1346

SUMMARY

The performance of phase-locked, semiconductor laser arrays is investigated. The array is first analysed as a passive structure. Coupled mode theory is utilised to calculate the eigenmodes of the parallel multiple, parallel waveguide structure. These modes (commonly referred to as "supermodes") are investigated first for uniform arrays where all waveguides are identical and on a constant pitch and, secondly, for non-uniform arrays where waveguide widths and pitches are varied. It is shown that the first structure promotes operation in the anti-phase highest order supermode, whilst the non-uniform array can be adjusted to promote various supermodes. In order to be most effective in telecommunication systems, coupling to single-mode fibre is preferred - this drives the requirement for devices to operate in a stable, fundamental supermode.

Having investigated the performance of simple phase-locked laser array structures, two alternative designs are proposed that incorporate mode selection mechanisms. The first utilises a phase-shift at the laser facet to induce phase-changes in the propagating mode, whilst the second uses an integral mode filter to increase discrimination between supported modes. Both of these designs have drawbacks that prevent them from being used universally as solutions to achieving high power, fundamental supermode propagation.

Lastly, the phase-locked array is analysed in its active mode - the threshold currents of the supermodes are calculated and the resultant carrier densities are used to determine effects on the lateral dielectric profile. It is shown that carrier-induced dielectric changes have a significant effect on the propagating modes.

ACKNOWLEDGEMENTS

The author wishes to thank the Science and Engineering Research Council and British Telecom Research Laboratories for funding this work.
Also, the author is very grateful for the many useful discussions with his colleagues at Bath University - Dr. I. Middlemast, Dr. Paul Lambkin and Dr. J. Sarma, and Dr. M.J. Adams of BTRL. In particular, I thank Dr. K.A. Shore for his perseverance and encouragement as well as for his technical support and advice.

CHAPTER 1

INTRODUCTION.

1.1 Review of Semiconductor Lasers.

Since the development of the first semiconductor injection lasers in 1962, lasers have found increasing numbers of uses as the fabrication technologies and understanding of their operating principles have improved. The first semiconductor laser, a GaAs single heterostructure device, had to be cooled to under 100K and required very high drive currents (amps) for operation. With improvements in fabrication processes and epitaxial growth techniques, together with the advent of multiple heterostructure designs, CW operation is now possible at temperatures over 100°C (373K) and operating drive currents can be as low as a few tens of milliamps. The introduction of multiple heterostructure, quantum well designs have produced significant improvements in terms of power consumption, quantum efficiency, total output power and reliability.

Despite the significant improvements already made, there is always a drive towards achieving better performance - higher output powers, lower drive currents, greater stability etc. Recent advances have opened up new fields of uses for semiconductor injection lasers - in particular, the advent of very high power (>1 Watt) CW semiconductor laser diodes has meant that diode pumping of solid state lasers (Nd-doped YAG, Erbium-doped fibres) is possible. Further improvements in the mode stability of these devices would be of great benefit in optical transmission systems including long-haul data links, distributed networks and inter-satellite links. In support of these requirements, considerable

research effort has been directed towards producing a high-power, single-(zero-order)-mode laser diode.

The design of single-emitter laser diodes to produce high-power, single-mode outputs is already well advanced. Single-mode outputs of 175mW with a single longitudinal mode have already been reported by Daniel, Buckley et al. (ref. 24) using a Multiple Quantum Well, Metal-Clad Ridge Waveguide (MQW, MC-RWG) laser. However, the prospect of utilising many single-mode emitters to produce a stable, single-mode output has led to intense interest in the field of phase-locked laser arrays where the performance attributes of the individual elements are combined to produce a single mode output.

This thesis concentrates on the design of a high-power, single-(zero-order)-mode, phase-locked laser array for coupling into single-mode fibre. The particular application is the design of such an array for use in long-haul, telecommunication networks (e.g. submarine systems). Thus, an operating wavelength of 1.55μm is considered.

1.2 Designing High-Power, Single-Mode Arrays.

The basic method of achieving a coherent, single-mode output from a multiple emitter device is by coupling the individual emitters to form a phase-locked output - if coupling is not achieved, the nett output is simply the incoherent sum of the outputs from each element (refs. 1, 26, 35).

An early coupled multiple stripe laser (ref. 85) utilised curved waveguide sections to join neighbouring stripes and, thus, phase-lock the array. However, whilst the emitted far-field pattern was narrow (width~5^{o})

with a dominant main mode of width $<0.6^{o}$, the structure in the far-field pattern intimated the presence of other higher-order modes. Other early attempts at producing phase-locked outputs (refs. 2, 6, 49, 50, 103) have also achieved some success - the far-field patterns exhibit a main central lobe; however, structure in the far-field has, once again, led to the conclusion that other higher-order modes are present. The early evaluation of some of these structures was limited - the understanding of the coupling mechanism and the propagation of higher order modes was limited.

In 1984, two independent groups developed coupled-mode models of the behaviour of passive arrays (refs 12 and 45) based on the earlier coupled mode formalism of Yariv (ref. 127). These models predicted the existence of array modes (now called 'supermodes' after ref. 45) made up of phase-locked combinations of the modes of the individual elements. Based on the shape of the eigensolutions derived from these methods, the preference for higher order laser modes to propagate above the lasing threshold was identified (ref. 45). The reason given for this was that since the higher order modes have reduced field intensity between the guides where the loss-factor is highest, the effective loss seen by that mode is minimised. Thus, the highest order mode, with the maximum number of intensity nulls in the highest loss regions, requires the lowest injected gain to reach threshold.

Even though the above coupled-mode formalisms have been improved to produce more accurate eigenmode solutions (refs 36, 37), the basic problem of higher order mode propagation remains and much effort has been directed at obtaining single, zero-order mode operation in arrays.

In a simple laser aray (made up of coupled elements only and not utilising any other form of mode control), the array mode solutions

depend on the strength of the coupling between adjacent elements. This, in turn, is ultimately governed by the array geometry and the waveguiding mechanism of the structure (i.e. refractive index guiding or gain-guiding). The simplest array consists of a number of parallel oxide-stripe lasers coupled together (refs. 78-82, 84, 86). These arrays guide light by the gain-guiding mechanism - carriers are generated beneath the stripe contacts and these produce local regions of gain. The light is then weakly confined to each stripe whilst a large proportion of the field overlaps with the mode of the adjacent guide causing coupling. However, due to the variation of injected gain as a function of drive current and temperature, the stability of the guided mode is suspect and changes in the far-field pattern with changing drive conditions are common (see previously listed references). From this point of view, the use of gain-guided, phase-locked arrays in producing stable zero-order mode outputs is limited. However, their ability to produce very high-power outputs (including incoherent outputs) is proven (refs. 38, 39, 102, 110, 112, 115, 118).

The theoretical modelling of gain-guided arrays is very complicated. However, simplified models have been generated (refs. 13, 46, 47). These models do not use the coupled-mode theory mentioned above since it does not take into account the continuous, lateral variation of carriers and, also, it has been shown to be limited in the calculation of higher-order, gain-guided modes (ref. 14, 32, 33). Instead numerical methods are employed to find the eigenmodes. These reveal that even small changes in the gain-guiding profile affect the eigenmodes (ref 4, 34) - a fact verified in practice by the mode instability with changing drive conditions.

The second waveguiding mechanism, refractive index guiding, can produce much stronger optical confinement leading to weaker coupling

between adjacent guides. However, the variation of the lateral index-guiding profile with changes in drive current above lasing threshold are much smaller than with gain-guided lasers. Thus, index-guided lasers are , potentially, more stable with respect to changes in temperature and drive current. It should be noted though that the modal performance of this laser is limited by other effects - notably, spatial hole burning and self-focussing (refs, 22, 100).

Uniform index-guided arrays (i.e. ones in which the guide widths and element pitches are constant) have been reported to operate in phase-locked modes (refs 6, 25, 27, 70, 95, 101, 104). Once again though, multiple-lobed far-field patterns have been observed, indicative of the presence of higher order modes. Thus, alternative array designs have been derived in an attempt to aid zero-order mode selection.

One of the first designs to be tested for its suitability to single mode operation was the offset gain configuration (refs. 89) - the injected gain was introduced in the regions corresponding to the minima in the field intensity profile. The proposed concept was that since the zero-order mode has the greatest relative proportion of photon density in the inter-guide regions, then this mode would benefit most when the injected gain profile matched these regions. However, by doing this, the nett overlap of the gain and photon distributions is drastically reduced resulting in higher drive currents and, ultimately, lower efficiencies.

A direct alternative to the uniform arrays mentioned previously is the chirped array in which either the guide width and/or separation are varied across the array to match the intensity distribution of the required mode (refs. 2, 27, 42, 43, 48, 49, 120). However, by chirping the guiding structure, the resulting eigenmode profile can be distorted so much that the likelihood of high power operation is unlikely as spatial

hole-burning and self-focussing effects will set in at lower powers. The design of a high uniformity array was suggested by Streifer (90) and further investigated by Buus (ref. 15, 16) where the outer guide strengths are adjusted to create a uniform eigenvector distribution across the array. The modal behaviour of this design is not as straightforward as suggested. This array is investigated in greater detail in this thesis (chapters 4 and 8).

Because of the problems associated with the types of coupling mentioned in the aforementioned arrays (i.e nearest neighbour, evanescent field coupling), some researchers have re-directed their effort to designing phase-locked arrays utilising alternative coupling methods. Two of the main methods proposed rely on coupling being introduced via Y-branching waveguides (refs. 21, 23, 88, 91, 92, 93, 94, 97, 111, 113, 114) and diffraction of the field off the facet into adjoining elements (refs. 54, 69, 108, 121, 122, 126). A third method recently employed involves strengthening the coupling of adjacent guides by creating an array of anti-guides (ref. 8, 67). Many other methods have been proposed for obtaining phase-locked behaviour from an array (e.g. lateral offset stripe arrays, ref. 116, X-branch arrays, ref. 7, interferometric arrays, ref. 9). However, their ability to produce a single-zero-order-mode output has been limited.

It has been proposed that the highest order mode is favoured and is self-stabilising (ref. 100) - this leads to the possibility that arrays are designed to support this mode and methods of phase-correction are used to convert it into an equivalent zero-order mode (refs. 61). The use of phase-corrector plates has been investigated (ref. 40, 68). However, the suitability of this method to manufacturing processes is questionable but it is noted that this method provides a possible alternative solution if a zero-order mode device cannot be fabricated.

Thus, it is seen that many alternative methods of producing a stable, zero-order mode, high power laser array are possible. What started as a simple design has become an extremely complicated problem involving the analysis of optical modes in active devices subject to variations in temperature and carrier redistribution.

1.3 Outline of Thesis.

This thesis addresses the problem of designing a stable, zero-order mode laser array operating at a wavelength of 1.55μm suitable for use in telecommunications networks.

Before considering the complexities of this design, the concepts of waveguiding and lasing threshold action in a single element laser is considered (Chapter 2) - for analysis purposes , the waveguide considered is the Ridge Waveguide (RWG). This device is dominantly refractive index-guided and has been shown to support a stable zero-order mode (ref. 24). Furthermore, it has demonstrated reliability compatible with telecommunication systems with typical predicted lifetimes greater than 25yrs.

Having presented a simple explanation of some of the characteristics of the single element, RWG laser, the multiple-element RWG laser array is analysed. First, a coupled mode approach is developed which allows the behaviour of an array of coupled elements to be analysed based on the behaviour of each individual element (Chapter 3). Two important parameters are identified - the coupling constant, κ, and the induced phase change, M. These are evaluated for the case of two parallel waveguides in close proximity. The eigenmodes of the structure are then derived from a matrix equation. The modes of an idealised, uniform RWG array are derived and the corresponding far-field patterns computed.

A more complete analysis of uniform and chirped arrays is presented in Chapter 4 - investigations of the RWG array modal behaviour as a function of ridge width, separation and injected gain are presented. The special case of a high uniformity array is presented after ref. 16. It will be seen that the behaviour is not as straightforward as might be thought. The higher order modes still have the lowest modal losses.

Having looked at the uniform and non-uniform arrays, Chapter 5 investigates two alternative array designs - the angled facet laser array and an array with mode filter. These produce two alternative methods of mode control - the first by introducing phase-changes at the facet and the latter by coupling the modes of the RWG array to the modes of a broad area structure. The first case is seen to produce degenerate modes when the phase between adjacent stripes is π radians whilst the latter can produce noticeable changes in the threshold modal gain values compared to the ordinary array.

Lastly, in Chapter 6, the analysis of RWG arrays switches from the passive structure to the active structure. A rate equations analysis is presented which calculates approximate values for the threshold currents and L/I characteristics for each supermode. The equations are extended to consider the effects of the lateral variation of carrier density on the refractive index guiding profile. The modes of a RWG array are computed in the presence of carriers for the threshold condition. The analysis is completed by considering the high uniformity array of Chapter 4 under carrier injection.

Chapter 7 presents the conclusions of the thesis.

CHAPTER 2.

BASIC WAVEGUIDE AND LASER THEORY.

2.1 Introduction.

This chapter investigates the behaviour of a simple ridge-waveguide laser. The concepts of waveguiding, energy confinement and lasing threshold are introduced.

Mode guidance in a real, lossless dielectric slab waveguide - the propagation of energy along a waveguide, is introduced in section 2.2. After briefly investigating the properties of this simple structure, the analysis of the 2-dimensional ridge waveguide is presented (section 2.3) - the effective dielectric constant approximation is used to reduce the two-dimensional ridge waveguide structure to an effective slab waveguide.

The concept of mode confinement is introduced in section 2.4. A parameter is defined quantifying the amount of mode confinement in a specified area. A simple expression is then derived relating the threshold gain of a laser to the internal semiconductor losses, the facet losses, the cavity length and the mode confinement parameter. The distinction between modal gain and threshold gain is clarified.

Section 2.5 presents the conclusions of the chapter.

2.2 Waveguiding in the 3-layer Dielectric Slab Waveguide.

This theory is covered in many text books on electromagnetic waveguide theory [e.g. refs. 3, 19, 99]. Electromagnetic wave propagation

through a medium is governed by Maxwell's equations. For a lossless medium, these may be written as:

$$\nabla \times \underline{E} = -\partial \underline{B} / \partial t \qquad (2.2.1)$$

$$\nabla \times \underline{H} = \partial \underline{D} / \partial t \qquad (2.2.2)$$

$$\nabla . \underline{E} = 0 \qquad (2.2.3)$$

$$\nabla . \underline{H} = 0 \qquad (2.2.4)$$

$\underline{E}$ is the electric field vector, $\underline{H}$ the magnetic field vector, $\underline{B}$ the magnetic flux vector and $\underline{D}$ is the electric flux vector. The latter fields are related to $\underline{E}$ and $\underline{H}$ in a non-magnetic, homogeneous, isotropic medium by:

$$\underline{B} = \mu_0 \underline{H} \qquad (2.2.5)$$

$$\underline{D} = \varepsilon \underline{E} \qquad (2.2.6)$$

where μ_0 is the permeability of free-space and ε is the permittivity of the medium. The latter is related to the permittivity of free-space by $\varepsilon = \varepsilon_r \varepsilon_0$ where ε_0 is the permittivity of free-space and ε_r is the relative permittivity of the medium.

By taking the curl of (2.2.1) and using equations (2.2.2), (2.2.5) and (2.2.6) to simplify the result, the Helmholtz wave equation may be derived for the homogeneous, isotropic medium. This equation is stated below for a vector field $E(x,y,z,t)=\underline{E}$ (with co-ordinates given in fig.2.2.1.).

$$\nabla^2 \underline{E} = \mu_0 \varepsilon(r) \frac{\partial^2 \underline{E}}{\partial t^2} \qquad \ldots\ldots(2.2.7)$$

where $\varepsilon(r)$ is the permittivity of the medium at co-ordinate r.

(An analogous equation can be derived for the magnetic field, H)

When considering the types of fields that dominate in simple laser structures, major interest centres on guided-fields i.e. fields in which energy is channeled along a given, guiding path. In the case of a laser, the desired axis of propagation lies along the length of the resonator cavity. The diagram below illustrates this principle where light energy is guided along the central layer if the value of its refractive index, n_2 (dielectric constant ε_2) is greater than those surrounding it ,n_1 and n_3 (dielectric constants ε_1, ε_3 respectively). The dielectrics are considered constant within the regions defined.

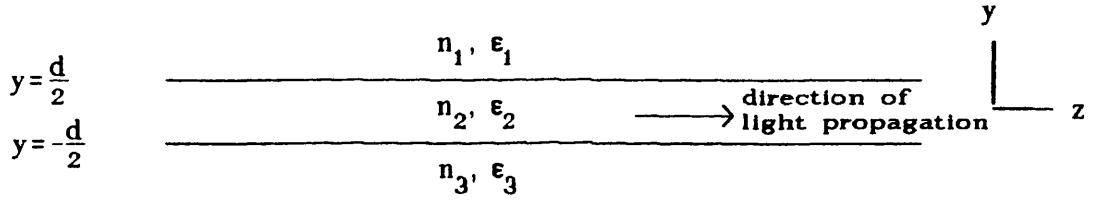

FIGURE 2.2.1 A SIMPLE THREE-LAYER, LOSSLESS, SLAB WAVEGUIDE

$(n_2 \geq n_1 \geq n_3)$

A wave travelling in the positive z-direction may be represented by:

$$\underline{E}(x,y,z,t) = E = \underline{E}(x,y).\ \exp j(\omega t - \beta z) \qquad .....(2.2.8)$$

This function represents an arbitrary-shaped forward travelling wave with angular frequency ω and propagation constant β. After

substituting this in the wave equation and setting $\partial/\partial x=0$:

$$\frac{\partial^2}{\partial y^2}\underline{E}(y) + (\beta^2 - \mu_0\varepsilon_k\omega^2).\underline{E}(y) = 0 \qquad \text{.....(2.2.9)}$$

This is the one-dimensional (or reduced) wave equation.

It is now worth considering the sets of solutions obtained from the Maxwell's equations for the three-layer, dielectric slab waveguide. Making use of equations (2.2.1) and (2.2.2) and setting $\partial/\partial x=0$ and $\partial E(y,z)/\partial z = i\beta E(y)\exp(-i\beta z)$ then:

$\nabla xE = -\mu_0\frac{\partial H}{\partial t} =$		$\nabla xH = \varepsilon_0\frac{\partial E}{\partial t} =$	
$\frac{\partial E_x}{\partial y} = i\omega\mu_0 H_z$	(2.2.10a)	$\frac{\partial H_x}{\partial y} = -i\omega\varepsilon_k E_z$	(2.2.10b)
$\beta E_x = \omega\mu_0 H_y$	(2.2.11a)	$\beta H_x = -\omega\varepsilon_k E_y$	(2.2.11b)
$i\beta E_y + \frac{\partial E_z}{\partial y} = -i\omega\mu_0 H_x$	(2.2.12a)	$i\beta H_y + \frac{\partial H_z}{\partial y} = i\omega\varepsilon_k E_x$	(2.2.12b)

Two orthogonal mode sets are now defined:

(i) E_x, H_y, H_z (E_z set to zero) - known as Transverse Electric (TE) modes as they have no component of the E-field in the direction of propagation. The field components are related via equations 2.2.10a, 2.2.11a and 2.2.12b

(ii) H_x, E_y, E_z (H_z set to zero) - known as Transverse Magnetic (TM) modes as they have no component of the H-field in the direction of propagation. The field components are related via equations 2.2.10b, 2.2.11b and 2.2.12a

Now that the mode sets are apparent, it is possible to solve the one-dimensional wave equation (equation 2.2.9) and, thus, find the components of the TE and TM modes. We start by calculating one vector component and then use equations (2.2.10) to (2.2.12) to determine the others. The requirement for bound modes implies that no energy should radiate away from the guide. Thus, the time averaged Poynting vector decays to zero as the distance from the guide increases. Analysing TE mode solutions first, we consider fields of the form:

TE MODE FUNCTIONAL FORM

$$E_x(y) = A\cos(\varphi)\exp(-p_1 (y-\tfrac{d}{2})) \qquad \text{for } y \geq \tfrac{d}{2}$$

$$E_x(y) = A\cos(h\,[y-\tfrac{d}{2}] + \varphi) \qquad \text{for } |y| \leq \tfrac{d}{2}$$

$$E_x(y) = A\cos(-hd+\varphi)\exp(p_3(y+\tfrac{d}{2})) \qquad \text{for } y \leq -\tfrac{d}{2} \qquad (2.2.13)$$

where A is the electric field amplitude

d is the width of the guide

p, h are related to the propagation constant, β by:

$$p_k^2 = (\beta^2 - \varepsilon_k k_0^2) \qquad (k=1,3) \qquad (2.2.14)$$

$$h^2 = (\varepsilon_2 k_0^2 - \beta^2) \qquad (2.2.15)$$

and φ is a phase-term to be determined.

The magnetic fields are then derived using (2.2.10a) and (2.2.11a):

$$H_y = \frac{\beta}{\omega\mu_0} E_x \qquad (2.2.16)$$

$$H_z = -\frac{i}{\omega\mu_0} \frac{\partial E}{\partial y}_x \qquad (2.2.17)$$

The unknowns in the field equations are now found by matching the tangential field components at the boundaries - both E_x and H_z are continuous across a charge-free boundary. Equation (2.2.13) already caters for the E-field continuity whilst the H-field continuity is the same as specifying a continuous E-field gradient ($\partial E/\partial y$) across the boundary. The equation obtained is in an eigenvalue form which allows calculation of the propagation constant, β.

TE MODE EIGENVALUE EQUATION:

$$\tan(hd) = \frac{h(p_1+p_3)}{h^2-p_1 p_3} \qquad \text{.....(2.2.18)}$$

The TM mode equations may be found similarly using an analogous field distribution:

TM MODE FUNCTIONAL FORM

$$H_x(y) = B\cos(\psi)\exp(-p_1 (y-\tfrac{d}{2})) \qquad \text{for } y \geq \tfrac{d}{2}$$

$$H_x(y) = B\cos(h[y-\tfrac{d}{2}] +\psi) \qquad \text{for } |y| \leq \tfrac{d}{2}$$

$$H_x(y) = B\cos(-hd+\psi)\exp(p_3(y+\tfrac{d}{2})) \qquad \text{for } y \leq -\tfrac{d}{2} \qquad (2.2.19)$$

where B is the magnetic field amplitude

and ψ is a phase-term to be found.

The corresponding eigenvalue equation is:

$$\tan(hd) = \frac{\frac{h}{\varepsilon_1}\left(\frac{p_3}{\varepsilon_3} + \frac{p_1}{\varepsilon_1}\right)}{\left(\frac{h^2}{\varepsilon_2} - \frac{p_1 p_3}{\varepsilon_1 \varepsilon_3}\right)} \qquad (2.2.20)$$

In the case of symmetric guides, the outer dielectric layers are the same, $\varepsilon_1=\varepsilon_3$ and the eigenvalue equations for the fundamental mode take on the form :

$$u\tan(u) = w \qquad \text{(TE modes)} \qquad \text{.....(2.2.21)}$$

$$u\tan(u) = \frac{\varepsilon_2}{\varepsilon_1} w \qquad \text{(TM modes)} \qquad \text{.....(2.2.22)}$$

where $u = h\frac{d}{2}$; $w = p\frac{d}{2}$

and $u^2 + w^2 = \left(\frac{2\Pi}{\lambda_0} \frac{d}{2} \sqrt{\varepsilon_2 - \varepsilon_1}\right)^2$

From equations 2.2.21 and 2.2.22, the values of u and p can be determined. The propagation constant of the mode, β, can then be readily evaluated. Thus, knowledge of the shapes of the modes and their z-dependence is obtained. For the waveguides considered in this thesis, typical values of ε_1 and ε_2 lie in the range 11.4 to 11.6. Since the ratio of ε_1 to ε_2 is very close to unity, there will only be a very small difference between the TE and TM mode sets. Values of β will lie in the range of $\sqrt{\varepsilon_1}.k_0$ to $\sqrt{\varepsilon_2}.k_0$ i.e. approximately $1.36\text{-}1.38\times10^7$ rads. m^{-1}. Plots of typical field profiles for TE and TM modes in a symmetric guide with $\varepsilon_1=\varepsilon_3=11.4$, $\varepsilon_2=11.6$ and $w=1.5\mu m$ are shown in figures 2.2.2(a) and (b). Note that the guide is capable of supporting only one TE and one TM mode. This mode is known as the fundamental mode. As stated above, the mode profiles are indistinguishable on the scale shown since the ratio $\varepsilon_1/\varepsilon_2$ is approximately one. As the strength of the guide ($w\Delta\varepsilon$) is increased, higher order modes may be supported. This is achieved by either increasing the width of the

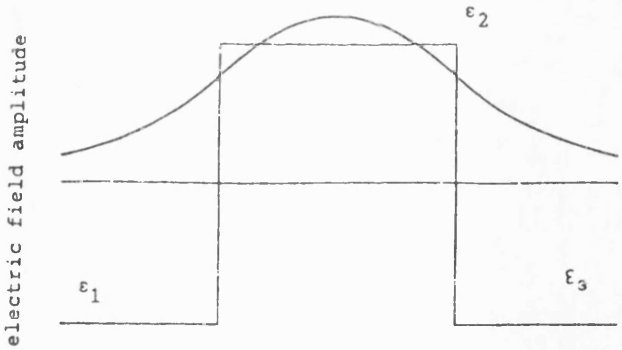

Figure 2.2.2(a) Fundamental TE mode of a 1.5μm wide slab waveguide with $\varepsilon_1=\varepsilon_3=11.4$ and $\varepsilon_2=11.6$

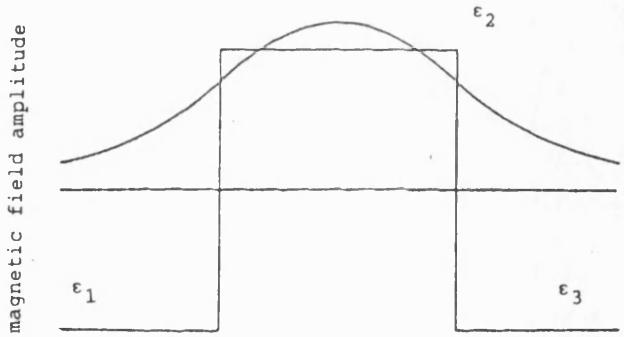

Figure 2.2.2(b) Fundamental TM mode of a 1.5μm wide slab waveguide with $\varepsilon_1=\varepsilon_3=11.4$ and $\varepsilon_2=11.6$

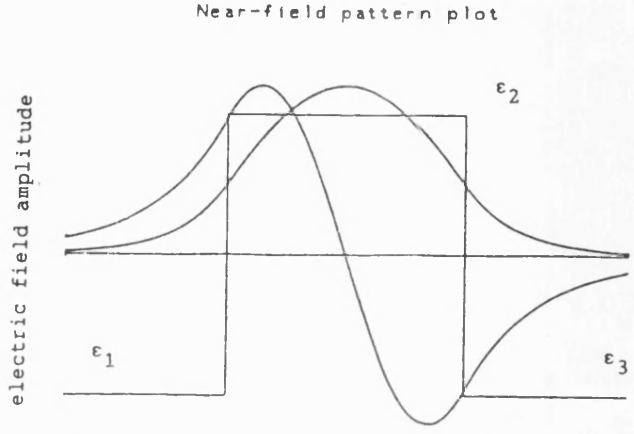

Figure 2.2.3 Fundamental and first-order TE modes of a 3μm wide slab waveguide with $\varepsilon_1=\varepsilon_3=11.4$ and $\varepsilon_2=11.6$

guide, w, or increasing the dielectric step, $\Delta\varepsilon$. Figure 2.2.3 shows the TE mode profiles for the same guide as its width is increased to 3μm. Two TE mode solutions are now present. To illustrate this principle further, figures 2.2.4(a) and (b) show the effective relative permittivities (defined by $(\beta/k_0)^2$) of the TE modes for a symmetric guide as w and $\Delta\varepsilon$ are varied. As the strength of the guide increases, higher order mode solutions are found. The corresponding TM mode solutions are shown in figures 2.2.5(a) and 2.2.5(b). The difference between the TE and TM mode sets are not noticeable on the scale shown.

2.3 The Ridge Waveguide.

The laser structure to be considered in this thesis is the Ridge Waveguide (RWG) laser (figure 2.3.1(a)) made from GaInAsP. This structure has variations of the refractive index in both the x and y directions. Thus, it forms a two-dimensional waveguide which serves to confine the energy in the transverse and lateral planes. To find the guided modes of this structure, an effective index approximation is first used to reduce the two-dimensional problem to one dimension. This, then, enables the method introduced in section 2.2 to be used to find guided mode solutions.

The effective index method is now applied to the semiconductor laser since it is a weak dielectric waveguide with low aspect ratio (see, for example ref. 3). The method involves finding the slab modes of the vertical structure of the RWG and converting their propagation constants into effective dielectric constants for the ridge and channel regions. If the vertical structure is assumed to support a single, TE mode then its effective dielectric constant is:

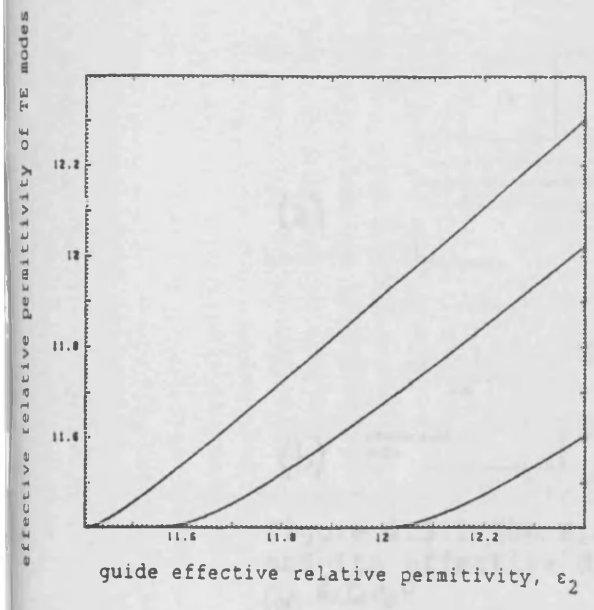

Figure 2.2.4(a) Effective relative permittivity of TE modes as guide permittivity, ε_2, is increased.

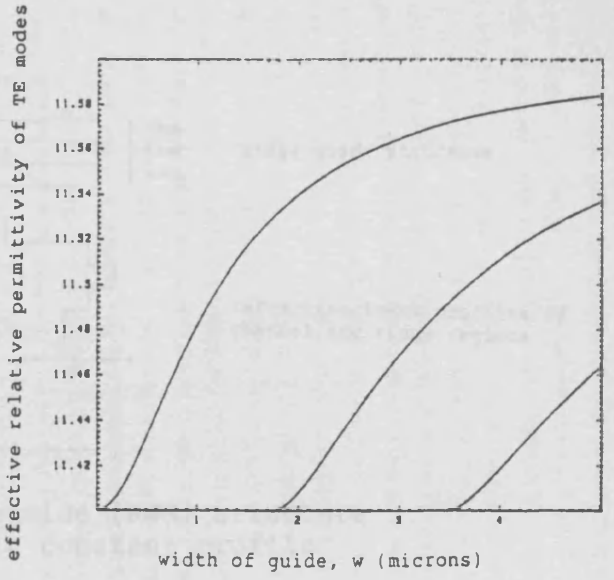

Figure 2.2.4(b) Effective relative permittivity of TE modes as guide width, w, is increased.

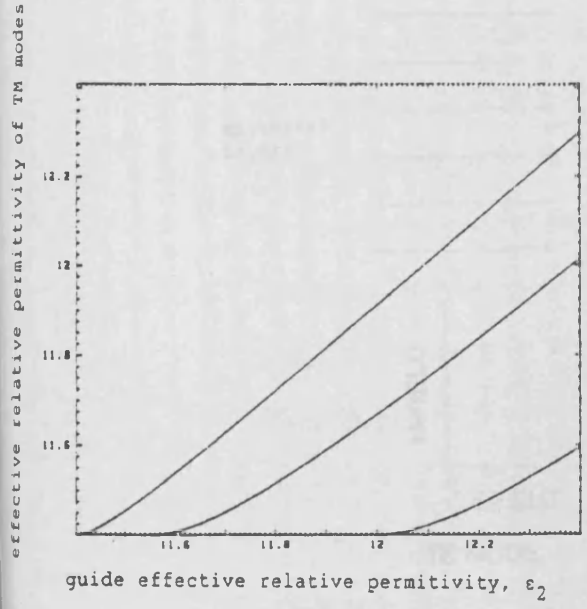

Figure 2.2.5(a) Effective relative permittivity of TM modes as guide permittivity, ε_2, is increased.

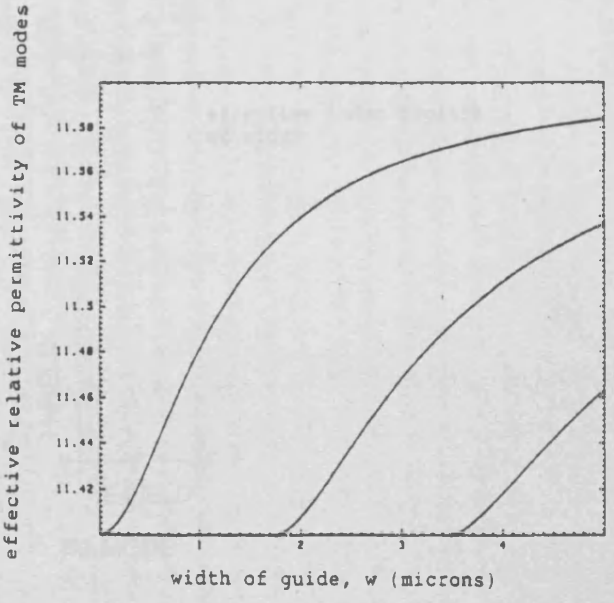

Figure 2.2.5(b) Effective relative permittivity of TM modes as guide width, w, is increased.

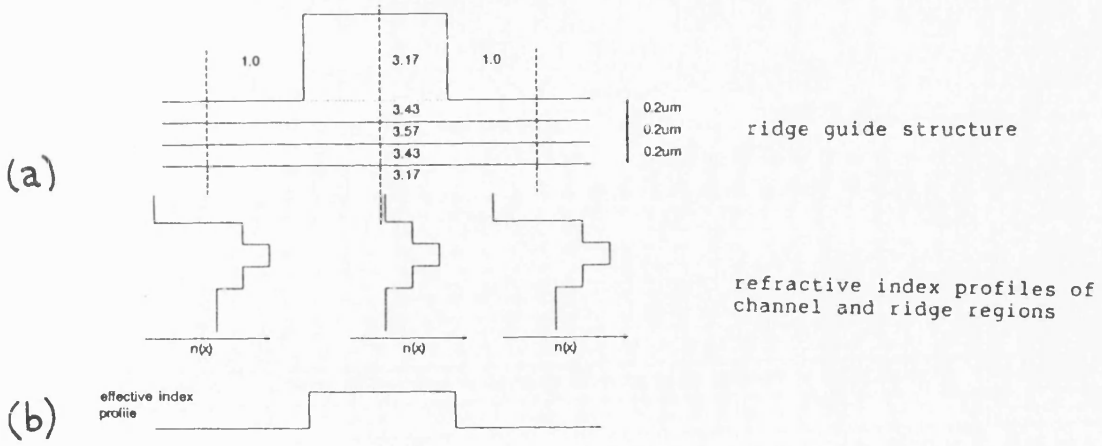

Figure 2.3.1 The Ridge Waveguide (RWG) structure and its effective dielectric constant profile for GaInAsP

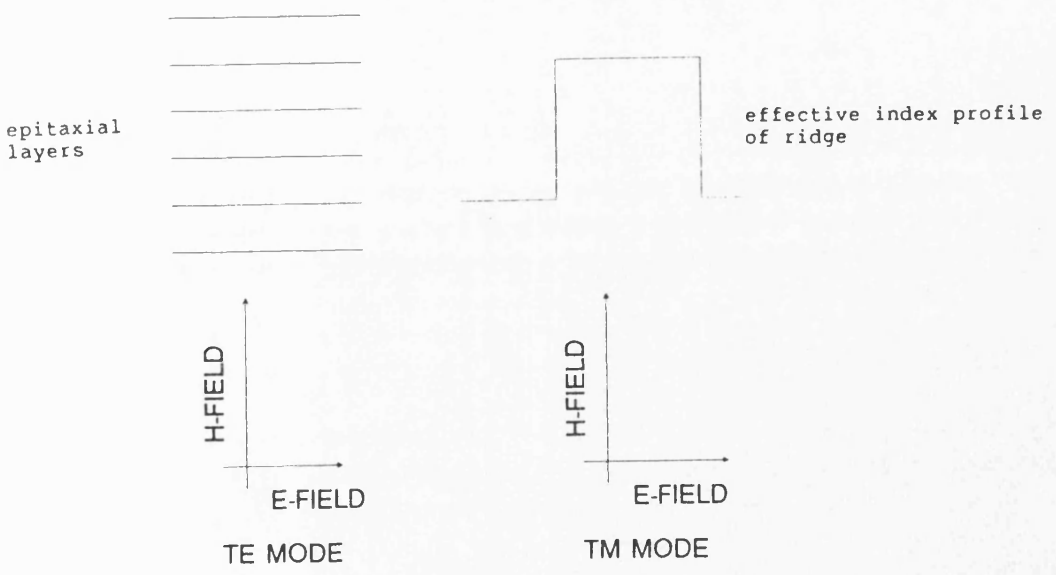

Figure 2.3.2 The TE and TM mode polarisations in dielectric slab waveguides

$$\varepsilon_{eff} = (\beta/k_0)^2 \qquad (2.3.1)$$

where β is the propagation constant of the TE mode of the ridge or channel region.

Since the vertical modes in the ridge and channel regions differ, a one-dimensional effective index profile can be calculated due to the different values of ε_{eff} for these regions (see fig.2.3.1(b)). The method of section 2.2 can then be employed to calculate the modes of the RWG structure. One point to emphasise is that the TE modes of the RWG structure are the TM modes of the effective index profile (see fig.2.3.2). Thus, one must calculate the effective dielectric constant of each region for the transverse fundamental TE mode and then use this to determine the TM mode of the effective index profile - the latter mode equates to a TE mode of the RWG structure.

For the structure shown in fig.2.3.1(b), the calculated values for the effective dielectric constants and dielectric steps are :

TE mode propagation constant beneath ridge= 1.3781265×10^7 rads m^{-1}

TE mode propagation constant between ridges= 1.3695269×10^7 rads m^{-1}

effective dielectric constant beneath ridge= 11.5579

effective dielectric constant between ridges= 11.4141

effective dielectric constant step= 0.1438

2.4 Mode Confinement and the Threshold Gain Condition.

So far the optical modes of the structures have been

calculated for lossless guides only i.e. ones in which photon loss is negligible. This is not a true representation of a dielectric waveguide formed from epitaxially grown layers. In such structures, optical losses may occur within the semiconductor layers and at the material interfaces (between layers of different composition). These losses can be dealt with theoretically by making the dielectric constant of the material complex. If one considers an effective dielectric constant $\hat{\varepsilon}$

$$\hat{\varepsilon} = \varepsilon_r + i\varepsilon_i$$

where ε_r and ε_i refer to the real and imaginary components of the dielectric constant, then the z-directed mode propagation function is:

$$E(z) \alpha \exp(-i\hat{\beta}z)$$

$$\alpha \exp(-i\beta_r z).\exp(\beta_i z)$$

where $\hat{\beta} = \beta_r + i\beta_i$

and $\beta_r = \sqrt{\varepsilon_r}.\ k_o$

$\beta_i = \sqrt{\varepsilon_i}.\ k_o$

It is seen that the "real" propagation constant is a wave propagation function related to the real part of the dielectric constant whilst the imaginary component is related to an exponentially growing or decaying term and is related to the imaginary part of the dielectric constant. If the exponential decays, the medium is said to be lossy whilst positive values of β_i represent gain. By using complex values of the dielectric constant, complex mode solutions can be found for waveguide structures. These

complex modes have a propagation constant (real part of the propagation constant) and a modal gain (loss). However, for the ridge waveguide laser, the ratio of $\varepsilon_i/\varepsilon_r$ is very small and it is not necessary to invoke the complicated analysis mentioned above. Instead the modal loss may be calculated with a high degree of accuracy from a knowledge of the field losses in the various layers and the mode distribution in those layers. If the gains in the ridge and channel regions in a ridge waveguide are denoted g_{ridge} and $g_{channel}$ and the proportion of field in these regions is denoted Γ_{ridge} and $\Gamma_{channel}$, then an approximation to the modal gain is, simply:

$$g_m = \Gamma_{ridge} \cdot g_{ridge} + \Gamma_{channel} \cdot g_{channel}$$

where g_m represents the modal gain

However, the sum of Γ_{ridge} and $\Gamma_{channel}$ are unity since they are relative proportions which sum to unity. Thus, a knowledge of Γ_{ridge} will yield a value of $\Gamma_{channel}$.

The values of gain in the ridge and channel regions can be determined experimentally or calculated approximately whilst the value of the parameter Γ_{ridge} may be determined theoretically using the mode shape determined from the slab waveguide calculations. If the lateral mode solution of the RWG is $E_m(x)$, then Γ_{ridge} is:

$$\Gamma_{ridge} = \int_{ridge} |E_m(x)|^2 dx \Big/ \int_{-\infty}^{+\infty} |E_m(x)|^2 dx$$

Function, Γ, is normally referred to as the mode confinement factor (or,

sometimes, the power filling factor) since it determines the relevant confinement of the optical mode or photon power to a given region. For waveguiding structures such as the ridge waveguide, the stronger the waveguiding effect, the higher the confinement of the mode to the ridge region. To realise how this affects the behaviour of the laser, it is now necessary to derive the threshold gain condition.

A laser is simply an optical amplifier which oscillates when the round-trip gain imparted on the optical mode is sufficient to overcome the internal and external (mirror) losses of the resonator itself. In mathematical form, this is simply

$$R_1 R_2 . \exp\left(2(G_m - \bar{\alpha})L\right) = 1$$

where R_1, R_2 are the facet (power) reflectivities,

$\bar{\alpha} = \Gamma_{ridge}\bar{\alpha}_{ridge} + (1-\Gamma_{ridge})\bar{\alpha}_{channel}$ = modal loss

($\bar{\alpha}_{ridge}$, $\bar{\alpha}_{channel}$ are the photon losses beneath the ridge and channel)

L is the cavity length

and G_m is the threshold gain of mode m.

Thus, the trheshold gain of mode m may be written as the sum of the modal loss and the mirror losses:

$$G_m = \bar{\alpha} + \frac{1}{2L} . \exp\left(\frac{1}{R_1 R_2}\right)$$

2.5 Conclusions.

The concept of electromagnetic mode families in refractive index guiding structures has been presented. A method of calculating the transverse electric (TE) and transverse magnetic (TM) modes in simple three-layered slab waveguides has been derived. Practical waveguide structures in the form of multiple ridge waveguides have been introduced. The modes in these structures can be analysed using the the effective index method.

With a knowledge of the modes supported by a waveguide, the mode confinement factor can be determined. This parameter determines the relative proportion of the total energy that exists in a specified area - it is used when specifying the modal gain/loss and threshold gain of each mode supported by the waveguide. A simple relation between the threshold modal gain of a mode, m, and the corresponding mode loss was derived. In simple terms, the threshold gain of a mode is equal to the sum of its modal loss and the mirror losses.

CHAPTER 3.

GUIDED MODE SOLUTIONS OF COUPLED WAVEGUIDES.

3.1 Introduction.

The previous chapter was concerned with calculating the modes and threshold gains of a single element, RWG laser. However, to achieve very high output powers, the output can be obtained from a number of coupled lasers. Before considering the multiple-emitter, rwg array, a method of analysis needs to be developed to analyse this structure.

Coupled mode theory can be used to find the eigenmodes of coupled multiple waveguide structures. The method has been used by Yariv [ref. 127] to find the eigenmodes of parallel, coupled waveguides in terms of the known modes of the individual waveguides. Before deriving these coupled mode equations, it is necessary to obtain a perturbation form of the wave equation which relates the modes of the coupled multiple guide structure to the modes of the individual waveguides. Thus, section 3.2 is concerned with deriving a perturbation form of the wave equation for a set of parallel waveguides. Section 3.3 derives the coupled equations for the case of N coupled, index-guided waveguides supporting TE modes only. It will be seen that the calculation of the eigenmodes of the composite guide using the coupled-mode theory requires the calculation of several mode overlap parameters. Two of the dominant parameters are the coupling constant (which determines the strength of the interaction of the modes supported by adjacent guides) and the correction to the propagation constants of the individual guided modes (due to the presence of the

neighbouring guides). The latter will be shown to represent an induced phase-change in the individual waveguide propagation constants caused by the proximity of the adjacent guides. A simplification of the last case is introduced in which the following assumptions are made. First, the guides are assumed to support the fundamental TE-like mode only. Secondly, nearest neighbour coupling is assumed to be strongest so that all other coupling coefficients can be ignored. Both points serve to simplify the calculation of the composite eigenmodes. The coupled mode format then reduces to the form presented by Hardy and Streifer [ref.s 36 and 37].

Section 3.4 is concerned with evaluating the coupling constant of adjacent guides and the induced phase-change due to these guides for the ridge structures introduced in the last chapter. These calculations are dependent on a knowledge of the modes of the individual ridge guides. First, the lateral modes of the parallel guides are determined and then, the relevant mode-overlap equations can be used to determine the coupling constants and induced phase-changes.

Lasly, in section 3.5, the phase-locked modes (also known as 'supermodes') of a multiple, coupled waveguide structure are calculated in terms of the individual waveguide modes using the previously defined coupled mode analysis.

The main conclusions of the chapter are detailed in section 3.7.

3.2 The Perturbed Field Equation for N, Parallel, Index-Guided Waveguides.

Consider N, parallel, index-guided waveguides whose respective refractive index profiles are shown overleaf. $n_k(x)$ is the refractive index profile of guide k , whilst $n_c(x)$ is the profile for the composite guide:

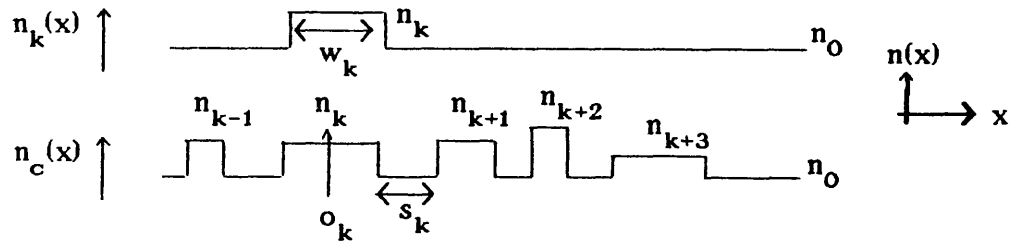

where w_k is the width of guide k, s_k is the distance between guides k and k+1 and o_k is the co-ordinate of guide k relative to the origin.

It is proposed that the total field of the guide may be approximated by a weighted sum of the fields supported by each guide:

$$E_x^c(x,y,z,t) = \sum_{k=1}^{N} \left\{A_k(z).E_x^k(x,y).\exp(i[\omega t-\beta_k z])\right\}$$

where $E_x^c(x,y,z,t)$ is the x-directed (TE-like) field of the composite structure at point x, y, z and time t,

$E_x^k(x,y)$ is the x-directed lateral mode of guide k at point x, y with longitudinal propagation constant β_k,

$A_k(z)$ is the weighting coefficient for guide k due to coupling with the other guides and the z-dependence accounts for any induced phase-changes

and ω is the angular frequency of the EM fields.

If there is no variation in the y direction then $\partial/\partial y$ is zero and the field can be assumed to be independent of y. The total field may then be expressed as:

$$E_x^c(x,z,t) = \sum_{k=1}^{N}\left\{A_k(z).E_x^k(x).\exp(i[\omega t-\beta_k z])\right\} \qquad .....(3.2.1)$$

(In the case of RWGs, the effective index method provides the one-dimensional guiding profile).

The method detailed by Yariv [ref.127] is now employed to relate the total field in the composite guide to the polarisation caused by each component of the field, ($E_x^k(x)$). The basis of this analysis is the perturbed form of the wave equation which relates the eigenmodes of the multi-element structure to the individual waveguide modes and the perturbation on the medium polarisation caused by the individual modes, P_{pert}. The details of the analysis are presented in Appendix 3.1; the result of the analysis is presented here. By first considering the wave equation for the coupled guide structure and redefining it in terms of the polarisation caused by the composite medium; then substituting equation 3.2.1:

$$\sum_{k=1}^{N} \left\{ -i2\beta_k \frac{\partial A_k}{\partial z}(z).E_x^k(x).\exp(i[\omega t-\beta_k z]) \right\} = \mu.\frac{\partial^2}{\partial t^2}[P_{pert}(x,z,t)]_x \qquad .....(3.2.2)$$

and $$\underline{P}_{pert}(\underline{r},t) = \sum_{k=1}^{N} [\varepsilon_c(\underline{r},t) - \varepsilon_k(\underline{r},t)]\, E_x(\underline{r},t) \qquad .....(3.2.3)$$

This equation forms the foundation of the following coupled-mode analysis.

3.3 The Coupled Mode Equations for a Coupled Waveguide Structure.

Following the method of Yariv (ref. 127), multiply the perturbation equation, (3.2.2), by $E_x^l(x)$ (where l=1, 2.....N), the mode supported by guide l and integrate over $x=-\infty$ to $x=+\infty$:

$$\sum_{k=1}^{N} \left\{-i2\beta_k \frac{\partial A_k}{\partial z}(z).\exp(i[\omega t-\beta_k z])\right\} \int_{-\infty}^{+\infty} E_x^k(x)E_x^l(x)\,dx$$

$$= \mu.\frac{\partial^2}{\partial t^2} \int_{-\infty}^{+\infty} [P_{pert}(x,z,t)]_x E_x^l(x)\,dx$$

where the x-dependent integral has been taken inside the second order differential term on the right hand side since it is independent of time, t. The method now departs from that of Yariv [ref.127] and follows that of Hardy et al (ref. 37). The latter method differs from the former since it includes a cross-product term of the overlap of the modes supported by adjacent guides. Yariv makes the assumption that this is negligible - which is only the case for weak coupling.

Thus the term $\int_{-\infty}^{+\infty} E_x^k(x)E_x^l(x)\,dx$ is not assumed to be negligible if $l \neq k$

If the above equation is re-arranged to keep all terms involving k on the left hand side then:

$$\sum_{k=1}^{N} \left\{\beta_k \frac{\partial A_k}{\partial z}(z).\exp(-i\beta_k z) I_{kl}\right\}$$

$$= \frac{i\mu}{2} \exp(-i\omega t) \frac{\partial^2}{\partial t^2} \int_{-\infty}^{+\infty} [P_{pert}(x,z,t)]_x E_x^l(x)\,dx$$

where I_{kl} denotes the integral of the overlap of $E_x^k(x)$ with $E_x^l(x)$.

$$I_{kl} = \int_{-\infty}^{+\infty} E_x^k(x)E_x^l(x)\,dx \qquad \text{.....(3.3.1)}$$

The perturbation of the medium $[P_{pert}(x,z,t)]_x$ is now expressed in terms of the modes supported by the coupled guide:

$$[\underline{P}_{pert}(x,t)]_x = \exp(i\omega t) \sum_{k=1}^{N} \{A_k(z)\, E_x^k(x) .\exp(-i\beta_k z).\Delta\varepsilon_k(x)\}$$

.....(3.3.2)

where $\Delta\varepsilon_k(x) = \varepsilon_0(\varepsilon_c(x) - \varepsilon_k(x))$ k=1, 2...N

$\varepsilon_c(x)$ is the coupled guide relative permittivity profile and

$\varepsilon_k(x)$ is the relative permittivity profile of guide k.

The coupled equation becomes:

$$\sum_{k=1}^{N} \left\{\beta_k \frac{\partial A_k}{\partial z}(z) . \exp(-i\beta_k z)\, I_{kl}\right\}$$

$$= \frac{-i\mu\omega^2}{2} \sum_{k=1}^{N} \left\{A_k(z) \exp(-i\beta_k z) \int_{-\infty}^{+\infty} E_x^k(x)\, E_x^l(x)\, \Delta\varepsilon_k(x)\, dx\right\}$$

.....(3.3.3)

Since l can go from 1 to N, there are N coupled equations of this form.

3.3.1 Simplification of the Coupled Mode Equations.

Let $A_k'(z) = A_k(z).\exp(-i\beta_k z)$, therefore:

$$\frac{dA_k'(z)}{dz} = -i\beta_k A_k'(z) + \exp(-i\beta_k z) \frac{dA_k(z)}{dz}$$

By re-arranging the above to obtain an expression for $\frac{dA_k(z)}{dz}$ in terms of $\frac{dA_k'(z)}{dz}$ and $A_k'(z)$ and substituting the result into the perturbation equation to eliminate the term $\exp(-i\beta_k z)$ then:

$$\sum_{k=1}^{N} \left\{ \beta_k \left(\frac{dA'_k(z)}{dz} + i\beta_k A'_k(z) \right) I_{kl} \right\}$$

$$= \frac{-i\mu\omega^2}{2} \sum_{k=1}^{N} \left\{ A'_k(z) \int_{-\infty}^{+\infty} E_x^k(x)\, E_x^l(x)\, \Delta\varepsilon_k(x)\, dx \right\}$$

This may be manipulated to express $\frac{dA'_k(z)}{dz}$ in terms of $A'_k(z)$:

$$\sum_{k=1}^{N} \left\{ \beta_k \frac{dA'_k(z)}{dz} I_{kl} \right\}$$

$$= \sum_{k=1}^{N} \left\{ -i\beta_k^2 I_{kl} - \frac{i\mu\omega^2}{2} \int_{-\infty}^{+\infty} E_x^k(x)\, E_x^l(x)\, \Delta\varepsilon_k(x)\, dx \right\} . A'_k(z)$$

.....(3.3.1.1)

Introducing the following matrices:

$\bar{A}$ representing a column matrix with components $\frac{dA'_k(z)}{dz}$

A representing a column matrix with components $A'_k(z)$

B , an NxN matrix with elements $B_{jk} = \beta_k I_{jk}$

C , an NxN matrix with elements $C_{jk} = \beta_k^2 I_{jk}$

and D , an NxN matrix with elements;

$$D_{jk} = \frac{\mu\omega^2}{2} \int_{-\infty}^{+\infty} E_x^k(x)\, E_x^j(x)\, \Delta\varepsilon_k(x)\, dx \qquad .....(3.3.1.2)$$

then the above equation can be expressed as:

$$\bar{A} = -i.\ B^{-1}(C+D).A \qquad .....(3.3.1.3)$$

3.3.2 Adjacent-Guide Coupled Equations.

The coupled equations derived at the end of the last section relate the modes of a coupled, multiple guide structure to the modes supported by each guide. If we consider the coupled multiple ridge waveguide structure mentioned earlier, practical designs will utilise ridge guides with widths greater than 1.5μm and ridge separatons of the same order. Under these circumstances, the coupling effects due to distant ridges are negligible and further simplifications may be introduced. If adjacent-guide coupling is dominant, then the matrix equation (3.3.1.3) contains tri-diagonal matrices B, C and D, with all other terms being negligible:

$$\overline{A} = -i\, B^{-1}(C+D)A$$

with

$$B_{jk} = \beta_k I_{jk} \qquad (k=j-1,\ j,\ j+1)$$

$$C_{jk} = \beta_k^2 I_{jk} \qquad (k=j-1,\ j,\ j+1)$$

$$D_{jk} = \frac{\mu\omega^2}{2} \int_{-\infty}^{+\infty} E^j(x)E^k(x)\Delta\varepsilon_k(x)\,dx \qquad (k=j-1,\ j,\ j+1)$$

When j=k, the value of D is related to the overlap of the mode intensity with adjacent guides - from the matrix equation, D_{jj} adds to the propagation constants. Thus, D_{jj} represents a phase correction term. For the purpose of the analysis, this term will be denoted M_{jj} and shall be referred to as the 'induced-phase' term.

When k=j-1 or j+1, the value of D_{jk} is the familiar coupling constant, $\varkappa_{jk}$, after ref.127. Thus, this term will also be separated out for discussion as the coupling constant: $\varkappa_{jk} = D_{jk}$

Further simplifications can be obtained if the coupling is very weak such

that $I_{jj} >> I_{jk}$ (j=/k). The matrix equations then reduce to the form proposed by Yariv (ref. 127):

$$\bar{A} = -i \begin{pmatrix} \beta_1 & \varkappa_{12} & & \underline{o} \\ \varkappa_{21} & \beta_2 & \varkappa_{23} & \\ & \underline{o} & & \\ & & & \varkappa_{N,N-1} \beta_N \end{pmatrix} \qquad \text{.....(3.3.2.1)}$$

where use has been made of the time-averaged Poynting vector, from which the following relationship can be derived:

$$\int_{-\infty}^{+\infty} |E_j(x)|^2 \, dx = \frac{2\mu\omega}{\beta_j}$$

and $\varkappa_{jk}$ is the value of equation (3.3.1.2) when $j \neq k$.

3.4 Calculating the Coupled Mode Parameters.

The previous section was concerned with deriving the coupled mode equations for a set of parallel waveguides in terms of the unperturbed modes of each isolated guide, the coupling coefficient, $\varkappa$, and the induced phase-change, M. Values of M and $\varkappa$ are now derived for the ridge-waveguide shown in section 3.2. Since nearset neighbour coupling is considered, the values of $\varkappa_{jk}$ and M_{jk} are restricted to k=j-1 and k=j+1.

3.4.1 Calculation of the Phase-change, M, of the Stripe Propagation Constant due to an Adjacent Guide.

The integral form of $M_{j,k}$ is given as the value of equation (3.3.1.2) when $E^j = E^k$. It is referred as the induced phase-change since it represents the effective change in β due to the presence of adjacent guides

- the leading diagonal of the matrix summation (C+D) from equation 3.3.1.3 represents a modified propagation constant term.

$$M_{j,k} = \frac{\omega}{4} \int_{-\infty}^{+\infty} \Delta\varepsilon_k(x).\{E_x^j(x)\}^2.dx \qquad \text{.....(3.4.1.1)}$$

$$k=j-1,\ j+1$$

To evaluate this for the array structure, the form of the field given by equation 2.2.13 is used. $\Delta\varepsilon_k(x)$ is zero everywhere except over the width of stripe k where its value is $\varepsilon_0\ (n_1^2 - n_0^2)$. This reduces the bounds of the integral to $o_k - w_k/2 \le x \le o_k + w_k/2$.

By carrying out the relevant substitutions and simplifying the equations, the expression for the real part of $M_{j,k}$ is found to be:

$$M_{j,k} = \frac{\omega}{4} a_e^{j2} \cos^2(h_e^j w_j/2).\ \frac{1}{2p_e^j}.\exp(-2p_e^j s_j).(1-\exp[-2p_e^j w_k]) \qquad \text{....(3.4.1.2)}$$

where a_e^j is the normalised fundamental TE mode field amplitude beneath guide j

$$h_e^j = \sqrt{n_j^2 k_o^2 - \beta_e^{j2}}$$

$$p_e^j = \sqrt{\beta_e^{j2} - n_j^2 k_o^2}$$

(n_j is the effective refractive index beneath guide j

β_e^j is the mode propagation constant for guide j)

and s_j is the distance between stripes j and k

a_e^j is normalised such that the power flowing in the mode is equal to 1Watt per unit of y-dimension, i.e.:

$$\frac{1}{2}\left| \int_{-\infty}^{+\infty} E \times H^*.dx \right| = 1$$

Since the real index guide supports the fundamental TE-mode, then the

above normalsiation is equivalent to:

$$\frac{\beta_e}{2\omega\mu_0}\int_{-\infty}^{+\infty} |E_x^j(x)|^2\,dx = 1$$

The variation of the real part of $M_{j,k}$ for two parallel guides has been investigated for a refractive index step of 0.012 ($\Delta\varepsilon$=0.1438) and w_2 fixed at 2μm. The variations of $M_{1,2}$ and $M_{2,1}$ have been calculated as functions of w_2 and s_1 (figures 3.4.1.1(a) and (b) , respectively). It can be seen that $M_{2,1}$ decreases rapidly as w_2 increases and s_1, w_1 remain fixed. This may be attributed to the increase in the lateral confinement of the fundamental TE-mode of guide 2 as w_2 increases which reduces the overlap of this mode with stripe 1 which, in turn, reduces $M_{2,1}$. Note also how $M_{2,1}$ decreases with s_1 due to the exponential fall-off of the E-field outside the stripe which, once again, reduces the relative amount of field beneath stripe 2.

The variation of $M_{1,2}$ with w_2 is hardly noticeable since, for a 2μm stripe, the mode beneath guide 2 is tightly confined. Thus, any change in the second stripe does not influence the phase-change beneath guide 1 since the penetration of the exponential field tail from mode 1 only reaches a fraction of guide 2. The change in $M_{1,2}$ as a function of s_1 is the same as $M_{2,1}$.

3.4.2 Calculation of the Coupling Constant, κ, Between Two Parallel Guides.

Similar to the above procedure, the coupling constant is obtained by substituting the relevant field equations into (3.3.1.2) and integrating

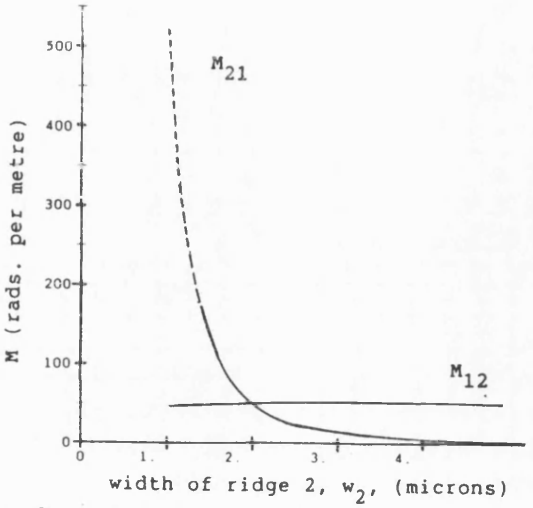

Figure 3.4.1.1(a) Variation of the modification of the propagation constant, M, due to an adjacent waveguide as the width of guide 2, w_2, is changed. (w_1=2μm, s=2μm, $\Delta\varepsilon$=0.144)

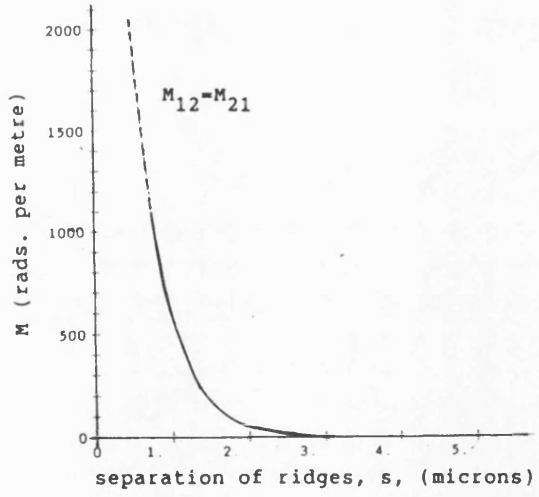

Figure 3.4.1.1(b) Variation of the modification of the propagation constant, M, due to an adjacent waveguide as the separation of the waveguides, s, is changed. (w_1=w_2=2μm, $\Delta\varepsilon$=0.144)

over the correct range. In this case, when evaluating $\kappa_{j,k}$, the range of integration is over stripe j, $o_j - w_j/2 \leq x \leq o_j + w_j/2$ where the dielectric difference, $\Delta\varepsilon$, is non-zero. The general form for the real part of the coupling constant is [ref. 11]:

$$\kappa_{j,k} = \frac{\omega\varepsilon_0}{2} \frac{(n_1^2 - n_0^2)}{(h_e^{j2} + p_e^{k2})} a_e^j a_e^k \cos(h_e^k w_k/2) \exp(-[p_e^k s_j + \varphi_1]) \times \left\{ h_e^j \sin(\varphi_2).\cosh(\varphi_1) + p_e^k \cos(\varphi_2).\sinh(\varphi_1) \right\} \quad \text{.....(3.4.2.1)}$$

where $\varphi_1 = p_e^k w_j/2$ and $\varphi_2 = h_e^j w_j/2$

and a_e^j , a_e^k are the normalised amplitudes of the fields beneath stripes j and k.

An analogous expression can be derived for $\kappa_{k,j}$ by interchanging the k's and j's and the 1's and 2's in (3.4.2.1).

$$\kappa_{k,j} = \frac{\omega\varepsilon_0}{2} \frac{(n_1^2 - n_0^2)}{(h_e^{k2} + p_e^{j2})} a_e^j a_e^k \cos(h_e^j w_j/2) \exp(-[p_e^j s_j + \varphi'_2]) \times \left\{ h_e^k \sin(\varphi'_1).\cosh(\varphi'_2) + p_e^j \cos(\varphi'_1).\sinh(\varphi'_2) \right\} \quad \text{.....(3.4.2.2)}$$

where $\varphi'_1 = p_e^j w_k/2$ and $\varphi'_2 = h_e^k w_k/2$

It should be noted that, for two, non-identical guides, $\kappa_{j,k}$ does not equal $\kappa_{k,j}$.. This can be seen by interchanging the j's and k's in the two equations above.

Plots of the real part of $\kappa_{1,2}$ and $\kappa_{2,1}$ for two parallel waveguides with a refractive index step of 0.0212 ($\Delta\varepsilon$= 0.1438) are shown in

figs. 3.4.2.1a and 3.4.2.1b. w_1 is fixed at 2μm while s_1 and w_2 are varied. To explain the variation of $\kappa_{1,2}$ with w_2, consider the shape of the fundamental mode beneath guide 2 as the guide dimension is varied. When w_2 is very small, mode 2 spreads out over a large area and the net overlap of the modes (of the two guides) beneath guide 1 is small. Hence, $\kappa_{1,2}$ is small. As w_2 increases mode 2 becomes more tightly confined and the field overlap of the modes beneath guide 1 increases until a maximum is reached - this corresponds to a maximum in $\kappa_{1,2}$. As the width of guide 2 increases further the exponential tail of mode 2 falls off rapidly across guide 1 since the offset of stripe 1 is effectively moved further away. As a result of this, the field overlap decreases and $\kappa_{1,2}$ decreases.

The variation of $\kappa_{2,1}$ with w_2 is almost exponential. The cause of this is that as w_2 increases, the offset of the centre of stripe 1 from stripe 2 increases. The field of guide 2 becomes more tightly confined whilst mode 1 remains unchanged. Hence, $\kappa_{2,1}$ falls off exponentially with w_2.

The effect of varying s_1 is the same for both $\kappa_{1,2}$ and $\kappa_{2,1}$. Since the dimensions of the guides are not changing, the modes beneath them remain unchanged in shape. The effects of increasing the separation of the guides is that the overlap of the modes decays evanescently. The coupling constants $\kappa_{1,2}$ and $\kappa_{2,1}$ decrease accordingly.

3.5 Supermode Theory.

Following the method of Kapon, Katz and Yariv (ref. 45) , phase-locked modes may propagate in a coupled waveguide structure. These modes are also referred to as 'supermodes' and they can be

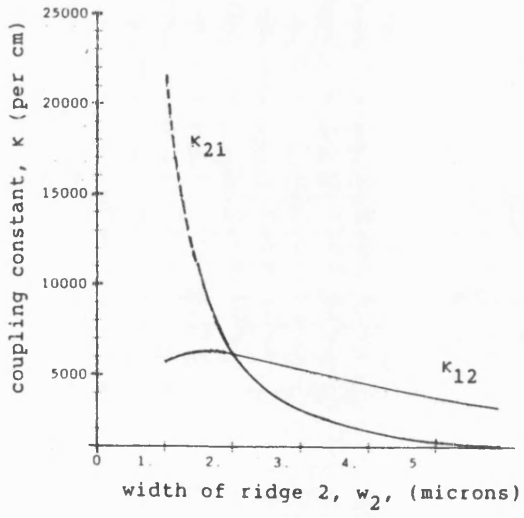

Figure 3.4.2.1(a) Variation of the coupling constant, κ, as the width of guide 2, w_2, is changed. (w_1=2μm, s=2μm, $\Delta\varepsilon$=0.144)

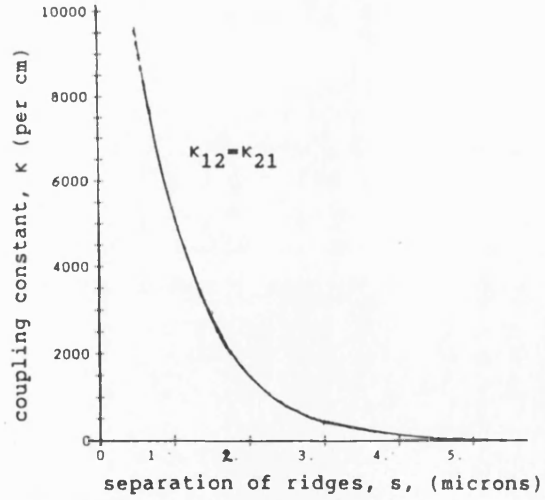

Figure 3.4.2.1(b) Variation of the coupling constant, κ, as the separation of the waveguides, s, is changed. ($w_1=w_2$=2μm, $\Delta\varepsilon$=0.144)

represented by:

$$E^r(x,z) = E^r(x)\exp(-i\sigma_r z)$$

where $E^r(x)$ represents the lateral distribution of supermode r with propagation constant σ_r.

By finding the z-derivative of the above equation, the supermodes can be calculated using coupled mode theory. Firstly:

$$\frac{dE^r(x,z)}{dz} = -i\sigma_r E^r(x).\exp(-i\sigma_r z)$$

$$= -i\sigma_r E^r(x,z) \qquad \text{.....(3.5.1)}$$

Now $E^r(x,z)$ can be found from the modes of the individual guides (coupled mode theory):

$$E^r(x,z) = \sum_{k=1}^{k=N} A'_k(z).E^k(x).\exp(-i\beta_k z)$$

Thus, $$\frac{dE^r(x,z)}{dz} = -i\sigma_r \sum_{k=1}^{k=N} A'_k(z)E^k(x,z)$$

Using (3.3.1.3)

$$-iB^{-1}(C+D)A = -i\sigma_r A$$

$$\Rightarrow \quad \left(B^{-1}(C+D) - \sigma_r I\right)A = 0 \qquad \text{.....(3.5.2)}$$

where I represents the NxN unit matrix.

The above equation, when solved, will yield eigenvalues (i.e. propagation constants) σ_r with eigenvectors A^r_j where r is the supermode number and j is the guide number. By applying this technique to the ridge guide structure of section 3.2, the phase-locked eigenmodes (supermodes) are found. For N=5, w=2μm and s=2μm, the near-field and far-field patterns are shown in figures 3.5.1 and 3.5.2. For a 5 element array comprising

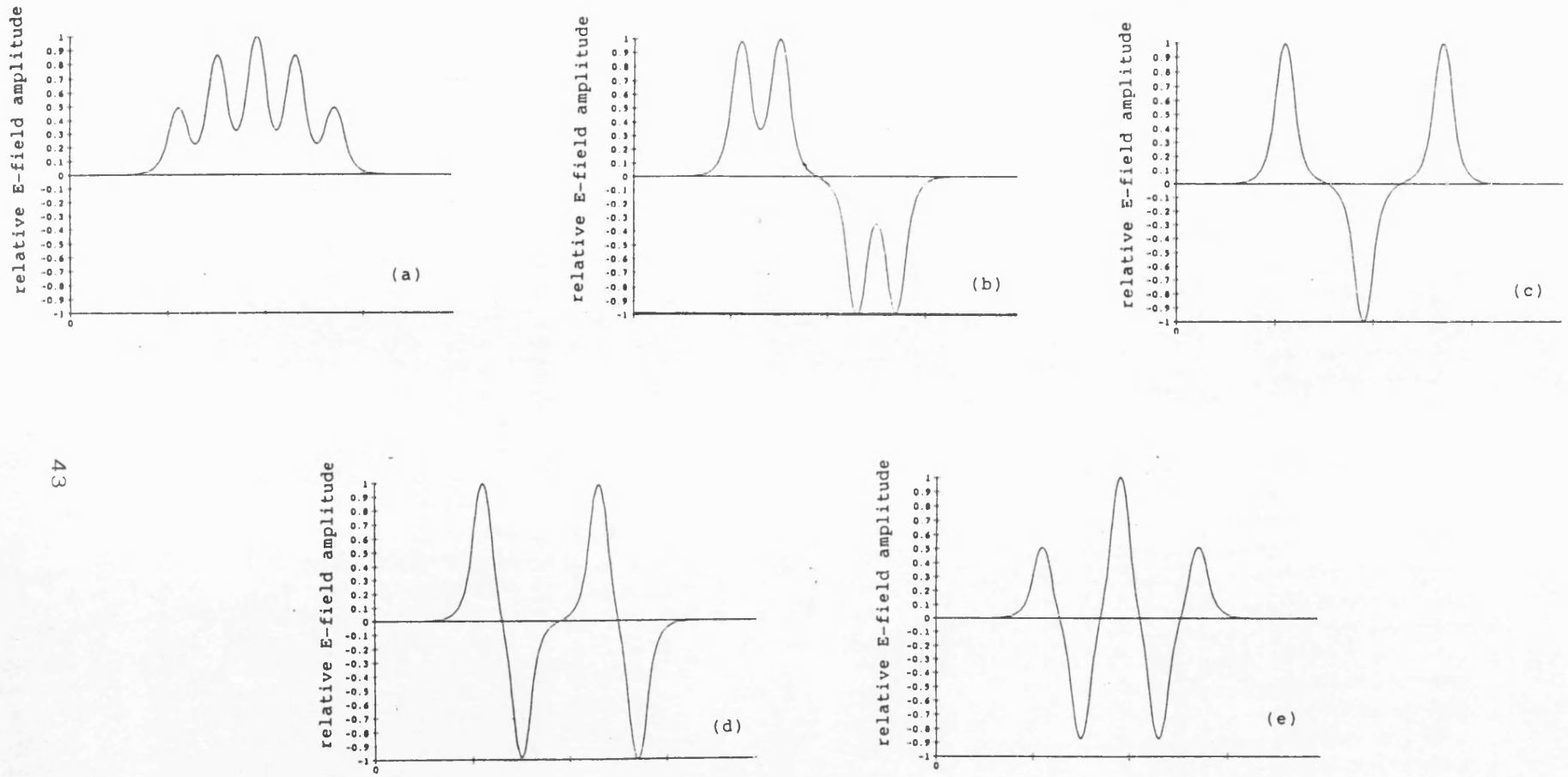

Figure 3.5.1 The 5 supermodes of a 5 element array ($w_1=w_2=w_3=w_4=w_5=2\mu m$, $s=2\mu m$, $\Delta\varepsilon=0.144$)
(a) zero-order (or fundamental) mode,
(b) first-order mode,
(c) second-order mode,
(d) third-order mode,
(e) fourth-order (or highest-order) mode.

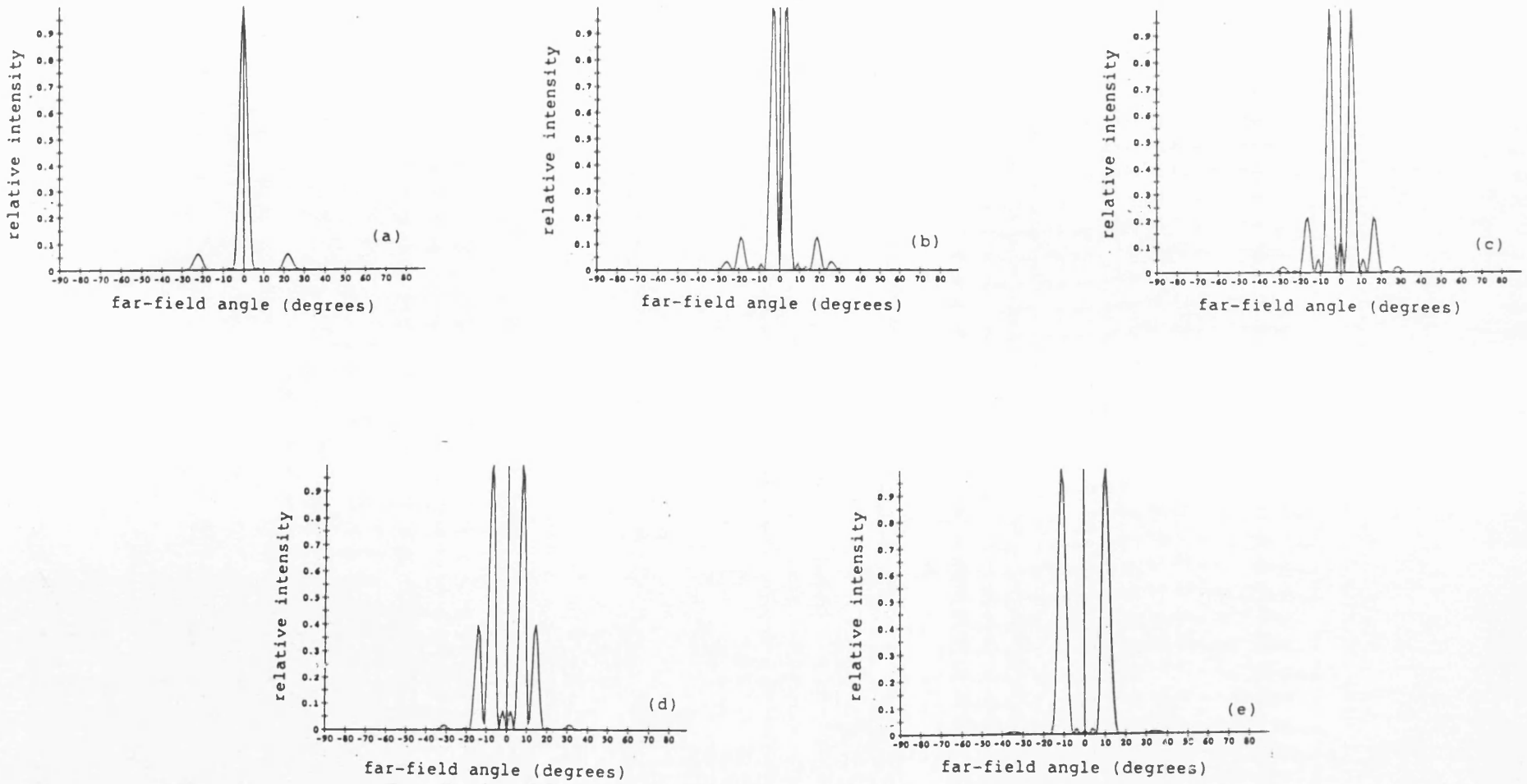

Figure 3.5.2 The 5 far-field patterns corresponding to figure 3.5.1(a)-(e)
(a) zero-order (or fundamental) mode,
(b) first-order mode,
(c) second-order mode,
(d) third-order mode,
(e) fourth-order (or highest-order) mode.

single-mode ridges, the total number of supermodes is 5. These supermodes have a similar form to that of a multi-mode, single ridge guide in that the envelope functions of the composite modes are comparable to the shape of the single guide mode functions. The supermode number is directly related to the number of times the electric field crosses the x-axis. Furthermore, as the order of the supermode increases, anti-phase electric field components cause destructive interference in the far-field, fig.3.5.2. This is consistent with basic diffraction theory. Since the waveguiding mechanism is real and symmetric, the far-field distribution is symmetric about the normal axis (ref. 20).

From the eigenvector distribution, it is clearly seen that the lowest order supermode has the greatest amount of its field distribution within the channel regions. Usually these regions experience the lowest gain and/or the greatest loss and, so, intuition leads one to conclude that the lowest order mode will experience the highest modal loss or lowest modal gain. On the other hand, the highest order supermode, which has the lowest amount of field in to the channel regions, will experience the lowest modal loss/highest modal gain.

3.6 Conclusions.

A method of determining the eigenmode solutions of coupled, multiple waveguide structures has been presented. Particular attention has been paid to the multiple coupled ridge waveguide array. The coupling of the individual ridges has been investigated and the eigenmodes determined. It is found that two important parameters dictate the performance of the coupled waveguide system - the coupling constant, κ, and the induced phase-change, M. These parameters have been evaluated for the case of

two parallel ridge waveguides as functions of ridge separation and ridge width.

The development of the coupled mode equations into a set of matrix equations determining the phase-locked behaviour of coupled arrays has been included. The analysis of a 5-element array consisting of 5 identical ridges on a constant pitch has been presented. It is found that 5 phase-locked 'supermodes' can be supported by this structure. However, the mode with the lowest modal losses is found to be the highest order mode which exhibits a twin-lobed far-field pattern.

APENDIX 3.1

The Perturbed Field Equation for N, Parallel, Index-Guided Waveguides.

Consider N, parallel, index-guided waveguides whose respective refractive index profiles are shown below. $n_k(x)$ is the refractive index profile of guide k , whilst $n_c(x)$ is the profile for the composite guide:

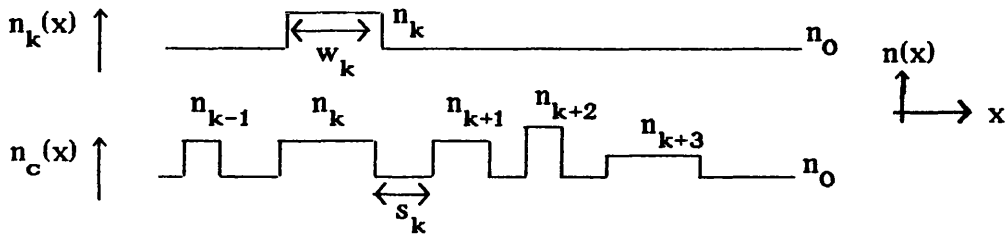

where w_k is the width of guide k and s_k is the distance between guides k and k+1.

It is proposed that the total field of the guide may be approximated by a weighted sum of the fields supported by each guide:

$$E_x^c(x,y,z,t) = \sum_{k=1}^{N} \left\{ A_k(z).E_x^k(x,y).\exp(i[\omega t-\beta_k z]) \right\}$$

where $E_x^c(x,y,z,t)$ is the x-directed (TE-like) field of the composite structure at point x, y, z and time t,

$E_x^k(x,y)$ is the x-directed lateral mode of guide k at point x, y with longitudinal propagation constant β_k,

$A_k(z)$ is the weighting coefficient for guide k due to coupling with the other guides,

and ω is the angular frequency of the EM fields.

If there is no variation in the y direction then $\partial/\partial y$ is zero and the field can be assumed to be independent of y. The total field may then be

expressed as:

$$E_x^c(x,z,t) = \sum_{k=1}^{N}\left\{A_k(z).E_x^k(x).\exp(i[\omega t-\beta_k z])\right\} \qquad .....(1)$$

(In the case of RWGs, the effective index method provides the one-dimensional guiding profile).

The method detailed by Yariv [ref.127] is now employed to relate the total field in the composite guide to the polarisation caused by each component of the field, ($E_x^k(x)$). The basis of this analysis is the perturbed form of the wave equation which relates the eigenmodes of the multi-element structure to the individual waveguide modes and the perturbation on the medium polarisation caused by the individual modes.

The wave equation for the E-field may be written in terms of the modes supported by each guide (as if the guide was in isolation) and the polarisation due to the modes supported by the coupled multiple-element structure.

If we consider a single element guide with dielectric constant profile $\varepsilon_k(r,t)$, the electric flux is given by:

$$\underline{D}_k(\underline{r},t)= \varepsilon_0 \underline{E}_k(\underline{r},t) + \underline{P}_k(\underline{r},t) \qquad .....(2)$$

where $\varepsilon_0 \underline{E}_k(\underline{r},t)$ represents the flux in free-space due to mode $\underline{E}_k(\underline{r},t)$ and $\underline{P}_k(\underline{r},t)$ is the polarisation of the free-space medium due to guide k and mode $\underline{E}_k(\underline{r},t)$:

$$\underline{P}_k(\underline{r},t) = (\varepsilon_k(\underline{r},t) - \varepsilon_0)\underline{E}_k(\underline{r},t)$$

In a multi-element structure, the electric flux, D(r,t), may be formulated in the same way:

$$\underline{D}(\underline{r},t) = \varepsilon_0 \underline{E}_x^c(\underline{r},t) + \underline{P}_c(\underline{r},t)$$

where $\underline{E}_x^c(\underline{r},t)$ is now the mode of the multi-element structure and $\underline{P}_c(\underline{r},t)$ is given by:

$$\underline{P}_c = (\varepsilon_c(\underline{r},t) - \varepsilon_0)\underline{E}_x^c(\underline{r},t)$$

The wave equation for the electric field , E, may now be expressed as:

$$\nabla^2 \underline{E}_x^c(\underline{r},t) = \mu_0 \varepsilon_0 \frac{\partial^2}{\partial t^2} \underline{E}_x^c(\underline{r},t) + \mu_0 \frac{\partial^2}{\partial t^2} \underline{P}_c(\underline{r},t)$$

$\underline{P}_c(\underline{r},t)$ may be expressed alternatively as:

$$\begin{aligned} \underline{P}_c(\underline{r},t) &= \underline{P}_0(\underline{r},t) + \underline{P}_{pert}(\underline{r},t) \\ &= [\varepsilon_c(\underline{r},t) - \varepsilon_0] E_x^c(\underline{r},t) \end{aligned}$$

where $\underline{P}_0 = \sum_{k=1}^{N} [\varepsilon_k(\underline{r},t) - \varepsilon_0] E_x^c(\underline{r},t)$ is the polarisation induced in the individual waveguides ($\varepsilon_k(\underline{r},t)$) in the presence of $E_x^c(\underline{r},t)$.

and $\underline{P}_{pert}(\underline{r},t) = \sum_{k=1}^{k=N} [\varepsilon_c(\underline{r},t) - \varepsilon_k(\underline{r},t)]\ E_x^c(\underline{r},t)$

The wave equation may now be written in terms of the

perturbation to the medium polarisation :

$$\nabla^2 E_x^c(\underline{r},t) - \mu.\varepsilon_k(\underline{r},t).\frac{\partial^2 E_x^c(\underline{r},t)}{\partial t^2} = \mu_o.\frac{\partial^2}{\partial t^2}[P_{pert}(\underline{r},t)]_x \quad \text{.....(3)}$$

(Subscript x denotes the x-directed component of the field vector i.e. the TE mode)

If there is no variation of the field in the y direction then $\partial/\partial y$ is zero. The modes of the isolated waveguides, as well as the field for the multi-element guide are then solutions of the following reduced wave equation:

$$\left[\frac{\partial^2}{\partial x^2} - \beta_k^2\right].E_x^k(x) + \omega^2\mu\varepsilon_k(x).E_x^k(x) = 0 \quad \text{.....(4)}$$

where k=1, 2, 3, ..., N and c

By substituting equation (1) into (3) and re-arranging the result, the perturbation equation yields:

$$\sum_k \left\{A_k(z).\exp(-i\beta_k z).\left[\frac{\partial^2 E_x^k(x)}{\partial x^2} + (\omega^2\mu\varepsilon_k(x) - \beta_k^2).E_x^k(x)\right] + E_x^k(x).\exp(-\beta_k z).\left[\frac{\partial^2 A_k(z)}{\partial z^2} - i2\beta_k\frac{\partial A_k(z)}{\partial z}\right]\right\}.\exp(i\omega t) = \mu\frac{\partial^2}{\partial t^2}[P_{pert}(x,z,t)]_x \qquad k=1, 2, 3,...., N$$

If $A_k(z)$ varies slowly with z, then $|\beta_k\frac{\partial A_k(z)}{\partial z}| >> |\frac{\partial^2 A_k(z)}{\partial z^2}|$. Furthermore, note that the expression in the first bracket on the LHS of the equation is zero (as can be shown by substituting $E_x^k(x,z)$ into the wave equation - equation (4)). Upon simplifying the last equation, the following perturbed wave equation is obtained:

$$\sum_{k=1}^{N} \left\{ -i2\beta_k \frac{\partial A_k}{\partial z}(z).E_x^k(x).\exp(i[\omega t-\beta_k z]) \right\} = \mu.\frac{\partial^2}{\partial t^2}[P_{pert}(x,z,t)]_x \quad .....(5)$$

This equation forms the foundation of the coupled-mode analysis.

CHAPTER 4

UNIFORM AND NON-UNIFORM RIDGE WAVEGUIDE ARRAYS.

4.1 Introduction.

The last section of chapter 3 presented the eigenmode solutions of a 5 element array based on coupled mode theory. It was predicted that, for the structure shown, the highest order mode has the lowest modal loss. Alternatively expressed, the highest order mode requires the lowest amount of injected gain to reach its threshold condition. Under uniform carrier injection, this infers that the highest order mode will dominate the modal behaviour of thae array at and above threshold. Thus, alternative array designs are sought to meet the criterion for a single, fundamental mode laser array. Firstly, the uniform array of the last chapter is investigated in greater depth to account for variations in ridge width, ridge separation and numbers of coupled ridges (section 4.2). Various types of non-uniform array designs are then presented in section 4.3 - these illustrate how the array design parameters may be simply adjusted in an attempt to achieve the required fundamental mode output. However, fundamental mode operation at threshold is not the only criterion which will affect the laser's performance - the stability of this mode above threshold is important. Since the stability of this mode is linked to its uniformity (references 15, 16, 20), then mode uniformity becomes an important performance criterion and the array designs are assessed by considering the combined effects of modal loss and uniformity about threshold. The ideal case is one in which the fundamental supermode has the lowest modal loss and is uniformly distributed across the array. The

array designs presented in this section will be shown to meet some but not all of these criteria. Further, since the array theory is a passive guide analysis, the effects of injected gain (i.e. carriers) on the lateral dielectric profile are not considered. However, to investigate the effects of injected carriers on modal gain, the effect of tailoring the injected carrier distribution is treated simply. The effects of a non-uniform gain profile (and, thus, non-uniform carrier injection) on the gain discrimination between supermodes is analysed by changing the value of the material gain beneath the ridge and channel regions (section 4.4). The nett modal gains for different lateral gain profiles are calculated.

The conclusions of the chapter are presented in section 4.5.

4.2 Uniform Arrays.

The uniform array is made up of elements of equal ridge widths and equal ridge separations - though the separations are not necessarily the same as the widths. For this simple design, the individual, isolated guides have identical propagation constants and coupling constants.

Figure 4.2.1(a) shows the variation of the supermode effective refractive indices (β/k_0) with increasing ridge width, w, for a uniform 5 element array. All the ridges are separated by 2μm. As w increases, two effects are noted - firstly, the supermode effective refractive indices increase and, secondly, they draw closer together.

The first effect is due to the increasing value of the fundamental mode propagation constant of the individual ridges with increasing guide strength (see section 2.3) whilst the second effect may be attributed to the corresponding reduction in the coupling coefficients as the individual

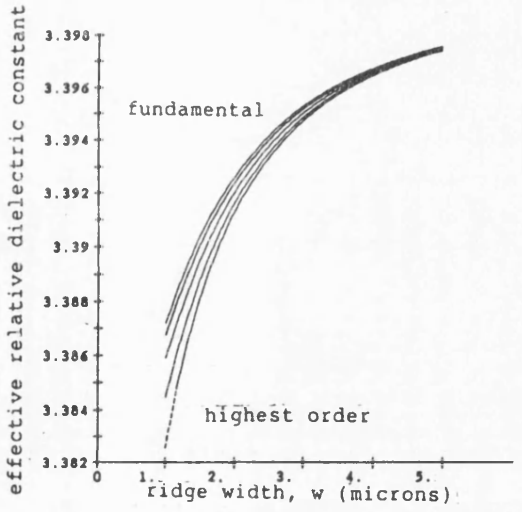

Figure 4.2.1(a) Variation of the effective refractive indices of the supermodes of a 5 element uniform array as the ridge widths are changed ($w_1=w_2=w_3=w_4=w_5=w$, $s=2\mu m$, $\Delta\varepsilon=0.144$)

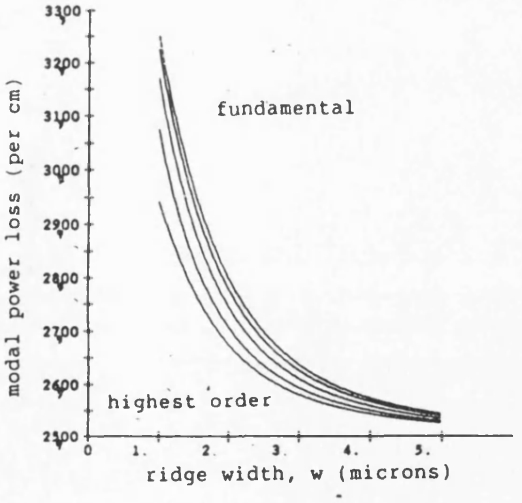

Figure 4.2.1(b) Variation of the mode loss of the supermodes of a 5 element uniform array as the ridge widths are changed ($w_1=w_2=w_3=w_4=w_5=w$, $s=2\mu m$, $\Delta\varepsilon=0.144$)

ridge modes become more tightly confined (see fig.3.4.2.1). Hence, since the splitting of the supermode propagation constants is dependent on the coupling constants, κ, [ref 45] then the splitting of the supermodes decreases as κ decreases.

The variation of the modal loss with w is also explained by the increase in mode confinement as w increases. Since the individual ridge guide modes are confined more tightly to the lower loss ridge regions and the overlap of the photon distribution with the higher loss channel regions decreases as w increases then the absolute value of modal loss decreases.

However, note that as w increases and κ decreases, there is the possibility that adjacent guides may become decoupled and phase-locking of the array breaks down. This brief discussion does not take into account the effects of injected carriers on the lateral dielectric profile. In practice, the injected carrier profile will reduce the effective dielectric step height of the individual ridges causing the coupling strength between adjacent guides to increase. However, the argument still holds that if κ gets too small then phase-locking conditions break down. A second effect not considered, is spatial hole-burning (reference 22). This occurs above threshold where high stimulated photon densities deplete the local carrier concentration at the intensity maxima. This leads to a localised increase in the effective dielectric constant which ultimately leads to self-focussing of the electric field and a reduction in the coupling constant. If the self-focussing effect is very strong other supermodes may begin to propagate as higher order supermodes make more effective use of the gain profile or, alternatively, the onset of a higher order mode of the individual ridge guide may occur. All of these effects are detrimental to the required output. For the purpose of illustration, it is assumed that the guided modes are not subject to self-focussing and the array is assumed to

operate in phase-locked mode - the coupling of adjacent guides is assumed to be sufficient to maintain a coupled output. Furthermore, the phase-locked output is assumed to be made up of a composition of the individual guide fundamental TE modes.

The near field distribution of the lowest and highest order supermodes are shown in figures 4.2.2a and 4.2.2b for w=1.0μm and w=3.0μm and fixed separation (s=2.0μm). It is seen that the mode profiles of the wide ridge array are very similar to those for the narrow ridge array. However, the amount of field in the channels differ slightly due to the higher ridge confinement factors for the wide ridge array.

The effects of varying the stripe separation, s, and keeping w constant in a uniform array are shown in figures 4.2.3a and 4.2.3b. Figure 4.2.3a displays how the effective refractive indices of the supermodes converge for large values of s. This is due to the decreasing value of the coupling constant with increasing s which decreases the separation between the supermode propagation constants. The effects on the supermode loss as s varies are shown in figure 4.2.3b. As previously noted, the higher order modes have a lower value of modal loss caused by the smaller proportion of light in the higher loss (channel) regions. However, three distinct characteristics are now obvious. For large ridge separations, the supermode loss approaches a constant value. This is intuitively understood by considering a number of free-running ridges which are in-phase or in anti-phase to each other - the amount of field between the ridges remains almost constant as long as s remains large and the width w does not change (the overlap of adjacent guides is so weak that the adjacent fields hardly interfere with one another). However, this may cause a break-down in the phase-locking of the supermode as mentioned earlier.

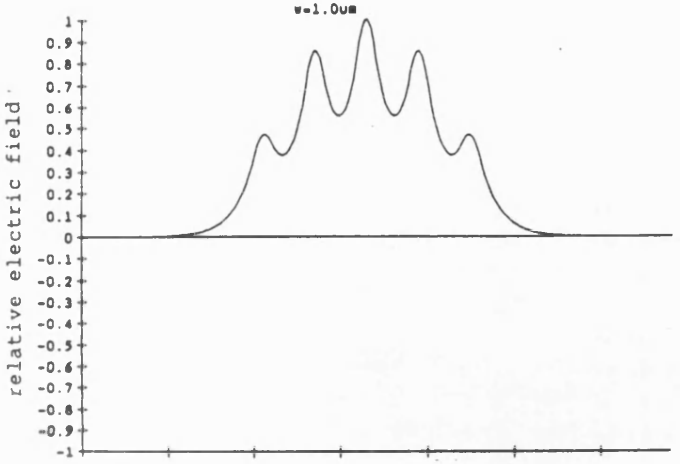

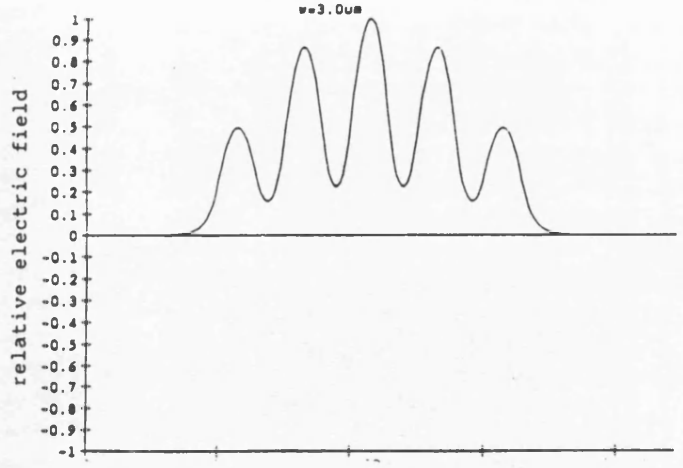

Figure 4.2.2(a) The fundamental supermode of a 5-element uniform array when w=1μm and w=3μm ($w_1=w_2=w_3=w_4=w_5=w$, s=2μm, $\Delta\varepsilon$=0.144)

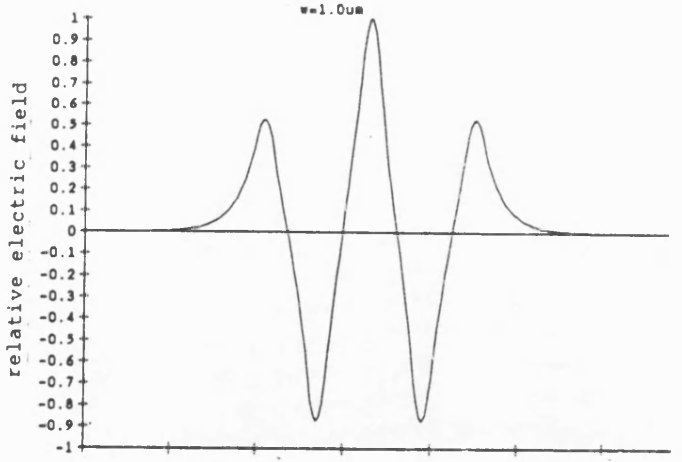

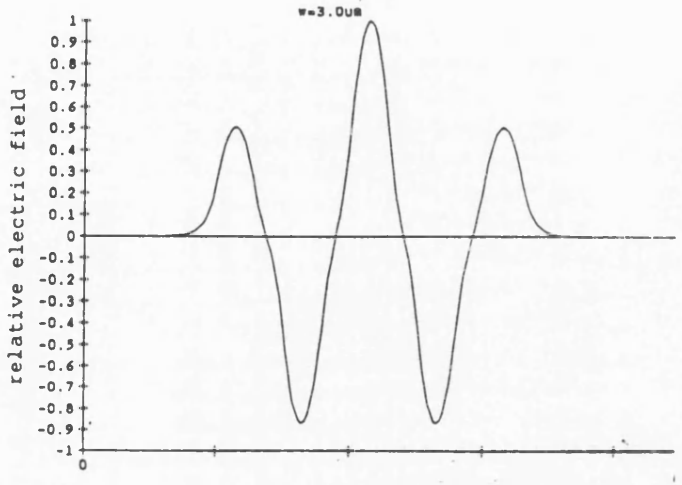

Figure 4.2.2(b) The highest-order supermode of a 5-element uniform array when w=1μm and w=3μm ($w_1=w_2=w_3=w_4=w_5=w$, s=2μm, $\Delta\varepsilon$=0.144)

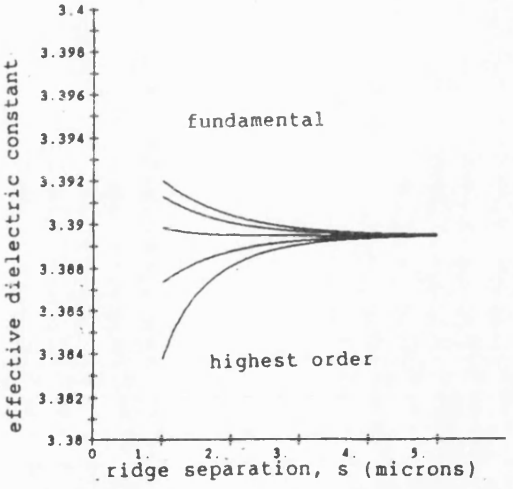

Figure 4.2.3(a) Variation of the effective refractive indices of the supermodes of a 5 element uniform array as the separation between the ridges, s, is changed ($w_1=w_2=w_3=w_4=w_5=1.5\mu m$, $\Delta\varepsilon=0.144$)

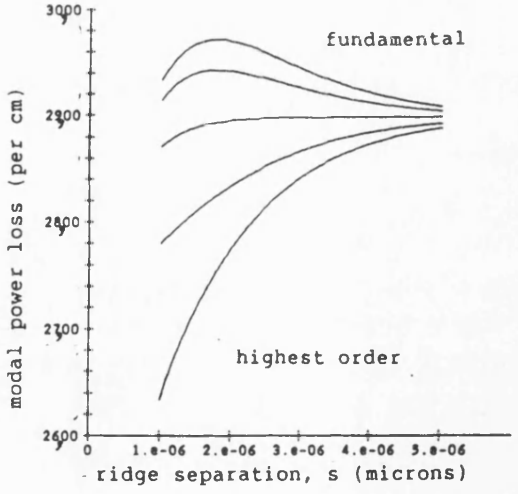

Figure 4.2.3(b) Variation of the mode loss of the supermodes of a 5 element uniform array as the separation between the ridges, s, is changed ($w_1=w_2=w_3=w_4=w_5=1.5\mu m$, $\Delta\varepsilon=0.144$)

As the ridge separation decreases the supermode losses diverge as the interference effects of the in-phase and anti-phase field components increase or decrease the relative proportions of field intensity in the channel and guide regions until a maximum in the loss of the lower order modes occurs at a separation of about 1.8μm.

Lastly, the absolute value of loss of the lower order modes decreases as s reduces further. This is, at first, surprising since the overlap of adjacent guided modes is still increasing as s reduces. However, another effect starts to come into play - the area of the channel region reduces uniformly as s decreases. Previously, this has been a secondary effect to the increase in the amount of mode overlap with decreasing s. Now, however, this reduced area results in a reduction of the relative amount of field intensity in the channel region and an increased field contribution to the field immediately under the adjacent guides. The net effect is that the mode loss reduces with further reduction of s.

The lowest and highest order eigenmodes corresponding to two separations of 1.0μm and 3.0μm for a ridge width of 1.5μm are shown in figure 4.2.4a and 4.2.4b. Once again, the closely coupled array experiences the greatest amount of neighbouring field overlap which results in larger mode discrimination.

Having effected changes in the ridge width and ridge separation of a uniform array, the last design freedom to consider is the behaviour of the array as the number of elements (ridges), n, increases. Figure 4.2.5 illustrate how the mode effective refractive indices and losses change as the number of ridges is increased from 2 to 7 (all ridge widths and separations are held constant at 2μm). As n increases, the number of guided modes supported increases in unison - each extra ridge adds

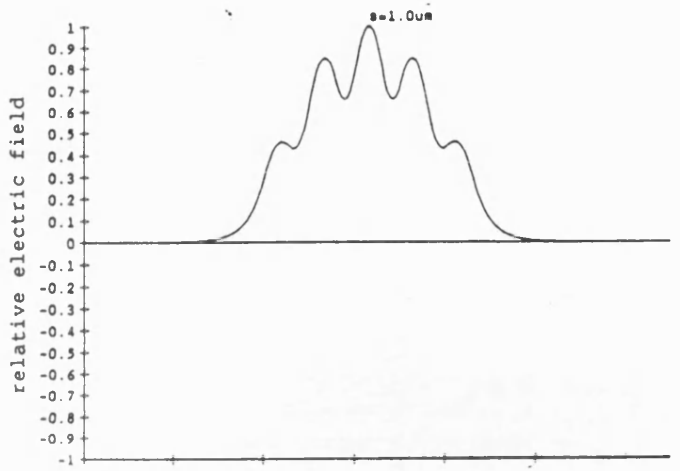

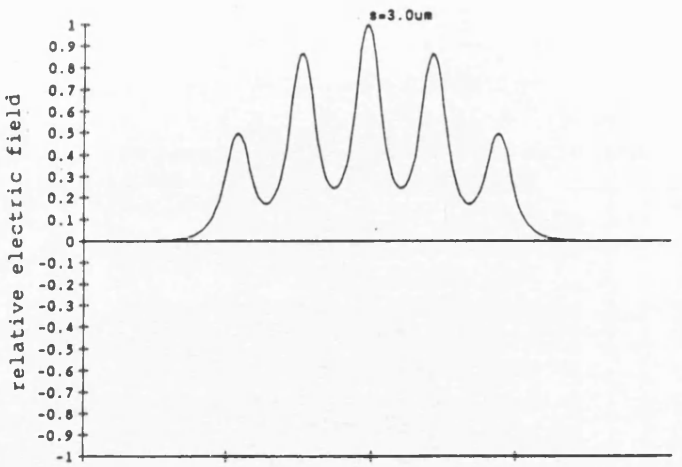

Figure 4.2.4(a) The fundamental supermode of a 5-element uniform array when s=1μm and s=3μm (w_1=w_2=w_3=w_4=w_5=1.5μm, $\Delta\varepsilon$=0.144)

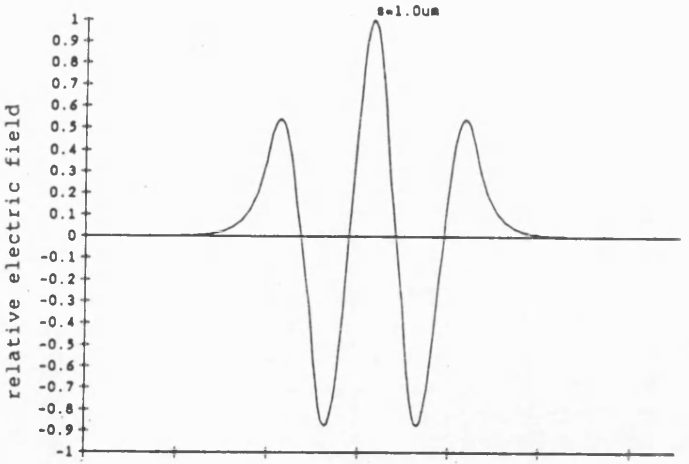

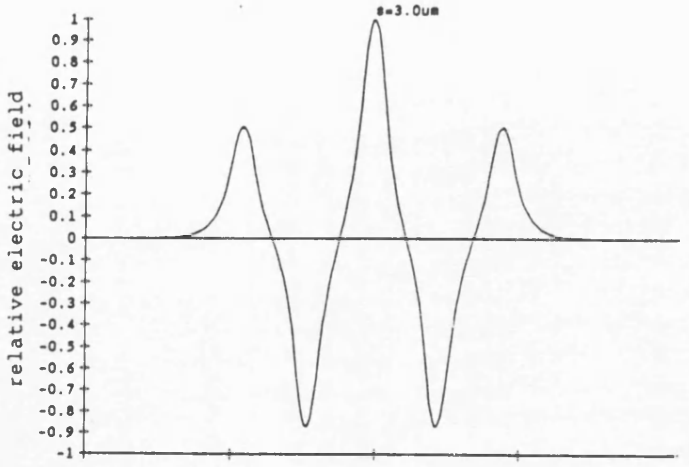

Figure 4.2.4(b) The highest-order supermode of a 5-element uniform array when s=1μm and s=3μm (w_1=w_2=w_3=w_4=w_5=1.5μm, s=2μm, $\Delta\varepsilon$=0.144)

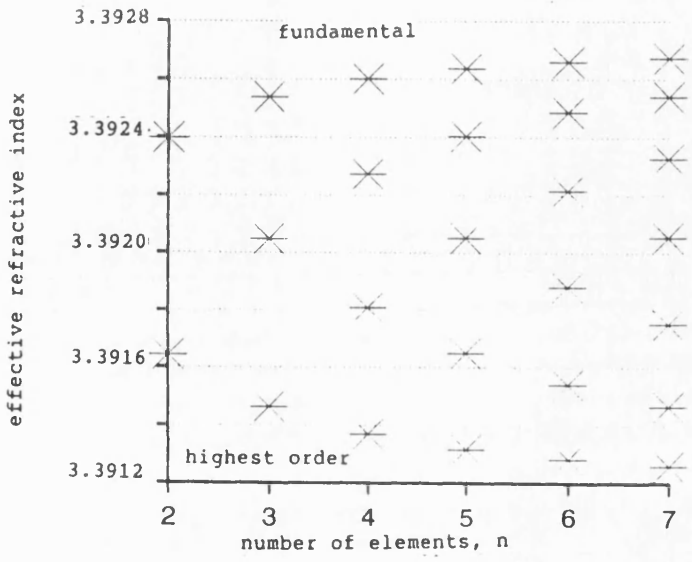

Figure 4.2.5(a) Variation of the effective refractive indices of the supermodes of a uniform array as the number of elements, n, increases. (w=2μm, s=2μm, $\Delta\varepsilon$=0.144)

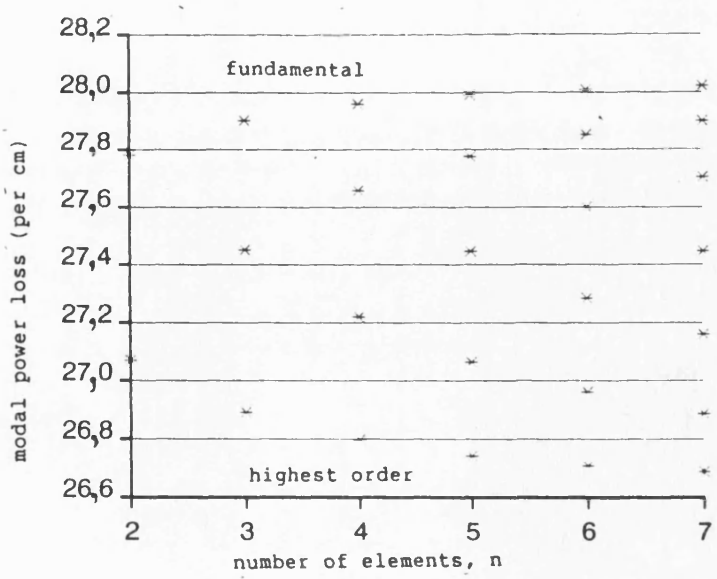

Figure 4.2.5(b) Variation of the mode loss of the supermodes of a uniform array as the number of elements, n, increases. (w=2μm, s=2μm, $\Delta\varepsilon$=0.144)

another TE mode to the nett ouput of the coupled array. Furthermore, since the coupling constant and propagation constants are not changing, the actual values of the eigen matrix elements remains the same - only the order of the eigen matrix changes. This means that the β-space occupied by the guided modes hardly changes as n increases. Thus, the separation of the propagation constants decreases since n is increasing. Similarly, the gain discrimination between the supermodes decreases as n increases (figure 4.2.5b)

4.3 Non-Uniform Ridge Waveguide Arrays.

Non-uniform ridge waveguide arrays are ones in which the individual ridges and/or channels differ in size. The basis of the designs in this section is the requirement to create a stable, fundamental mode device of practical use. As such, the modal loss of the fundamental must be lower than all higher order modes and, in order that the output is stable under high power drive conditions, the photon distribution should be as uniform as possible to reduce non-linearities in the output due to spatial hole-burning effects. Two types of non-uniform arrays are considered here - the first is the variable width array (i.e. the ridge widths are chirped across the array), the second is the variable separation array (where the ridge separations are chirped). Since it is desirable to produce a uniform light intensity distribution, symmetry of the array is maintained about its centre.

4.3.1 Variable Ridge Width Arrays

The first, most obvious case to consider is one in which the ridge widths are adjusted to complement the fundamental mode light distribution - i.e. the ridges are widest where the light intensity is greatest. This case may be considered as tailoring the lateral (real) dielectric guide for fundamental mode operation. The lateral guide of the array becomes an equivalent of an effective parabolic guide since the index is greatest at the centre of the guide to suit the fundamental mode intensity maximum. Figure 4.3.1.1 shows how the array behaves as the centre ridge varies in a 5 element array in which $w_1=w_5=1.5\mu m$, $w_2=w_4=2.0\mu m$ and w_3 is varied between 2.0 and 3.0μm. The ridge separations are held constant at 2.0μm. The number of ridges is arbitrarily set at 5 to illustrate the performance of this design without using a large array in which there will be many modes to analyse. It is seen that as long as $w_3>2.5\mu m$, the fundamental mode has the lowest modal loss. However, the field uniformity of this mode is poor (see figure 4.3.1.2) - the fundamental mode is almost totally confined to the centre element. Note how modes 2 and 4 are independent of w_3. From figure 4.3.1.2, the cause of this is apparent - neither of these modes have significant field distributions beneath the third ridge and, so, their characteristics are largely independent of the dimension of this ridge. Figure 4.3.1.3 shows the effects of varying the outer ridge dimensions of the array from 1.0 to 2.0μm - the fundamental mode has the lowest modal loss as long as w_1 and w_5 are less than 2.0μm wide. This is once again of secondary importance as the field uniformity is poor with most of the fundamental supermode occupying the central element.

In order to distribute the photon density more evenly across an array, an inverse of the last design is presented in which the guiding mechanism is strongest at the outer edges and decreases uniformly

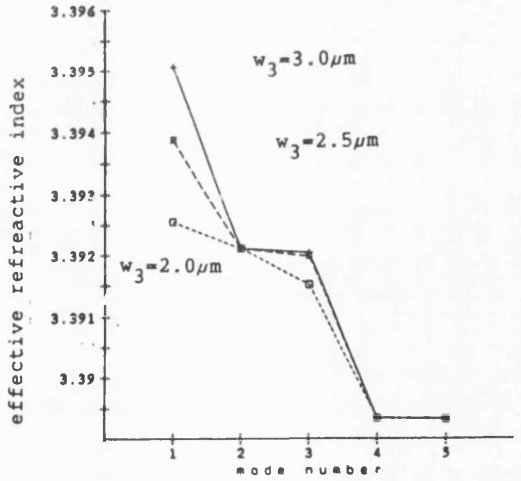

Figure 4.3.1.1(a) Variation of the effective refractive index of the supermodes of a 5 element, Λ-chirped array as w_3 changes. (w_1=w_5=1.5μm, w_2=w_4=2.0μm, s=2μm, Δε=0.144)

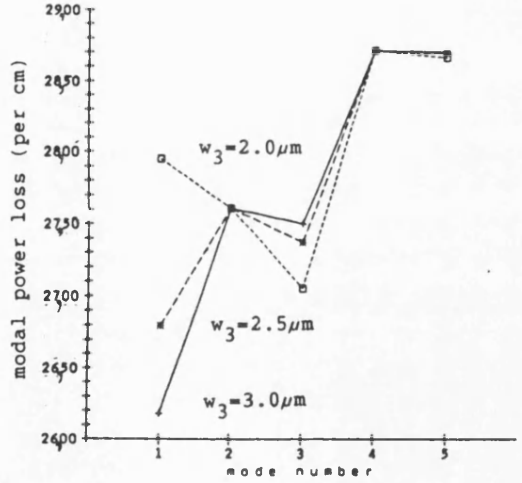

Figure 4.3.1.1(b) Variation of the mode loss of the supermodes of a 5 element, Λ-chirped array as w_3 changes. (w_1=w_5=1.5μm, w_2=w_4=2.0μm, s=2μm, Δε=0.144)

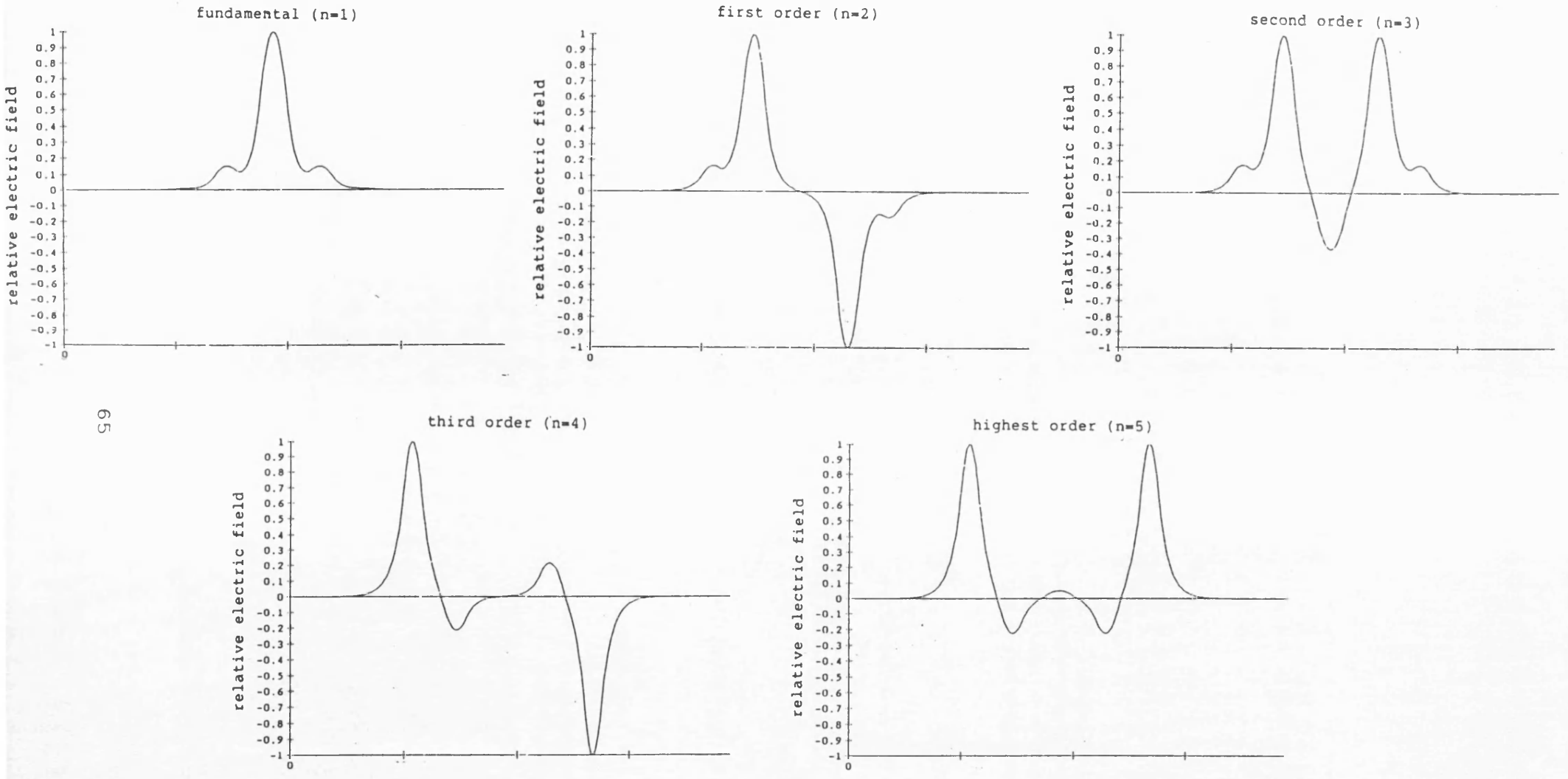

Figure 4.3.1.2 Near field pattern of a 5-element array in which $w_1=w_5=1.5\mu m$, $w_2=w_4=2.0\mu m$ and $w_3=2.5\mu m$ for a fixed separation , s, of $2.0\mu m$

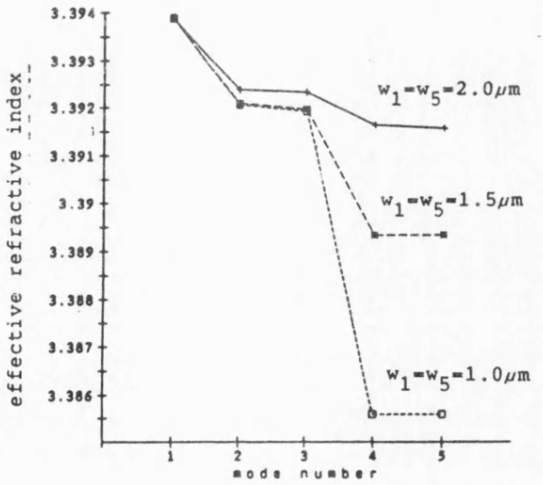

Figure 4.3.1.3(a) Variation of the effective refractive index of the supermodes of a 5 element, Λ-chirped array as w_1 and w_5 change. ($w_3=2.5\mu m$, $w_2=w_4=2.0\mu m$, $s=2\mu m$, $\Delta\varepsilon=0.144$)

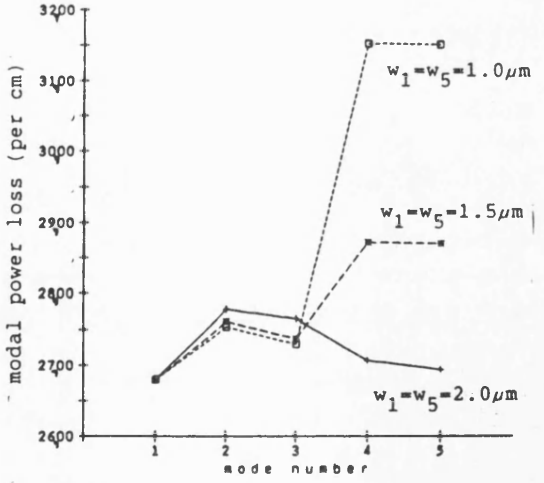

Figure 4.3.1.3(b) Variation of the mode loss of the supermodes of a 5 element, Λ-chirped array as w_1 and w_5 change. ($w_3=2.5\mu m$, $w_2=w_4=2.0\mu m$, $s=2\mu m$, $\Delta\varepsilon=0.144$)

towards the centre. Figures 4.3.1.4 and 4.3.1.6 show how this array behaves for the case where $w_1=w_5=2.5\mu m$, $w_2=w_4=2.0\mu m$ and $w_3=1.5\mu m$. Variations of this array due to variations of w_3 and w_1, w_5 are shown. It is seen that the fundamental and first order modes are almost indistinguishable in terms of the effective refractive index and modal loss. Figure 4.3.1.6 illustrates the cause of this - the fundamental and first order modes are almost identical to each other - the only difference between them being the phase difference occurring beneath guide 3. Since the field beneath guide 3 is negligible, the net overlap of the modes is practically identical for the fundamental and first order modes causing the effective refractive indices and mode losses to be indistinguishable on the scale shown in both cases. Furthermore, the absence of any field contribution beneath guide 3 for these modes eliminates their dependence on the width of this guide.

4.3.2 Variable Ridge Separation Arrays.

An equivalent way of achieving mode control is by adjusting the strength of the coupling between adjacent guides by altering the separation of the guides. Figures 4.3.2.1 and 4.3.2.4 show how variable spacing arrays achieve mode control. However, notice that in all cases the fundamental mode has the highest modal loss - the cause of this is that changing the separation of the guides changes the mode overlap parameters slightly whereas the effects of changing ridge width are two-fold. Firstly, there is a variation in the individual ridge propagation constants and, secondly, there is a change in the coupling constants. Both of these alter the original eigenmatrix. The latter effects have a much more pronounced effect on the supermode properties. In all cases, the effects of changing the separation will change both the coupling constant and the mode overlap equations but the individual propagation constants

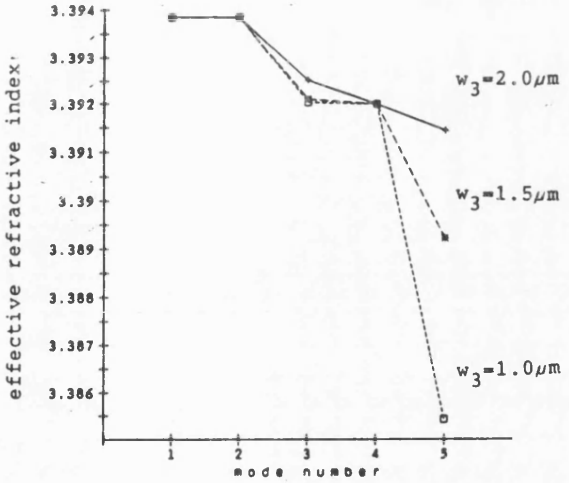

Figure 4.3.1.4(a) Variation of the effective refractive index of the supermodes of a 5 element, V-chirped array as w_3 changes. (w_1=w_5=2.5μm, w_2=w_4=2.0μm, s=2μm, $\Delta\varepsilon$=0.144)

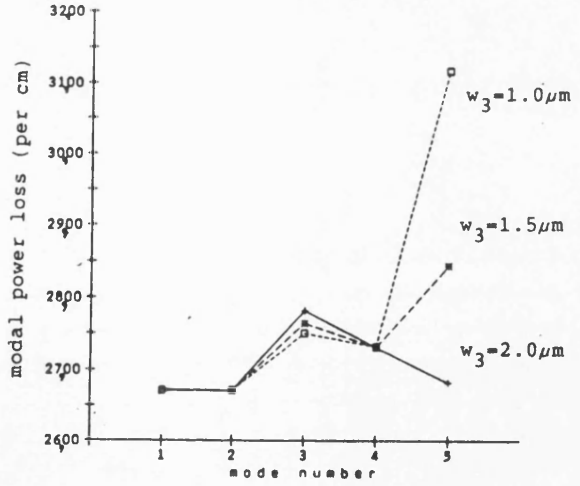

Figure 4.3.1.4(b) Variation of the mode loss of the supermodes of a 5 element, V-chirped array as w_3 changes. (w_1=w_5=2.5μm, w_2=w_4=2.0μm, s=2μm, $\Delta\varepsilon$=0.144)

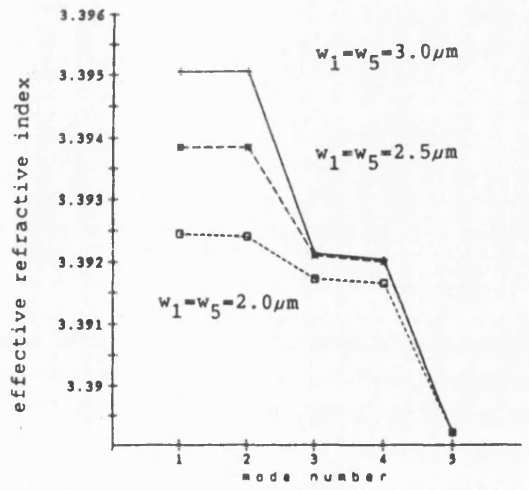

Figure 4.3.1.5(a) Variation of the effective refractive index of the supermodes of a 5 element, V-chirped array as w_1 and w_5 change. ($w_3=2.5\mu m$, $w_2=w_4=2.0\mu m$, $s=2\mu m$, $\Delta\varepsilon=0.144$)

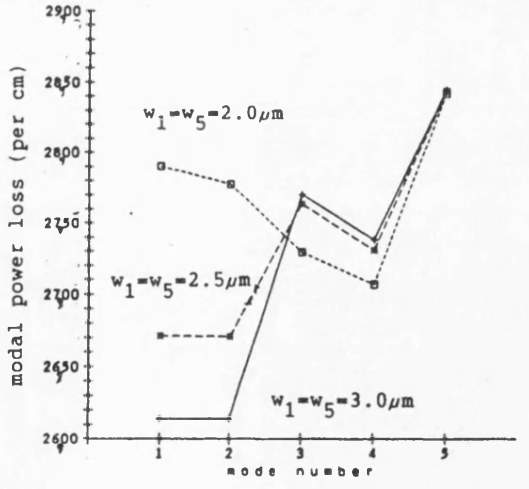

Figure 4.3.1.5(b) Variation of the mode loss of the supermodes of a 5 element, V-chirped array as w_1 and w_5 change. ($w_3=2.5\mu m$, $w_2=w_4=2.0\mu m$, $s=2\mu m$, $\Delta\varepsilon=0.144$)

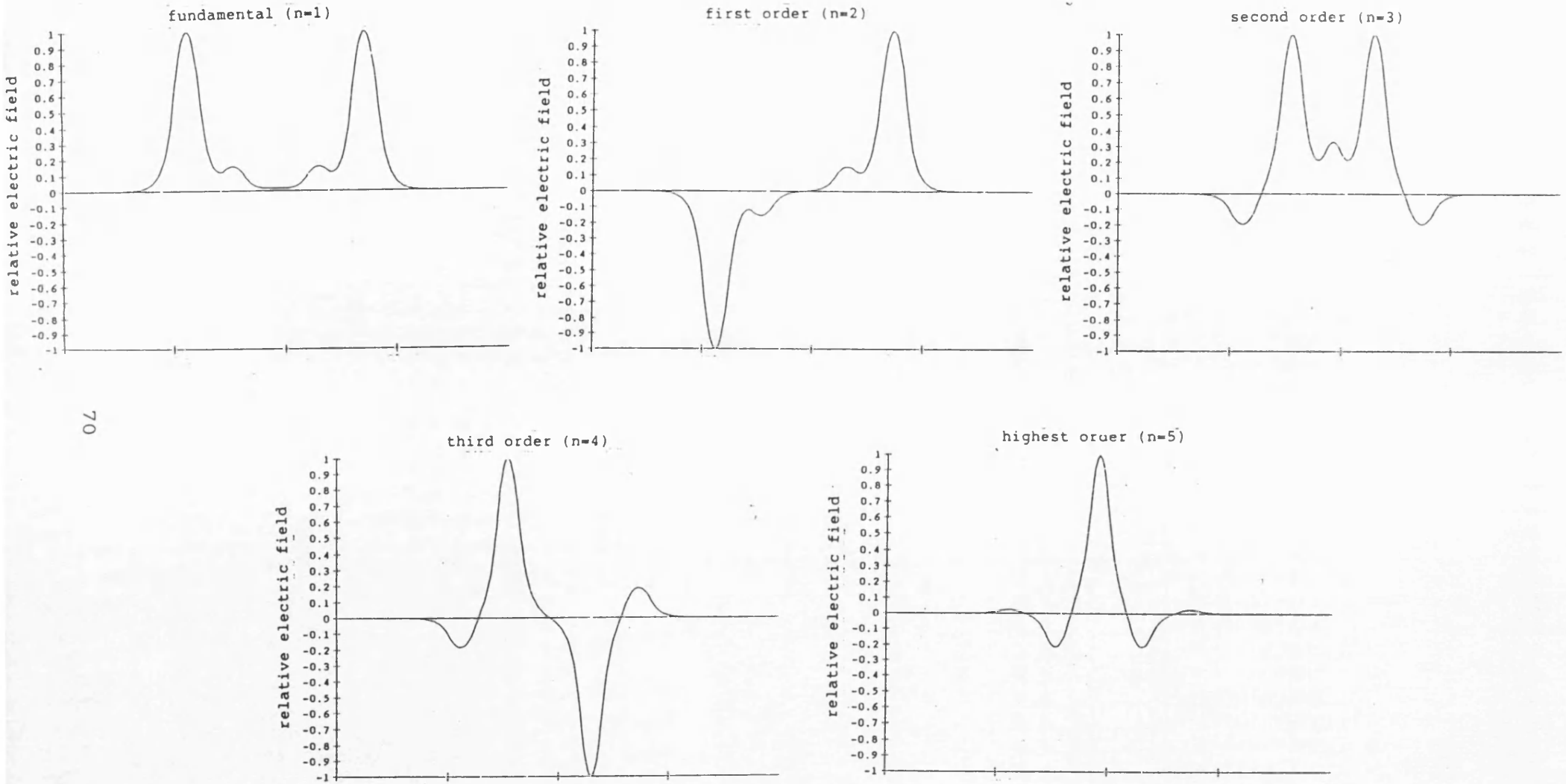

Figure 4.3.1.6 Near field pattern of a 5-element array in which $w_1=w_5=2.5\mu m$, $w_2=w_4=2.0\mu m$ and $w_3=1.5\mu m$ for a fixed separation , s, of $2.0\mu m$

remain fixed. Figure 4.3.2.1 shows the effects of having the strongest coupling (smallest separation) at the centre of the 5-element array. Likewise, figure 4.3.2.2 shows the inverse of this design where $\varkappa$ is strongest at the array edges. These designs are analogous to the earlier attempts to tailor the propagation constants (ridge widths) to suit the required intensity profile. However, the effects of these changes are significantly smaller than the previous case - changes in $\varkappa$ due to variations in separation, s, are orders of magnitude smaller than those effected by changes in the ridge propagation constants due to variations of the ridge widths, w. Most importantly, note that, without exception, the higher order modes have the lowest modal loss - the opposite to the desired result.

4.3.3 High Uniform-Intensity Arrays.

Apart from the non-uniform arrays presented above, other non-uniform arrays have been proposed. Perhaps the most significant of these is a perturbed form of the uniform array in which the outer ridge widths of a uniform array are adjusted to improve the uniformity of the light distribution [ref. 15, 16]. Consider the 5-element array in which all separations are 2μm and $w_2=w_3=w_4=2\mu m$. The effects of changing w_1, w_5 are shown in figure 4.3.3.1 where the uniformity factor and modal loss of the supermodes are plotted as the dependent variables. (The uniformity factor is a guide to the linearity of the supermode and is defined by $\eta=1-\left\{|E_{max}|-|E_{min}|\right\}$). It is seen that, as predicted by Buus, a highly uniform fundamental mode can be produced by tailoring w_1 and w_5. However, a slight intolerance on these dimensions may cause the array to propagate an equally uniform, anti-phase, highest order mode. Secondly,

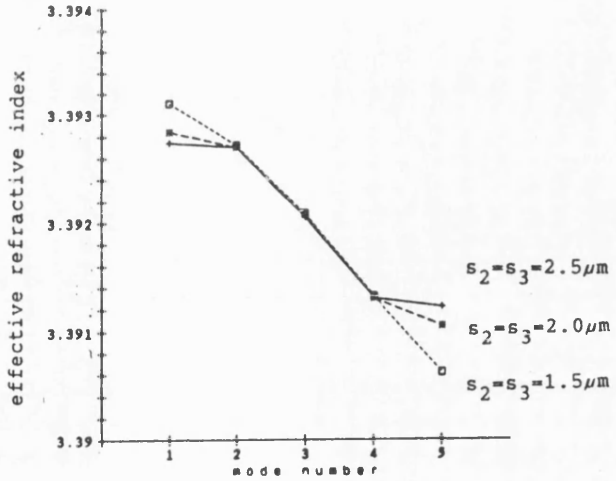

Figure 4.3.2.1(a) Variation of the effective refractive index of the supermodes of a 5 element, variable separation array as s2 and s_3 change. (w=2μm, $s_1=s_4=1.5\mu m$, $\Delta\varepsilon=0.144$)

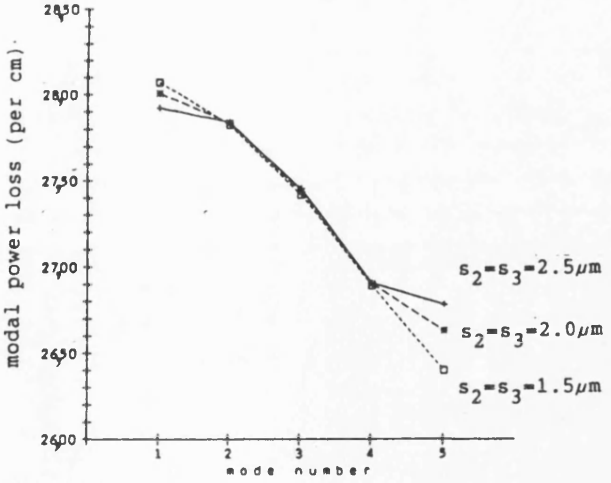

Figure 4.3.2.1(b) Variation of the mode loss of the supermodes of a 5 element, variable separation array as s_2 and s_3 change. (w=2μm, $s_1=s_4=1.5\mu m$, $\Delta\varepsilon=0.144$)

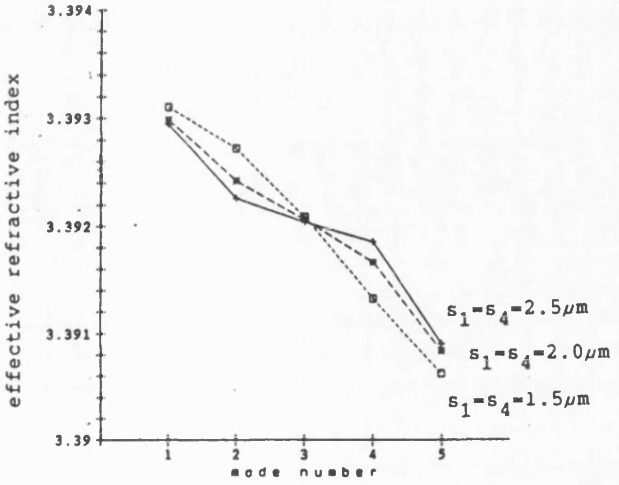

Figure 4.3.2.2(a) Variation of the effective refractive index of the supermodes of a 5 element, variable separation array as s_1 and s4 change. (w=2μm, s_2=s_3=1.5μm, Δε=0.144)

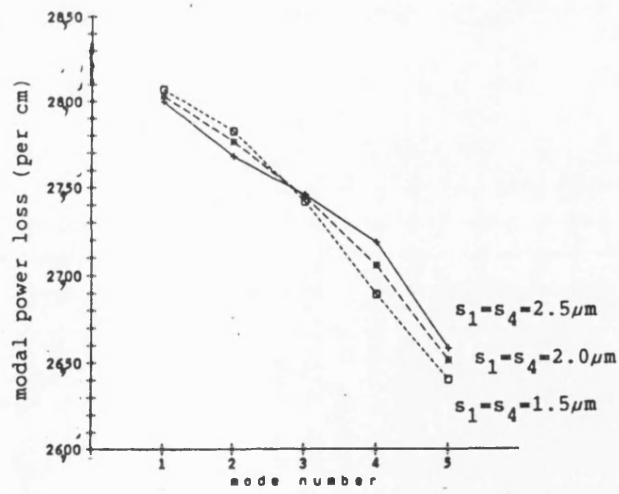

Figure 4.3.2.2(b) Variation of the mode loss of the supermodes of a 5 element, variable separation array as s_1 and s_4 change. (w=2μm, s_2=s_3=1.5μm, Δε=0.144)

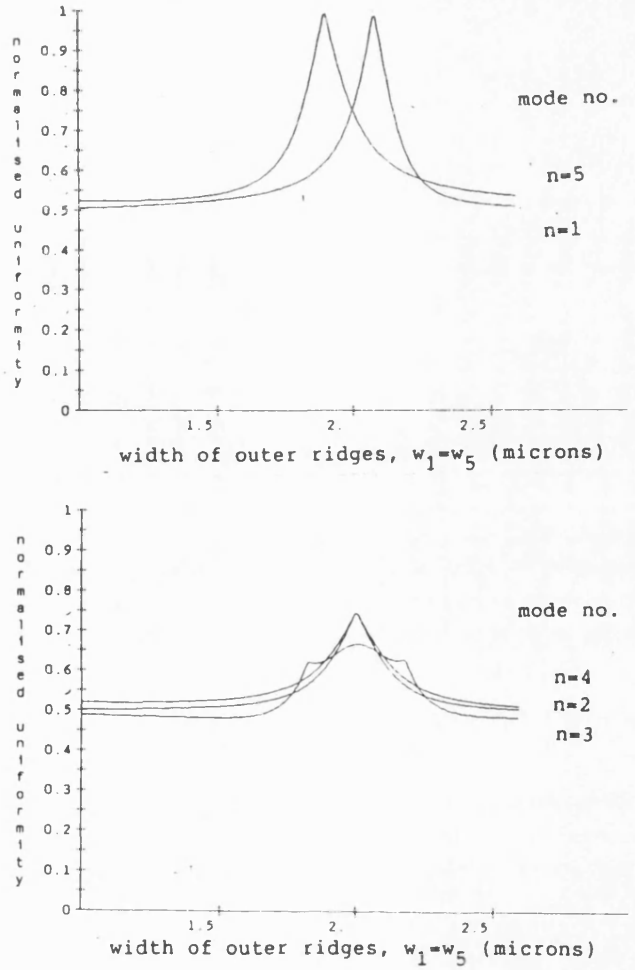

Figure 4.3.3.1(a) Variation of the uniformity, η, of the supermodes in a 5-element, non-uniform array in which the outer RWG widths, w_1=w_5, are changed. (w_2=w_3=w_4=2μm, s=2μm, $\Delta\varepsilon$=0.144)

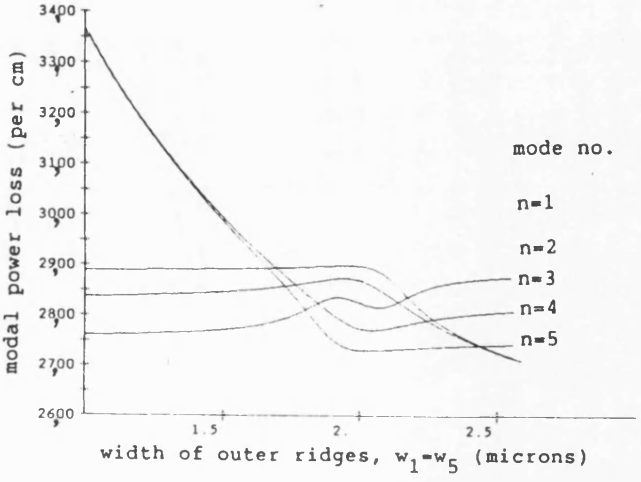

Figure 4.3.3.1(b) Variation of the mode loss of the supermodes in a 5-element, non-uniform array in which the outer RWG widths, w_1=w_5, are changed. (w_2=w_3=w_4=2μm, s=2μm, $\Delta\varepsilon$=0.144)

the modal loss of the fundamental mode when the array is designed to support this uniform distribution is still greater than the loss of the other higher order modes - this results in higher order mode operation. Thus, it is seen that the solution is not as suitable as appears at first. If, instead of strengthening the guiding mechanism at the edges of the guide, the guide strength at the centre of the array is changed, the results shown in figure 4.3.3.2 are obtained. The fundamental and higher order modes have uniformity maxima at about 1.8μm and 2.2μm but, yet again the higher order modes have lower values of modal loss. For the purpose of completeness, the uniformity and modal loss are plotted in figure 4.3.3.3 as functions of the separations, s_1 and s_4. This array design produces a reasonably uniform light distribution but, also, preferentially supports the higher order modes.

4.4 Tailoring the Gain in a Waveguide Array.

Apart from changing the simple physical dimensions of the array, another form of introducing mode control is by altering the contact stripe currents whereby the lateral gain profile is tailored to enhance the desired mode. This section presents a simplified approach to this design method. The introduction of gain is accounted for by altering the values of the material loss constants for the ridge and channel regions - i.e. the complex dielectric constant. The nett modal loss is then calculated as normal (via the matrix eigenvalue equation).

Table 4.4.1 shows values of modal gain in a uniform 5-element array with and without a tailored gain profile. It is seen that, even though the

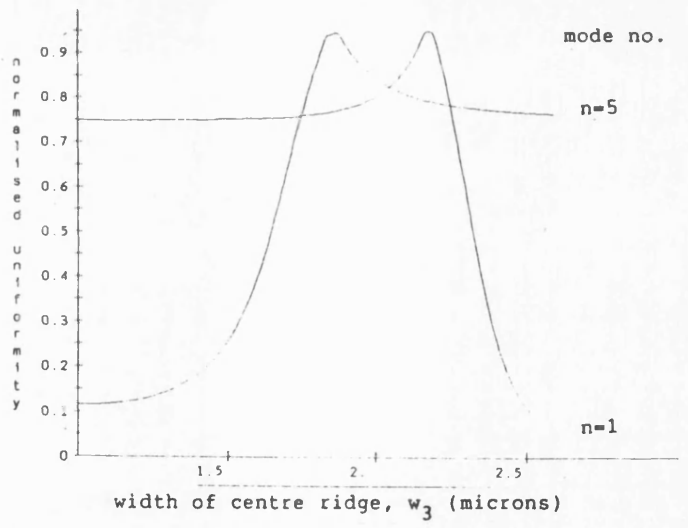

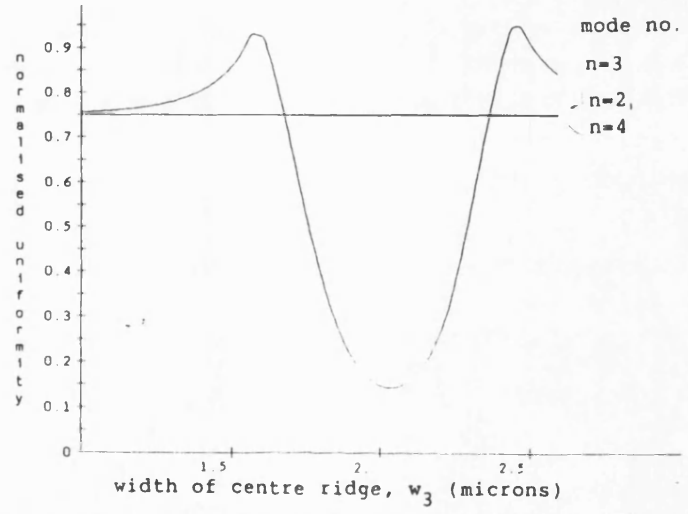

Figure 4.3.3.2(a) Variation of the uniformity, η, of the supermodes in a 5-element, non-uniform array in which the center RWG width, w_3, is changed. ($w_1=w_2=w_4=w_5=2\mu m$, $s=2\mu m$, $\Delta\varepsilon=0.144$)

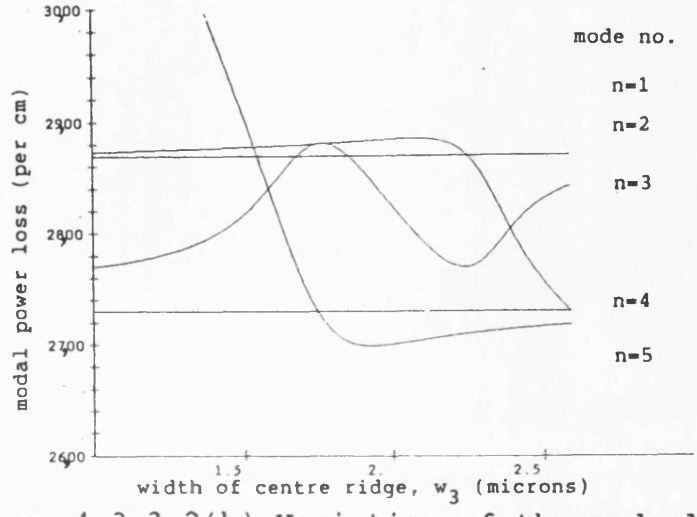

Figure 4.3.3.2(b) Variation of the mode loss of the supermodes in a 5-element, non-uniform array in which the center RWG width, w_3, is changed. ($w_1=w_2=w_4=w_5=2\mu m$, $s=2\mu m$, $\Delta\varepsilon=0.144$)

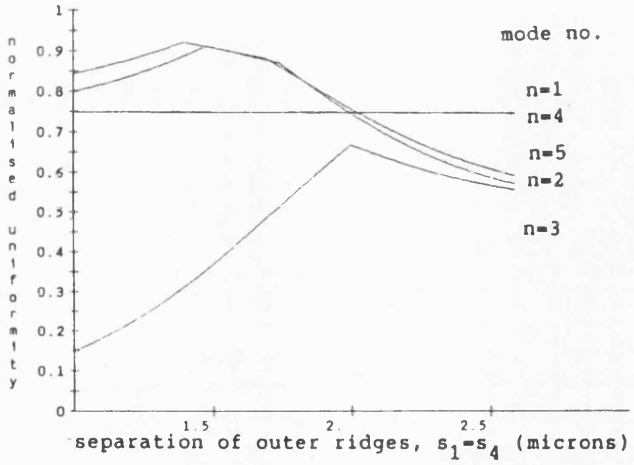

Figure 4.3.3.3(a) Variation of the uniformity, η, of the supermodes in a 5-element, non-uniform array in which the separation of the outer RWG's, $s_1=s_4$, is changed. ($w_1=w_2=w_3=w_4=w_5=2\mu m$, $s_2=s_3=2\mu m$, $\Delta\varepsilon=0.144$)

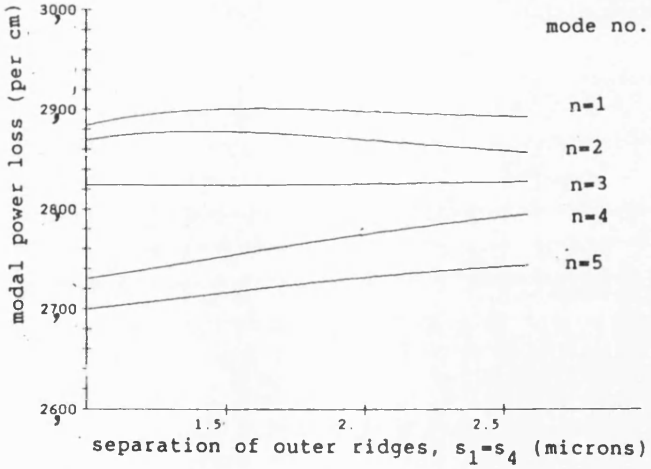

Figure 4.3.3.3(b) Variation of the mode loss of the supermodes in a 5-element, non-uniform array in which the separation of the outer RWG's, $s_1=s_4$, is changed. ($w_1=w_2=w_3=w_4=w_5=2\mu m$, $s_2=s_3=2\mu m$, $\Delta\varepsilon=0.144$)

TABLE 4.4.1
TAILORING THE GAIN IN A UNIFORM ARRAY

NETT GAIN BENEATH RIDGE (per cm)					MODAL GAINS (per cm)				
R1	R2	R3	R4	R5	G1	G2	G3	G4	G5
-25	-25	-25	-25	-25	-28	-27.8	-27.4	-27.1	-26.7
15	25	35	25	15	13.62	9.06	11.52	11.91	19.29
35	25	15	25	35	10.49	17.08	17.65	20.72	16.26
35	15	35	15	35	12.01	12.67	22.93	16.73	17.83

TABLE 4.4.2
TAILORING THE GAIN IN A HIGH UNIFORMITY INTENSITY ARRAY

NETT GAIN BENEATH RIDGE (per cm)					MODAL GAINS (per cm)				
R1	R2	R3	R4	R5	G1	G2	G3	G4	G5
-25	-25	-25	-25	-25	-27.9	-27.6	-27.3	-27.1	-26.8
15	25	35	25	15	10.8	7.87	13.82	13.73	20.44
35	25	15	25	35	13.81	19.8	16.54	18.86	14.91

modal gain can be changed by adjusting the lateral gain profile via controlling the current injection, the higher order modes remain the least lossy. Table 4.4.2 shows the mode discrimination obtained in the uniform intensity array of Buus as the lateral gain profile is changed. Without considering the complications that a non-uniform, lateral gain profile causes on the real guiding mechanism, it is seen that the fundamental mode still has a higher value of modal loss than other modes.

4.5 Conclusions

Supermodes of uniform and non-uniform structures have been predicted. Similarity between the supermode envelope and the individual waveguide modes exist for uniform arrays. Non-uniform arrays are shown to be capable of supporting highly uniform intensity distributions. However, in all cases, the fundamental supermode appears to have the highest loss associated with it, thus inhibiting it from lasing in preference to other modes.

CHAPTER 5

ALTERNATIVE LASER ARRAY DESIGNS - THE ANGLED FACET LASER ARRAY AND LASER ARRAY WITH MODE FILTER.

5.1 Introduction.

Chapter 4 has shown the limitations of the uniform and non-uniform laser arrays. The problems of achieving stable, fundamental mode operation with the power emitted in a single, narrow, far-field lobe are appreciable. One method proposed to solve the problem of highest order mode propagation is to introduce phase-changes beneath the guides. The highest order mode then undergoes a 180^{o} phase-shift beneath alternate stripes which converts it into an equivalent of the fundamental mode. Various methods of achieving this have been investigated [ref 40, 68]. One of these is the angled-facet laser where either the stripes are etched at an angle to the cleaved facets or the facet is etched at an incline to the crystal planes. The effect of this is that each stripe has a slightly different optical path length such that the additional path caused by the inclined facet introduces an extra phase-change in the mode supported by that stripe.

Section 5.2 looks at the derivation of the round-trip conditions for the angled-facet laser array using a matrix method developed by Chen and Wang [20]. The method involves breaking down the array into three distinct regions - the uniform length of the laser (not including the angled-facets) and the angled regions at each facet. One simplification introduced into this analysis is to model the angled-facet as a set of discrete steps. A matrix-formulation for the threshold condition is then

derived which yields values for the complex modal propagation constants and, hence, the modal gains and emitted wavelengths. However, a different form for the modal gain is used in this thesis which ultimately leads to a simple eigenvalue equation.

Section 5.3 looks at the analytic solutions to the matrix threshold equation for two simple cases. The first is the basic laser structure where the facets are perpendicular to the axis of the laser. The second has one facet perpendicular and the other one angled to the axis of the laser such that a 180° phase-shift is induced in the modes supported by alternate stripes. These examples provide a guide to the two extremes of the performance of the array. It will be seen that the second case yields a set of degenerate modes which all lase at the same wavelength and have the same modal gain.

Section 5.4 looks at the general performance of the angled-facet laser. It is shown that the threshold equation can be simplified such that the two angled-facets can be replaced in the model by one effective facet reflectivity with the other one assumed perpendicular. The values of injected gain and emitted wavelength are computed for various angles on the facets.

The simple angled facet laser array may be considered as a structure in which supermode selection may be aided by suitable design of a phase-correction mechanism. A second method of selecting supermodes is presented in section 5.5 where an integral filter is included in the array design. This takes the form of a broad area ridge connected to the end of an evanescently-coupled array. The structure will be referred to as a Laser Array with Mode Filter. The monolithic structure acts as a linear array with an in-line mode filter - the broad area ridge acts as a discriminator between various array and broad area modes. The wave overlap between

the supermodes and broad area modes is calculated for a simple structure. It will be shown that the discrimination between various supermode threshold conditions can be improved enhancing the stability of these modes. However, the application of the technique has its limitations - notably the dimension of the broad area region must be minimised to prevent filamentary oscillation leading to the collapse of the mode-selection mechanism. Various array designs are investigated.

Lastly, section 5.6 draws together the main conclusions of the chapter.

5.2 Angled-Facet Laser Arrays and The Threshold Condition.

Consider the laser array shown in fig. 5.2.1. The cavity is broken down into three regions - numbered I, II and III. In region II, the array is assumed to be phase-locked and the eigenvalues/eigenvectors given by [ref. 20]:

$$\sigma^k = \beta_0 + 2\varkappa\cos(k\pi/[N+1]) \qquad j=1,2,...N \qquad .....(5.2.1)$$

$$E_j^k = \sqrt{2/(N+1)}\,.\sin(jk\pi/[N+1]) \qquad j=1,2...,N,\ k=1,2,...N \qquad .....(5.2.2)$$

β_o = free-space propagation constant

$\varkappa$ = coupling constant

and β_0, $\varkappa$ are real.

The number of the guide is denoted by j and the order of the supermode by k.

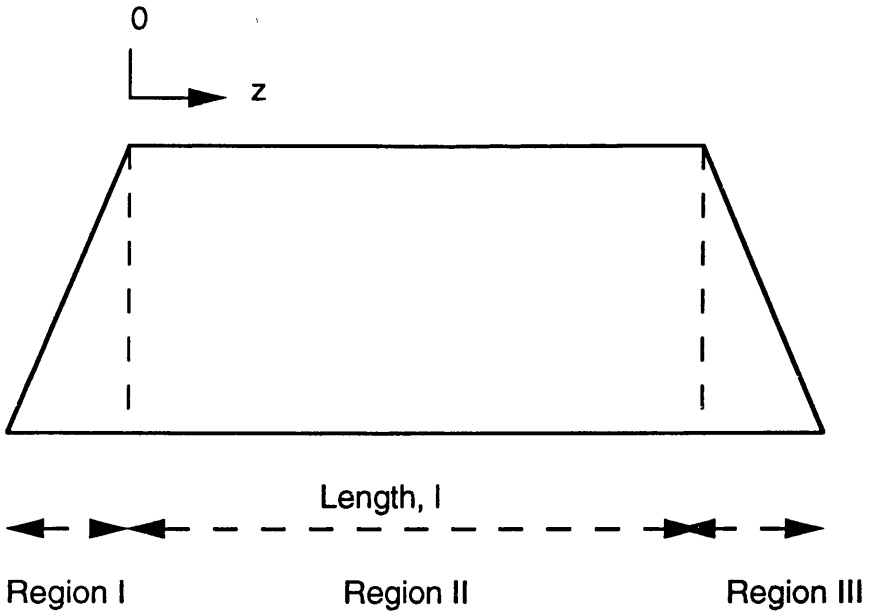

a) Angled Facet Laser Array

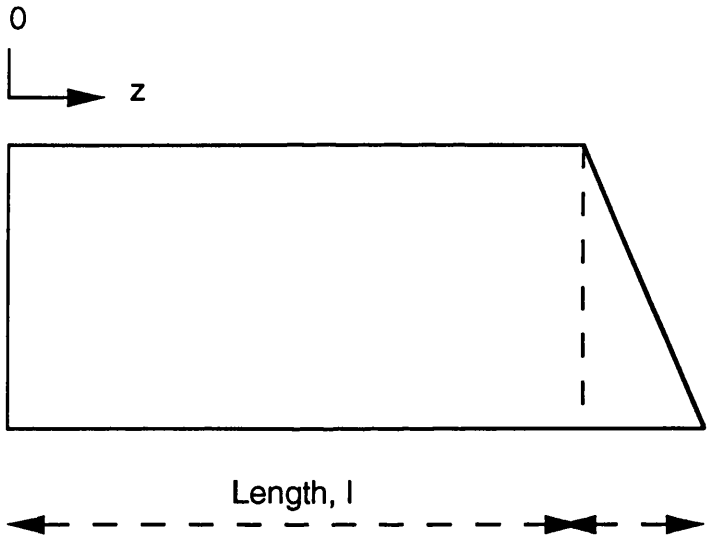

b) Angled Facet Laser Array - Simplified Model

Figure 5.2.1 Schematic Diagram of the Angled Facet Laser Array

The three regions of the laser are modelled according to the modes supported by its guides - the angled-facet regions are assumed to support locally the fundamental TE mode with propagation constant β_0 whilst the bulk of the laser, region II, supports the supermodes.

The effect of the angled-facets is that the supermodes of region II undergo a partial phase change defined by the extra optical path in each guide caused by the angle of the facets. The result of this is that the supermodes couple to one another and the array will contain a weighted distribution of supermodes. Denote a_k as the weighting coefficient for supermode k. Thus, at any point in region II, the field present will be $\mathbf{a}$, a column vector with elements a_k.

When the modes enter region III, the guides are modelled as a set of independent, uncoupled stripes supporting a mode with propagation constant β_0. If the amplitudes of the fields in each stripe are the elements of the column vector $\mathbf{b}$, then:

$$\mathbf{b} = \mathbf{T}\,\mathbf{a}$$

where the elements $T_{j,k}$ of matrix $\mathbf{T}$ are the amplitudes (eigenvectors) in stripe j for supermode k (E_j^k from above). The alternative process of finding the vector $\mathbf{a}$ from the field $\mathbf{b}$ is to multiply both sides of the above equation by the inverse of $\mathbf{T}$. However, it can be shown that $\mathbf{T}^{-1} = \mathbf{T}$.

$$\mathbf{a} = \mathbf{T}\,\mathbf{b}$$

The threshold equation is now derived for an N-stripe array with two angled facets.

At point z=0 (fig. 5.2.1a), the supermode distribution can be represented by the column matrix $\mathbf{a}$. This field propagates towards region III. Each supermode, has a characteristic, complex propagation constant β_k such that:

$$\hat{\beta}_k = \sigma^k - i g_k \qquad \text{.....(5.2.3)}$$

(g_k is the mode field gain of supermode k - σ^k, g_k are real).

At point z=L, the total field is $\mathbf{P}\,\mathbf{a}$ where $\mathbf{P}$ is a diagonal matrix with leading diagonal elements $\exp(i\hat{\beta}_k L)$ and all other elements are zero.

At this z=L, the supermodes are converted to the uncoupled mode representation to model the propagation of the stripe-modes through region III. The uncoupled field at point z=L is $\mathbf{T}\,\mathbf{P}\,\mathbf{a}$. This propagates through region III. If $\mathbf{M}_1$ represents propagation across this region to the facet then the field at the facet is $\mathbf{M}_1\,\mathbf{T}\,\mathbf{P}\,\mathbf{a}$ where $\mathbf{M}_1$ is a diagonal matrix with leading diagonal elements $\exp(i\beta_0 l_j)$ - l_j is the length of stripe j in region III. (l_j is dependent on the angle of the facet, ϑ_{III} as will be shown later). All other elements are zero.

The facet is assumed to take a step form to simplify the analysis. The reflection of the field at the facet is then given by the value of field reflectivity, r, for normal incidence. On returning to point z=L, the uncoupled field is given by: $r^2\,\mathbf{M}_1\,\mathbf{T}\,\mathbf{P}\,\mathbf{a}$.

The field is now converted to coupled-mode form by multiplying by the inverse of $\mathbf{T}$.

The effects of propagation of the fields back along the cavity and through region I, returning to the starting point yields the following threshold equation:

$$r^2 T^{-1} M_2^2 T \; P \; T^{-1} M_1^2 T \; P \; a = a \qquad \text{.....(5.2.4)}$$

where the original field has been reconstructed after one round-trip.

Consider now the value of the complex propagation constant, $\hat{\beta}_k$, given by equation (5.2.3). The two components of this are the real propagation constant, σ^k, and a gain term, g_k. This latter term does not include the effects due to end-losses - it is the effective material gain minus the losses associated with both the material (bulk losses e.g. absorption) and the ridge structure (e.g. scattering).The dependence of σ^k on β_0 is given in (5.2.1). The value of the gain term may be expressed in the following way :

$$g_k = g_0 - loss_k/2 \qquad \text{.....(5.2.5a)}$$

$$loss_k = \left\{ \Gamma_{str}^k \alpha_1 + (1-\Gamma_{str}^k).\alpha_2 \right\} \qquad \text{.....(5.2.5b)}$$

Γ_{str}^k is the relative amount of field confined to the stripe regions for supermode k (see section 2.4).

α_1 and α_2 are the optical (power) loss factors for the stripe and inter-stripe regions respectively and the factor 2 accounts for the conversion from power to field gain,

g_0 is an effective gain term representing the nett gain necessary beneath each channel to achieve the threshold condition.

Note that this form for the gain is different to that proposed in (20) where the gain experienced by the supermodes is assumed to be linearly dependent on the mode number k ($g_k \propto g_0.k$). However, this is corrected for above by accounting for the actual supermode losses in the bracketed term of (5.2.5b).

Since the values of α_1, α_2, $\varkappa$, N and Γ_{str} are known, the only unknown variables are g_0 and β_0 . The latter parameter is present in both the **M** and **P** matrices.

To solve the equation as it stands is, numerically, complicated. The unknown values include modal gains, propagtion constants and phase-changes. To eliminate the dependence of the phase-changes on the value of the propagation constants, the phase changes are specified beforehand and the actual facet angle required to produce these phase delays may be calculated last according to the matrix eigenvalue solutions. Hence, when evaluating the equation for an angled facet array, the matrices **M** assume a leading diagonal with terms exp(i[jϑ]), j is the stripe-number - where the effect of the angled-facet is introduced into the equations through the phase change jϑ. This is incorporated easily into the model since the phase-delay between each stripe can be directly specified as an input parameter. Thus, if the facet is made such that each stripe was assumed to be $\pi/2$ rads out of phase with its neighbour, then $\vartheta=\pi/2$ etc. Using this form for the phase delay allows the matrix equation to be solved easily since the terms invoving $\beta_0 l$ in the matrices **M** can be

replaced by the phase terms $j\vartheta$. Hence, β_0 will be present in the matrix P only. Once a set of solutions are obtained, the corresponding angle on the facet can be derived.

Using the above simplifications, the value $\exp(i[\beta'_0 - ig_0]2L)$ can be isolated from the threshold condition which gives an eigenvalue equation of the form:

$$\gamma T^{-1} M_1^2 T \; P' \; T^{-1} M_2^2 T \; P' \; a = a \qquad \text{.....(5.2.8)}$$

where P' is the modified form of P and contains a leading diagonal with elements $\exp(i[2x\cos\{k\pi/11\} - i\{loss_k\})$ and $\gamma = r^2.\exp(i[\beta_0 - ig_0]2L)$.

This gives a standard eigenvalue equation of the form:

$$(A - \frac{1}{\gamma} I)\, a = 0 \qquad \text{.....(5.2.9)}$$

where A is the product of the matrix terms in (5.2.8) and I is the unit matrix of order NxN.

5.3 Solutions of the Eigenvalue Equation for Two Special Cases.

Two design cases are now presented to investigate the behaviour of the array model in the extreme case of normal facets and then a 180° induced phase change to the propagating modes.

5.3.1 Both Facets Perpendicular.

The first case to be considered is when both facets are perpendicular to the plane of the active later. This is the most commonly encountered form for a semiconductor laser etalon.

Using equation (5.2.4) for the case where ϑ=0rads. then the threshold equation yields 10 solutions for the threshold condition given by:

$$r^2 P^2 a = a. \quad \text{.....(5.3.1.1)}$$

Each value of gain, g_0, is given by:

$$g_0 = \frac{1}{L}\ln\frac{1}{r} + \Gamma^k_{str}\alpha_1 + (1-\Gamma^k_{str}).\alpha_2 \quad \text{.....(5.3.1.2)}$$

k=1 to 10

and each value of β_0 yields solutions of:

$\sigma^k L = q\pi$ where q is an integer .....(5.3.1.3)

and σ^k is given by equation (5.2.1)

The result demonstrates that in the simple case of normal facets, the equations reduce to the mode threshold conditions.

5.3.2 One Facet Perpendicular, the Other Angled to Induce π Phase-Shift.

The purpose of this design is to introduce a π phase-shift on alternate stripes. Intuitively, this should convert the highest order, anti-phase mode into an equivalent, in-phase lowest order mode. One might suspect that this would result in an emitted field of the fundamental mode type (i.e. a 0^o phase-shifted mode).

The starting point is equation (5.2.6). The angle on facet 1 is 0^0 and so M_1^2 is equivalent to a unit matrix. The eigenvalue equation can be simplified to:

$$\gamma\, P'\, T\, M_2\, T\, P'\, a = a \qquad \text{.....(5.3.2.1)}$$

M_2^2 may be represented by a diagonal matrix with the leading diagonal given by $(-1)^j$, due to the π phase-shift on alternative stripes and all other elements being zero. The effect of the matrix multiplication $T^{-1} M_2^2 T$ is shown in Appendix 1 of this chapter.

The eigenvalue equation may now be written as:

$$\gamma \begin{vmatrix} 0 & 0 & 0 & 0 & 0 & 0 & 0 & 0 & 0 & e_1 \\ 0 & 0 & 0 & 0 & 0 & 0 & 0 & 0 & e_2 & 0 \\ 0 & 0 & 0 & 0 & 0 & 0 & 0 & e_3 & 0 & 0 \\ 0 & 0 & 0 & 0 & 0 & 0 & e_4 & 0 & 0 & 0 \\ 0 & 0 & 0 & 0 & 0 & e_5 & 0 & 0 & 0 & 0 \\ 0 & 0 & 0 & 0 & e_6 & 0 & 0 & 0 & 0 & 0 \\ 0 & 0 & 0 & e_7 & 0 & 0 & 0 & 0 & 0 & 0 \\ 0 & 0 & e_8 & 0 & 0 & 0 & 0 & 0 & 0 & 0 \\ 0 & e_9 & 0 & 0 & 0 & 0 & 0 & 0 & 0 & 0 \\ e_{10} & 0 & 0 & 0 & 0 & 0 & 0 & 0 & 0 & 0 \end{vmatrix} \quad a = a$$

where $e_j = r \exp(i[2x\cos\{j\pi/11\} - i \cdot loss_j])$

The solution of the above equation requires that the determinant of $\gamma D - I = 0$ where D is the expanded matrix above and I is the unit matrix. Hence, solutions are obtained when :

$$\text{DET}\begin{vmatrix} -1 & 0 & 0 & 0 & 0 & 0 & 0 & 0 & 0 & \gamma e_1 \\ 0 & -1 & 0 & 0 & 0 & 0 & 0 & 0 & \gamma e_2 & 0 \\ 0 & 0 & -1 & 0 & 0 & 0 & 0 & \gamma e_3 & 0 & 0 \\ 0 & 0 & 0 & -1 & 0 & 0 & \gamma e_4 & 0 & 0 & 0 \\ 0 & 0 & 0 & 0 & -1 & \gamma e_5 & 0 & 0 & 0 & 0 \\ 0 & 0 & 0 & 0 & \gamma e_6 & -1 & 0 & 0 & 0 & 0 \\ 0 & 0 & 0 & \gamma e_7 & 0 & 0 & -1 & 0 & 0 & 0 \\ 0 & 0 & \gamma e_8 & 0 & 0 & 0 & 0 & -1 & 0 & 0 \\ 0 & \gamma e_9 & 0 & 0 & 0 & 0 & 0 & 0 & -1 & 0 \\ \gamma e_{10} & 0 & 0 & 0 & 0 & 0 & 0 & 0 & 0 & -1 \end{vmatrix} = 0$$

which gives a multiple root at one value of g_0 and λ_0. Hence all the modes are degenerate with the same wavelength and the same threshold gain.

5.4 Varying the Phase Between Adjacent Emitters.

Figure 5.4.1 shows the modal gains and lasing wavelengths as the relative phase between adjacent emitters is increased linearly from 0° to 180° (π radians) induced phase-change. It is seen that, as expected, the supermodes are discrete at 0° induced phase-change, whilst at 180° induced phase-change the modes are degenerate (as predicted in section 5.3). Note how the supermodes converge smoothly on the degenerate state with the highest order mode requiring the lowest threshold gain. The relative amplitudes (the eigenvectors of the eigenvalue equation) of each supermode are shown in Table 5.4.1 for various relative phase-changes. The weightings are dominated by the real component in the complex values. However, it is not obvious that all the modes would actually be present

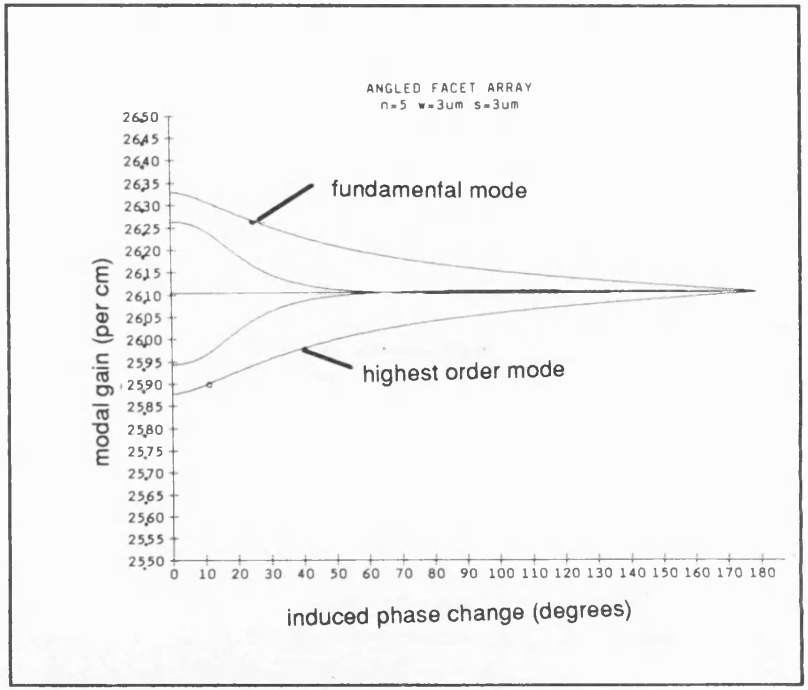

Figure 5.4.1 Variation of the Modal Loss of the Eigenvectors of a 5 Element Array (3um ridges separated by 3um) as a Function of Induced Phase-Change at the Angled Facet

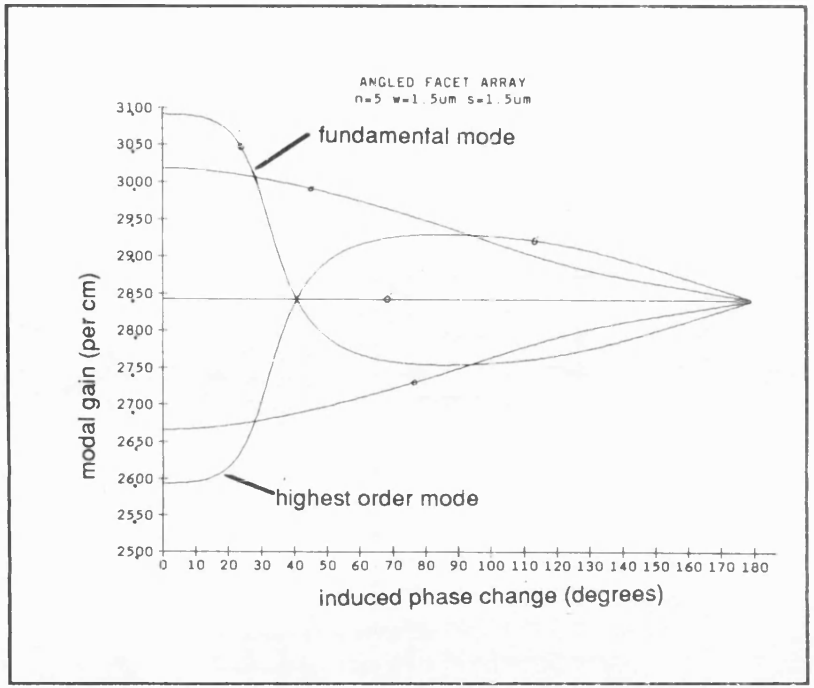

Figure 5.4.2 Variation of the Modal Loss of the Eigenvectors of a 5 Element Array (1.5um ridges separated by 1.5um) as a Function of Induced Phase-Change at the Angled Facet

TABLE 5.4.1
SUPERMODE WEIGHTING COEFFICIENTS FOR THE LOWEST LOSS MODE COMBINATION OF AN ANGLED FACET ARRAY AS A FUNCTION OF INDUCED PHASE-CHANGE

SUPERMODE WEIGHTING FACTORS	PHASE-CHANGE 0 deg.s LOWEST LOSS 26.82 cm	PHASE-CHANGE 45 deg.s LOWEST LOSS 26.99 cm	PHASE-CHANGE 90 deg.s LOWEST LOSS 27.00 cm
1	0+i0	0.1+i0.01	0.11+i0.01
2	0+i0	0.2+i0.01	0.22+i0.01
3	0+i0	0.36+i0.01	0.31+i0.01
4	0+i0	0.29+i0.01	0.38+i0.01
5	0+i0	0.41+i0.01	0.42+i0.01
6	0+i0	0.43+i0	0.43+i0
7	0+i0	0.41-i0.01	0.40-i0.01
8	0+i0	0.36-i0.01	0.34-i0.01
9	0+i0	0.26-i0.01	0.24-i0.01
10	1+i0	0.14-i0.01	0.13-i0.01

since no account of the active nature of the array has been taken.

As the strength of coupling increases and the separation of mode gains increases, a more subtle variation between the supermode effective threshold gains is observed as the angle of the facet is varied. Figure 5.4.2 shows a number of crossover points between various modes for a 5 element array. However, it is not entirely unexpected since there is a phase relationship between the eigenvectors of all supermodes. For example, if one considers the fundamental and first-order mode, as the phase-delay induced by the angled facet increases, there comes a point when the eigenvector components beneath stripes 2, 3, 4 and 5 are dramatically reduced or inverted. If the relative phase between adjacent emitters was approximately 30^{o}, stripe 1 remains unaffected (as it is the reference point), stripe 2 is phase shifted by 30^{o} ($\cos(30^{o})=0.87$), stripe 3 by 60^{o} ($\cos(60^{o})=0.5$) and stripe 4 by 90^{o}. Stripe 5 is then "partially" inverted - phase-shifted by 120^{o}. It is at this point that the first order mode eigenvector mode distribution is always positive and the fundamental mode has a negative component. In effect, the two modes reverse their order, thus explaining the crossover points of the modes. A similar relationship exists between the other supermodes.

5.5 Laser Array with Mode Filter.

The usefulness of the above array is limited since the zero-order mode is not preferentially excited and the practicalities of controlling the angle of the stripes relative to the facet (in order to control the phase between adjacent emitters) are questionable. Hence, an

alternative array design is proposed in which an evanescently-coupled array is "attached" to a broad area structure. The latter will support many modes depending upon its guide strength. The action of the broad area structure is then to select supermodes by the action of coupling between the broad area modes and the supermodes.

A diagram of the structure is given in Figure 5.5.1. The number of evanescently-coupled elements can be adjusted to suit the total width of the broad area guide, W. By adjusting the widths of the coupled guides, their spacing and their numbers, mode selection may be affected.

Consider the eigenvectors of the array structure, denoted E_j^k. Denote the modes of the broad area guide, Ψ_l. The coupling of the two wave functions may be written as:

$$\kappa_{lk} = \frac{\left| \int E_j^k \Psi_l \, dr \right|^2}{\left| \int E_j^k dr \right|^2 \left| \int \Psi_l \, dr \right|^2}$$

where r is the position vector of a point. By substituting for l=1 to n (the number of elements) and remembering that both guides are the same in the vertical plane, the above equation may be expressed as:

$$\kappa_{lk} = \sum_{j=1}^{j=n} \frac{\left| \int E_j^k \Psi_l \, dx \right|^2}{\left| \int E_j^k dx \right|^2 \left| \int \Psi_l \, dx \right|^2} \qquad \text{.....(5.5.1)}$$

Plots of the coupling coefficient for various array designs are shown in figure 5.5.2. Note that the coupling coefficient is dependent on the shape of the laser array - the ridge widths and separations, as these affect the

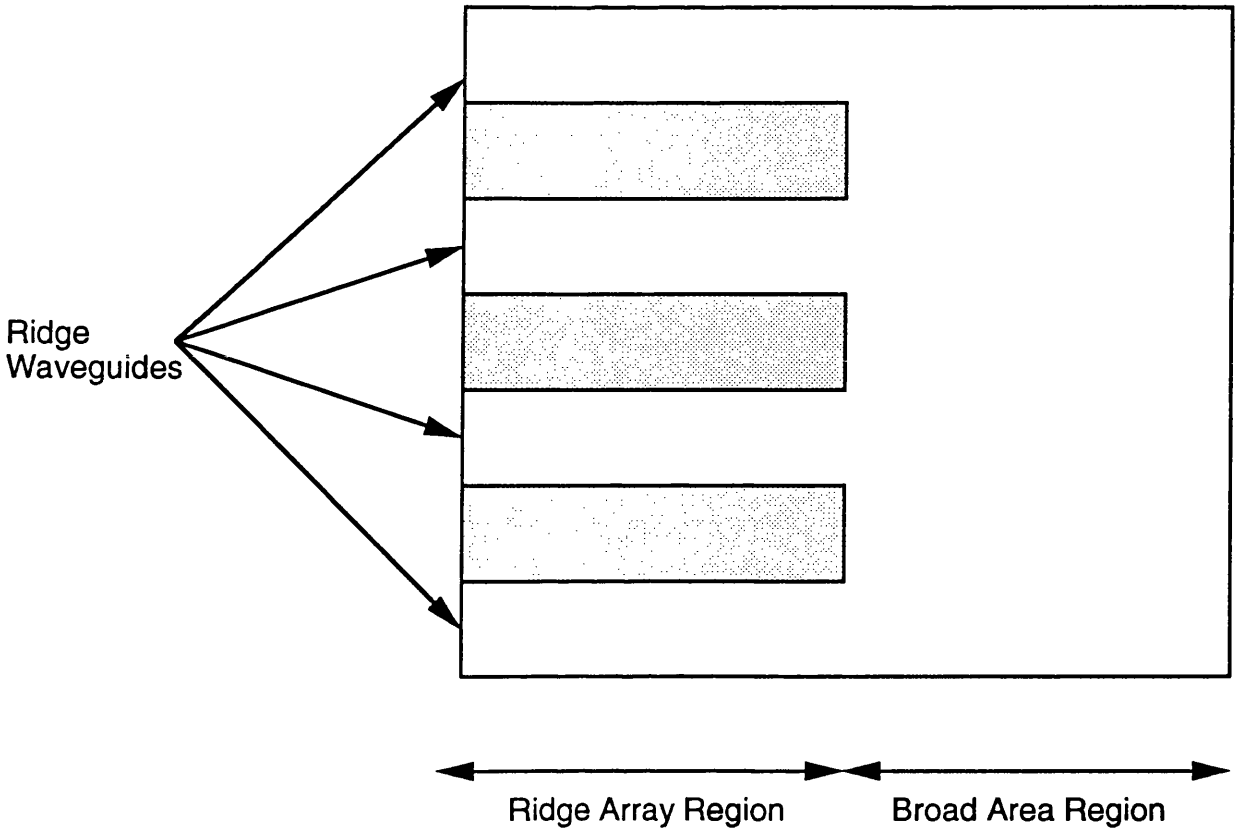

Figure 5.5.1 Laser Array With Mode Filter - Broad Area Mode Filter Attached to Multi-Element Ridge Array

Figure 5.5.2a COUPLING COEFFICIENTS OF 3 ELEMENT ARRAY
(3x1.5um RIDGES SEPARATED BY 3.75um)
TO 12um BROAD AREA STRUCTURE

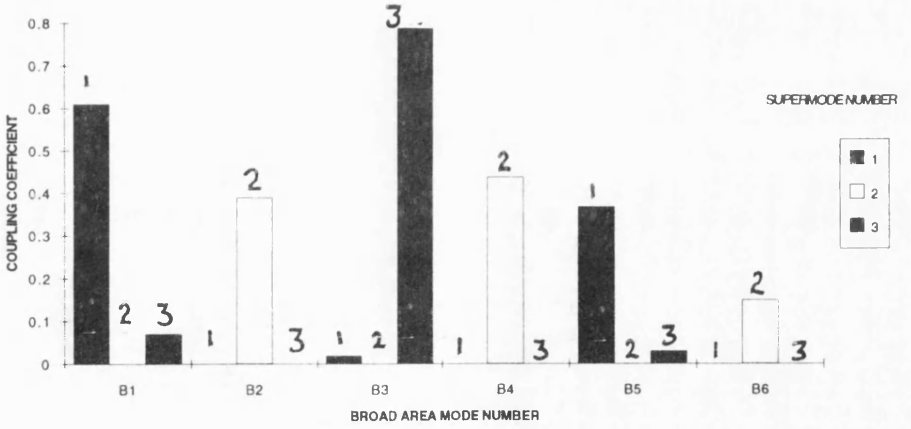

Figure 5.5.2b Variation of the Coupling Coefficients of a 3 Element Array (w1=w3=1.5um; s1=s2=(9-w2)/2 with the Centre Ridge Width, w2, Varied from 1.5um to 3.1um

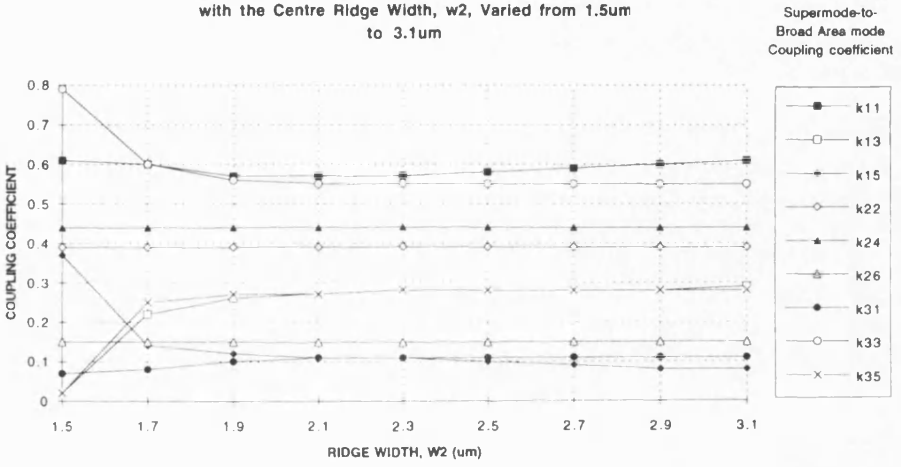

Figure 5.5.2c Variation of the Coupling Coefficients of a 3 Element Array (w2=1.5um; w1=w3; s1=s2=(10.5-(w1+w3))/2)) with the Outer Ridge Widths, w1=w3, Varied from 1.5um to 3.1um

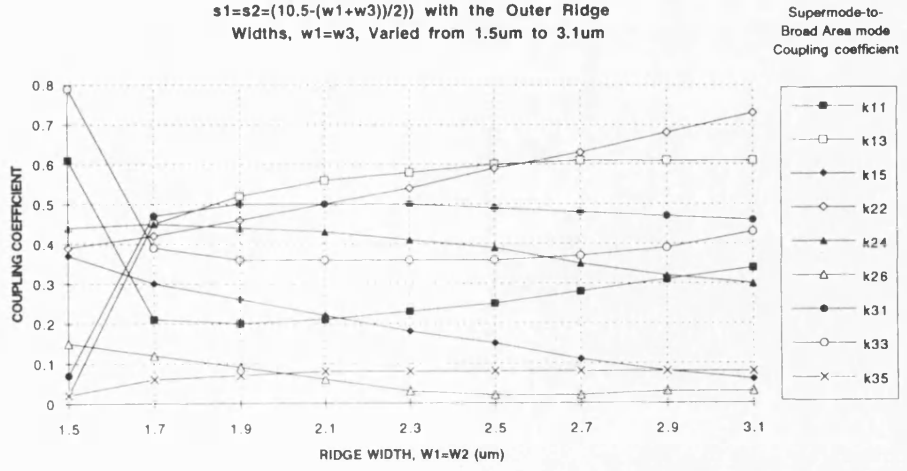

shape of the supermode and, hence, directly influence the coupling coefficient. It is especially interesting to note that for the symmetric laser array (all guides of equal widths), the highest order mode is coupled most strongly to one of the broad arera modes; however, in all cases except the symmetric case, there are at least two mode combinations with similar coupling values. The selection of the propagating mode will then be decided by the overlap of the mode pairs with the gain profile.

5.5.1 The Threshold Condition for the LAMF Structure.

The round-trip condition for the LAMF structure may be derived in a similar manner to that for the angled-facet laser array. By starting at point z=0 with a supermode weighting function, $\hat{a}$ and multiplying by the propagation and coupling matrices to obtain the round-trip journey, the threshold may be found by solving:

$$P_1 K_1 P_2 R_1 P_2 K_2 P_1 R_1 \hat{a} = \hat{a} \qquad \text{.....5.5.2}$$

where P_1 is the power gain (per cm) through region 1,

P_2 is the power gain (per cm) through region 2,

K_1 is the coupling of supermodes into slab modes,

K_2 is the coupling of slab modes into supermodes,

R_1 is the power reflection coefficient of facet 1

and R_2 is the power reflection coefficient of facet 2.

Now R_1 and R_2 have the same value, R, and P_2 is assumed to be be

independently controlled via a separate contact to induce whatever gain is required.

In order to prevent filamentary oscillation, it is necessary to keep the width of the broad area to a minimum. Since the same epitaxial (transverse) structure is continuous throughout the monolithic device and the same etch-depths are assumed for both the ridge and broad-area regions, the lateral effective index step is the same for the two different regions. Assuming a broad area width of 12μm and three identical ridges of 1.5μm in the structure separated by 3.75μm, the modal gains are given (Table 5.5.1.1) with the broad area region pumped to transparency. The mode with the lowest threshold gain is found to be the fundamental order supermode and the second order (n=3) broad area mode with a required threshold gain of 16.84cm^{-1} (not including end-losses).

Further examples of this laser design are given in figures 5.5.1.1 and 5.5.1.2. for a two element and three element array atttached to a 9μm broad area laser.. For these structures, the difference between the mode sets is not so clear as the coupling of the supermodes and broad area is not so discriminating.

5.6 Conclusions

Two models of laser arrays have been presented which are based upon phase-locked laser arrays with an extra mode filter. In the first case, the mode filter was a phase adjuster in the form of an angled facet. The concept of the design was to take a uniform laser array and convert the

TABLE 5.5.1.1
THRESHOLD MODAL GAINS FOR A 12um BROAD AREA STRUCTURE COUPLED TO A 3 RIDGE ARRAY (3x1.5um RIDGES, SEPARATED BY 3.75um)

SUPERMODE NUMBER	BROAD AREA MODE NUMBER 1	2	3	4	5	6
	MODAL GAINS (per cm)					
1	45.42	HIGH	16.84	HIGH	62.70	HIGH
2	HIGH	60.30	HIGH	56.33	HIGH	91.28
3	117.40	HIGH	36.69	HIGH	151.00	HIGH

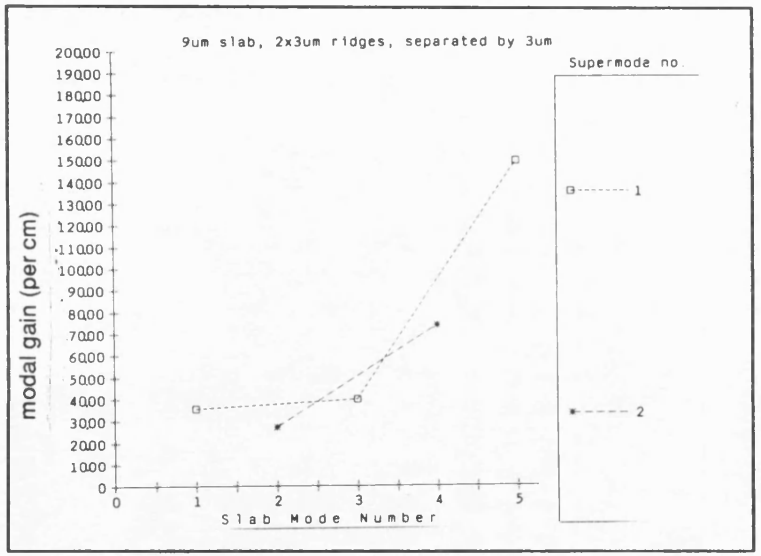

Figure 5.5.1.1Modal Gain of a 2-Element Array Coupled to a 9um Broad Area Structure

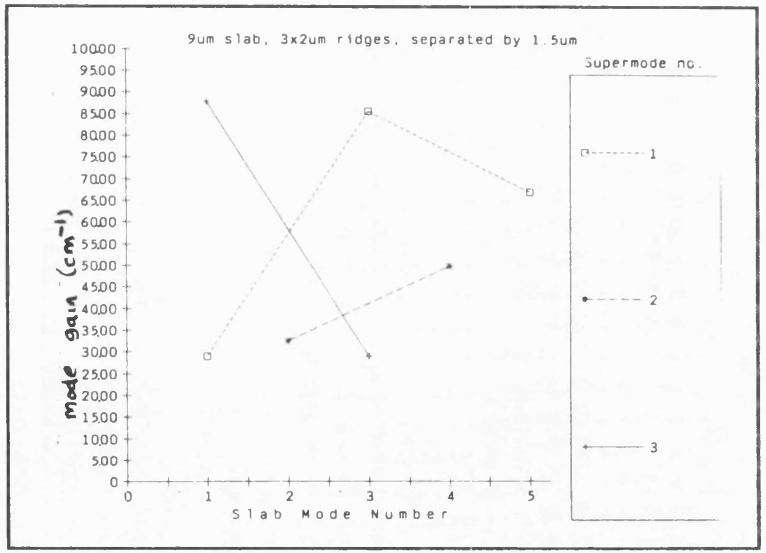

Figure 5.5.1.2 Modal Gain of a 3-Element Array Coupled to a 9um Broad Area Structure

highest order mode (which has the lowest threshold gain) into the zero-order mode by transforming its phase by 180°. However, it was found that the laser becomes degenerate when a 180° phase-change is induced at the laser facets.

The second model derived, was based upon the use of an in-line mode filter; this takes the form of a broad area guide on the end of the phase-locked array. By coupling from the array into the broad area structure, and back again, modes can be strengthened or discriminated against. However, in order to do this it is necessary to exercise care when selecting the width of the broad area structure as this section can break down into non-coherent filaments. The model predicts that the zero order mode might be stable if the array parameters are chosen carefully. However, small perturbations in the array can result in competing pairs of modes being generated as the discrimination between them becomes small.

APPENDIX 1.

Simplification of the Matrix Threshold Condition for an Array Where One Facet Induces a Π Phase-Shift on Alternate Stripes.

The matrix threshold condition is given by:

$$\gamma T^{-1} M_1^2 T \; P' \; T^{-1} M_2^2 T \; P' \; a = a \qquad \text{.....(7.8)}$$

where γ is the eigenvalue to be found.

Since one facet is perpendicular, say facet 1, then M_1 is the unit matrix. Furthermore, since facet 2 is inclined at an angle such that alternate stripes have associated with them a π phase-shift, then M_2 has a single, leading diagonal with elements $(-1)^{1+j}$, j is the row number. Equation (7.8) can now be replaced by:

$$\gamma \; P' \; T^{-1} M_2 T \; P' \; a = a \qquad \text{.....(A.2.1)}$$

where use has been made of $T^{-1} T = I$.

It should now be remembered that T and its inverse are equal and that they have elements

$$T_{j,k} = \sqrt{2/(N+1)} \cdot \sin(jk\pi/[N+1]) \qquad \text{.....(7.2)}$$

Hence, it can be shown that $T_{j,k} = (-1)^{j+1} T_{j,N+1-k}$ ant the product of T^{-1}, M_2 and T is:

$$\left(\sum_{m=1}^{N} T_{j,m} \sum_{l=1}^{N} (-1)^{1+m} \delta_{m,l} T_{1,k} \right) = \sum_{m=1}^{N} T_{j,m} (-1)^{1+m} T_{m,k}$$

but, using the above identity, $T_{m,k} = (-1)^{m+1} T_{m,N+1-k}$. Hence:

$$\left(T^{-1} M_2 T \right)_{j,k} = \sum_{m=1}^{N} T_{j,m} T_{m,N+1-k}$$

Now, due to the orthogonality of the eigenvectors, $\sum T_{j,m}\ T_{m,k} = \delta_{j,k}$ where the summation is carried out over m=1 to N and δ is the Kronecker Delta function. Hence, if the summation of $T_{j,m}T_{m,N+1-k}$ is carried out the result is that the orthogonality changes to;

$$\left(\sum_{m=1}^{N} T_{j,m}\, T_{m,N+1-k} \right)_{jk} = \delta_{j,N+1-k}$$

and equation (A.2.1) becomes:

$$\gamma \begin{vmatrix} 0 & 0 & 0 & 0 & 0 & 0 & 0 & 0 & 0 & e_1 \\ 0 & 0 & 0 & 0 & 0 & 0 & 0 & 0 & e_2 & 0 \\ 0 & 0 & 0 & 0 & 0 & 0 & 0 & e_3 & 0 & 0 \\ 0 & 0 & 0 & 0 & 0 & 0 & e_4 & 0 & 0 & 0 \\ 0 & 0 & 0 & 0 & 0 & e_5 & 0 & 0 & 0 & 0 \\ 0 & 0 & 0 & 0 & e_6 & 0 & 0 & 0 & 0 & 0 \\ 0 & 0 & 0 & e_7 & 0 & 0 & 0 & 0 & 0 & 0 \\ 0 & 0 & e_8 & 0 & 0 & 0 & 0 & 0 & 0 & 0 \\ 0 & e_9 & 0 & 0 & 0 & 0 & 0 & 0 & 0 & 0 \\ e_{10} & 0 & 0 & 0 & 0 & 0 & 0 & 0 & 0 & 0 \end{vmatrix} \quad \mathbf{a} = \mathbf{a}$$

where $e_j = r^2 \exp(i[2x\cos\{j\pi/11\} - i \cdot loss_j])$

CHAPTER 6

CURRENT TAILORING IN PHASE-LOCKED ARRAYS OF SEMICONDUCTOR LASERS WITH SEPARATE CONTACTS.

6.1 Introduction.

The previous chapters have been concerned with analysing the modal behaviour of phase-locked, multi-element ridge waveguide laser arrays. Two types of arrays have been discussed - those which are uniform along the axis of light propagation and those which have longitudinal variations in the laser structure. These analyses have considered the array behaviour in terms of the modal gains required for threshold and mode stability.

This chapter digresses from the eigenmode analyses and investigates the performance of a waveguide laser array under carrier injection. The type of laser considered is one in which each ridge guide has an isolated electrical contact (ref 11,18, 52). As such, each element can be individually controlled to effect the output modal characteristics.

The results of the analysis are that the individual drive currents can be calculated for specified modal output powers.

The method presented is an extension of that proposed by Kapon, Katz and Yariv (ref 53). The array laser is broken up into a number of discretised elements such that conservation equations can be written in terms of averaged carrier densities and averaged photon densities in each of the array's elements (Section 6.2). The conservation equations are then used to derive a condition in which either the photon output is maximised

for a specified lateral current distribution or, alternatively, the lateral gain distribution (and, hence, the carrier distribution) is minimised for a specified photon output distribution. The first case is inverted to derive minimum current requirements for a specified photon output. In both cases, the modal output power can be set and the required drive currents calculated for a specified output power distribution (Section 6.3). Section 6.4 presents examples of the analyses and compares the two methods. The averaged carrier densities can then be converted into an approximate spatial carrier distribution using an analytic function for the carrier distribution of a single ridge (which includes the hole carrier diffusion constant). Carrier-induced dielectric constant changes are then derived (Section 6.5).

The conclusions of the chapter are presented in Section 6.6.

6.2 The Steady-State Conservation Equations For the Laser Array.

An element of the phase-locked array is depicted schematically below. The ridge widths are denoted by w_i and ridge separations are s_i. The array is broken up into a number of discretised elements of width r_i, centred on ridge i, such that $r_i=w_i+0.5(s_i+s_{i-1})$:

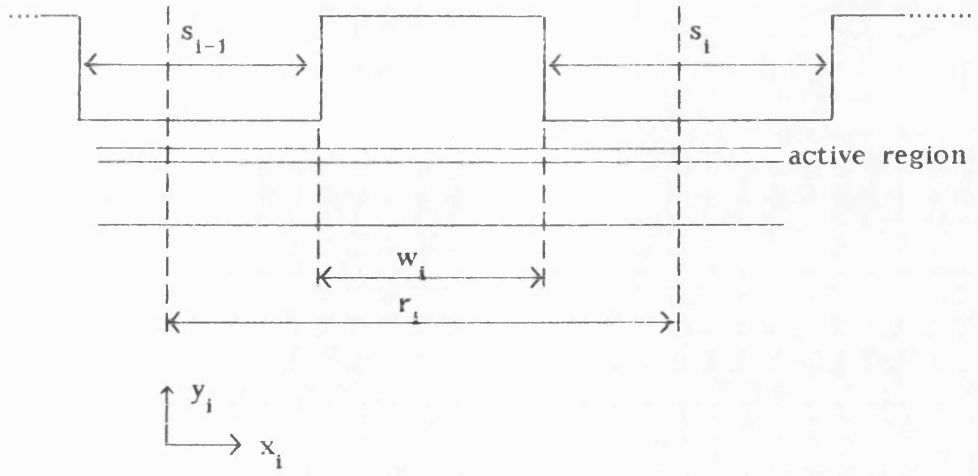

If the array is assumed to operate with a very narrow spectral width or in a single longitudinal mode, the carrier and photon density equations may be written in the following simple form - if longitudinal variation of the photon density and carrier diffusion are ignored (after ref 53):

$$\frac{dN_i(x_i,y_i)}{dt} = \frac{J_i(x_i,y_i)}{qd} - \bar{a}\left(N_i(x_i,y_i)-N_o\right)S_i(x_i,y_i) - \frac{N_i(x_i,y_i)}{\tau_s} \qquad .....(6.2.1)$$

$$\frac{dS_i(x_i,y_i)}{dt} = \bar{a}\left(N_i(x_i,y_i)-N_o\right)S_i(x_i,y_i) - \frac{S_i(x_i,y_i)}{\tau_{ph}} + \beta\frac{N_i(x_i,y_i)}{\tau_s} \qquad .....(6.2.2)$$

where $N_i(x_i,y_i)$ is the free-carrier density at point (x_i,y_i) in element i

$J_i(x_i,y_i)$ is the injected current density at that point,

$S_i(x_i,y_i)$ is the photon density at that point,

N_o is the carrier density for transparency,

q is the electronic charge,

d is the thickness of the active region,

$\bar{a}$ is the gain coefficient,

τ_s is the spontaneous lifetime (or free-carrier lifetime) which, for simplicity, is assumed to be constant above threshold, (i.e. bimolecular recombination is accounted for by a constant term)

τ_{ph} is the photon lifetime in the array due to internal and

mirror losses such that:

$$\frac{1}{\tau_{ph_\lambda}} = c/n.\left(\Gamma_{ridge_\lambda}\alpha_{ridge}+(1-\Gamma_{ridge_\lambda})\alpha_{channel}+\frac{1}{2L}\ln\left(\frac{1}{R_1R_2}\right)\right)$$

c = speed of light in vacuum,

n=effective index of array

Γ_{ridge_λ} = lateral confinement of field to ridge i

$$= \sum_{i=1}^{n}\int_{w_i}|E(x)|^2dx \Big/ \int_{-\infty}^{+\infty}|E(x)|^2dx$$

α_{ridge} = photon loss beneath ridge due to scattering and absorption.

$\alpha_{channel}$ = photon loss in channel regions due to scattering and absorption.

$\frac{1}{2L}\ln\left(\frac{1}{R_1R_2}\right)$ = mirror losses from the laser resonator of length L and with end reflectivities R_1 and R_2

and, β represents the fraction of spontaneous power coupled into the lasing mode.

By considering steady-state solutions of equations 6.2.1 and 6.2.2 and ignoring the amount of spontaneous power coupled into the lasing mode (after ref 53 , then

$$\frac{dN_i(x,y)}{dt} = \frac{J_i(x,y)}{qd} - \bar{a}\left(N_i(x,y)-N_o\right)S_i(x,y) - \frac{N_i(x,y)}{\tau_s} = 0 \quad .....(6.2.3)$$

$$\frac{dS_i(x,y)}{dt} = \bar{a}\left(N_i(x,y)-N_o\right)S_i(x,y) - \frac{S_i(x,y)}{\tau_{ph_\lambda}} = 0 \quad .....(6.2.4)$$

where the i-subscripts of x and y are implicitly assumed.

By integrating the above equations from $y_i=-\infty$ to $+\infty$ and $x_i=0$ to

$x_i = r_i$, (that is, the width of the i-th element), the steady-state equations become:

$$\frac{\bar{J}_i}{qd}.(w_i d) - \int_{-\infty}^{+\infty}\int_{0}^{r_i} g_i(x,y)S_i(x,y)\,.dx.dy - \frac{\int_{-\infty}^{+\infty}\int_{0}^{r_i} N_i(x,y)\,dx.dy}{\tau_s} = 0$$

and

$$\int_{-\infty}^{+\infty}\int_{0}^{r_i} g_i(x,y)S_i(x,y)\,.dx.dy - -\frac{\int_{-\infty}^{+\infty}\int_{0}^{r_i} S_i(x,y)\,dx.dy}{\tau_{ph_i}} = 0$$

where $\bar{J}_i$ is the average injected current density in the active region beneath the ridge waveguide:

$$\bar{J}_i = \frac{1}{w_i d}\int_{-\infty}^{+\infty}\int_{0}^{r_i} J_i(x,y)\,dx.dy$$

and $g_i(x,y)$ represents the injected gain term in the i-th element:

$$g_i(x,y) = \bar{a}\left(N_i(x,y) - N_o\right)$$

Now $\int_{-\infty}^{+\infty}\int_{0}^{r_i} g_i(x,y)S_i(x,y)\,.dx.dy$ can be approximated by averaged values of gain and photon density

$$\int_{-\infty}^{+\infty}\int_{0}^{r_i} g_i(x,y)S_i(x,y)\,.dx.dy = \bar{g}_i\bar{S}_i r_i d = \bar{g}_i\Gamma_{r_i}\Gamma_v\Psi$$

where $\bar{g}_i$ is the effective (average) gain over the i-th element

$\bar{S}_i$ is the effective (average) photon density over the i-th element

Γ_{r_i} is the lateral confinement factor of the optical field to the i-th element = $\int_{0}^{r_i} S_i(x)\,dx \Big/ \int_{-\infty}^{+\infty} S_i(x)\,dx$

Γ_v is the transverse (vertical) confinement factor of the optical field to the active region = $\int_0^d S_i(y)\,dy \Big/ \int_{-\infty}^{+\infty} S_i(y)\,dy$

and Ψ represents the number of photons emitted per unit length of the array

By letting $\int_{-\infty}^{+\infty}\int_0^{r_i} N_i(x,y)\,dx.dy = \bar{N}_i\, r_i d$, $\bar{N}_i$ representing an average carrier density in the active region of the i-th element, the steady-state conservation equations become

$$\frac{\bar{J}_i}{qd} - \frac{\bar{g}_i \Gamma_{r_i} \Gamma_v \Psi}{w_i d} - \frac{\bar{N}_i r_i}{\tau_s w_i} = 0$$

and $$\bar{g}_i \Gamma_{r_i} \Gamma_v \Psi - \frac{\Gamma_{r_i} \Psi}{\tau_{ph_i}} = 0$$

which may be alternatively expressed as:

$$\frac{\bar{J}_i}{qd}\frac{w_i}{r_i} - \bar{g}_i \bar{S}_i - \frac{\bar{N}_i}{\tau_s} = 0 \qquad \text{.....(6.2.5)}$$

$$\left(\bar{g}_i - \frac{1}{\tau_p}\right)\bar{S}_i r_i d = 0 \qquad \text{.....(6.2.6)}$$

where $\bar{S}_i = \frac{\Gamma_{r_i} \Gamma_v \Psi}{r_i d}$ and $\tau_{p_i} = \Gamma_v\, \tau_{ph_i}$

Equations 6.2.5 and 6.2.6 represent the behaviour of the i-th element acting as if it was in electrical and optical isolation from all other guides. However, in the case of phase-locked arrays, the mode structure is composed of contributions from all elements - the photon densities of the elements are not independent but coupled together to form the supermode output. On the other hand, the individual electrical contacts on the ridges

of a separate-contact, multi-element, ridge array are to a large extent independent - the main conducting path lies through the cladding and active layers (a distance of 1.5μm away from the contact) and the region between the ridges (the channels) is a non-conducting medium. Thus, one may consider the photon rate equation as consisting of the summation of the products of all elemental photon powers and gains - the nett supermode gain can be approximated by a discrete summation of the modal gain of each element within the array for a given supermode; the carrier equations for each element remain independent since coupling of the carriers is not considered. The nett photon conservation equation is then, from 6.2.6:

$$\sum_{i=1}^{n}\left(\bar{g}_i - \frac{1}{\tau_p}\right)\bar{S}_i r_i d = 0 \qquad \text{.....(6.2.7)}$$

Equations 6.2.5 and 6.2.7 are the simplified equations for steady-state operation of the phase-locked array. They differ from those proposed by Kapon, Katz and Yariv since they include parameters dependent on the array geometry. Ref 53 considers different elemental optical densities but does not include the element and ridge widths (r_i and w_i). This fact is not significant when considering 6.2.5 since the current density term $\frac{\bar{J}_i}{qd}\frac{w_i}{r}$ may be replaced by an effective value $\frac{\bar{\bar{J}}_i}{qd}$. Equation 6.2.7, on the other hand, includes the term r_i within the summation. This equation simplifies to the form proposed in ref 53 only when the array is uniform. Thus, the improved equations proposed here differ in the results derived for non-uniform (e.g. chirped) arrays.

6.3 Solution of the Steady-State Conservation Equations.

Before attempting to derive solutions to the steady-state equations,

6.2.5 and 6.2.7 are normalised using the following variables (after ref 53):

$$n_i = a\tau_{p_i} N_i \qquad \text{.....(6.3.1)}$$

$$n_{om_i} = \bar{a}\tau_{p_i} N_o \qquad \text{.....(6.3.2)}$$

$$n_{o_i} = \bar{a}\tau_{p_i}\tau_s \frac{\bar{J}_i}{qd}\left(\frac{w_i}{r_i}\right) \qquad \text{.....(6.3.3)}$$

$$s_i = \bar{a}\tau_s S_i \qquad \text{.....(6.3.4)}$$

$$p_i = n_{o_i} - n_{om_i} \qquad \text{.....(6.3.5)}$$

Equations 6.2.5. and 6.2.7 now become:

$$n_{o_i} - (n_i - n_{om_i})s_i - n_i = 0 \qquad i=1,2,3.....,n \qquad \text{.....(6.3.6)}$$

$$\sum_{i=1}^{n}\left((n_i - n_{om_i}) - 1\right)s_i r_i = 0 \qquad \text{.....(6.3.7)}$$

where all common constants have been eliminated.

The above sets of equations, representing the behaviour of an n-element array, have 3n variables (n of n_i , n of n_{oi} and n of s_i). In order to solve these equations it is necessary to eliminate one of the variable sets and introduce a constraint such that a method of maxi/minimisation can be used to reduce the resultant equation set to include only one dependent variable set and one independent variable set which may be arbitrarily specified. Two methods are presented here for comparison - the first is based on the method proposed by Kapon, Katz and Yariv (ref 53) and extended by Buckley and Shore (ref 10, 11) which involves the maximisation of the output power for a specified lateral current distribution. This process is then inverted to deduce the element currents for a specified mode and output power. The second method is

similar to the first in that the mode and output power are specified whilst the new constraint is that the lateral gain distribution will distribute itself to minimise the total number of carriers. In this way the required drive conditions for a given modal output is minimised. Once again the individual drive currents are found for a given lateral photon distribution - the latter is an extension of the first method and is its first documentation.

6.3.1 Method 1 - Maximising the Photon Output.

Considering an array in which the lateral current profile (i.e. the ridge currents) is specified. It is proposed that the total light output will be maximised for the given current input in which case the supported modes will be weighted to maximise the overlap with the injected gain distribution. The total light output is represented in normalised form by the function F:

$$F = \sum_{i=1}^{n} s_i r_i = \sum_{i=1}^{n} \bar{a}\tau_s \frac{\Gamma_v \Gamma_{r_i}}{r_i d} \Psi r_i \qquad \text{.....(6.3.1.1)}$$

Since $\sum \Gamma_{r_i} = 1$, it follows that

$$F = \bar{a}\tau_s \frac{\Gamma_v}{d} \Psi .$$

This equation demonstrates that F is representative of the total output power since all other parameters except Ψ are constants. Now, for given values of n_{oi} (the normalised parameter representing the current density terms J_i), the values of s_i need to be determined. Equations 6.3.6, 6.3.7 and 6.3.1.1 are re-written below to clarify the method to be used in determining

the values for s_i:

$$n_{o_i} - (n_i - n_{om_i})s_i - n_i = 0 \qquad i=1,2,3.....,n \qquad .....(6.3.6)$$

$$\sum_{i=1}^{n} \left((n_i - n_{om_i}) - 1\right) s_i r_i = 0 \qquad .....(6.3.7)$$

$$F = \sum_{i=1}^{n} s_i r_i \qquad .....(6.3.1.1)$$

As mentioned above, function F needs to be maximised subject to the constraints implied by equations 6.3.6 and 6.3.7. The method of Lagrange multipliers is used to maximise F. A function, G is defined in the following way:

$$G = \sum_{i=1}^{n} s_i r_i + \lambda \sum_{i=1}^{n} \left((n_i - n_{om_i}) - 1\right) s_i r_i \qquad .....(6.3.1.2)$$

where λ is the Lagrange multiplier.

Since the required variables are s_i and n_{oi}, 6.3.7 is re-written :

$$\sum_{i=1}^{n} \left(\frac{n_{oi} - n_{om_i} - 1}{1+s_i} \right) s_i r_i = 0$$

where use has been made of 6.3.6. Noting that $p_i = n_{oi} - n_{om_i}$ and substituting in the last equation:

$$\sum_{i=1}^{n} \left(\frac{p_i}{1+s_i} - 1 \right) s_i r_i = 0 \qquad .....(6.3.1.3)$$

where p_i is the new independent variable. Using 6.3.1.3 in 6.3.1.2, the function G can be written as:

$$G = \sum_{i=1}^{n} s_i r_i + \lambda \sum_{i=1}^{n} \left(\frac{p_i}{1+s_i} - 1 \right) s_i r_i$$

Since the term multiplied by λ is zero, maximising function F is the same as maximising G. To find the corresponding stationary points of G as s_i changes, the differential of G with respect to s_i needs to be set to zero:

$$\frac{dG}{ds_i} = r_i + \lambda r_i \left(\frac{p_i}{(1+s_i)^2} - 1 \right) = 0 \qquad \text{.....(6.3.1.4)}$$

In order to ascertain whether or not the corresponding value of G is a maximum, the second differential with respect to s_i is also determined:

$$\frac{d^2G}{ds_i^2} = -2\lambda r_i \frac{p_i}{(1+s_i)^3}$$

Since r_i, p_i and s_i are all positive, then the second differential is less than zero and G is a maximum if $\lambda > 0$. Returning to equation 6.3.1.4, s_i can be derived in terms of λ and p_i:

$$s_i = \sqrt{p_i} \sqrt{\frac{\lambda}{\lambda - 1}} - 1 \qquad \text{.....6.3.1.5}$$

or $$s_i = C\sqrt{p_i} - 1 \qquad \text{.....6.3.1.6}$$

where $$C = \sqrt{\frac{\lambda}{\lambda - 1}}$$

Using this formula for s_i in 6.3.1.3, C can be obtained in terms of the known variables p_i. After simplification:

$$\frac{1}{C} + C = \frac{\sum (p_i + 1) r_i}{\sum r_i \sqrt{p_i}}$$

Solving the above equation for C yields:

$$C = \frac{1}{2\sum r_i\sqrt{p_i}}\left(\sum(p_i+1)r_i + \sqrt{\left(\sum(p_i+1)r_i\right)^2 - 4\left(\sum r_i\sqrt{p_i}\right)^2}\right) \quad \text{.....6.3.1.7}$$

where the positive root has been taken to maximise C. The above equation may be clarified by re-writing it as:

$$C = \frac{\sum(p_i+1)r_i}{2\sum r_i\sqrt{p_i}} + \sqrt{\left(\frac{\sum(p_i+1)r_i}{2\sum r_i\sqrt{p_i}}\right)^2 - 1}$$

Since $p_i>0$, then $(p_i+1)>\sqrt{p_i}$ and $\frac{\sum(p_i+1)r_i}{\sum r_i\sqrt{p_i}} > 1$. Thus, $C > 0$ and G is a maximum.

When an array is uniform, all r_i's are the same and equations 6.3.3.6 and 6.3.1.7 reduce to the form proposed in ref 10,11. The important result derived here is that the photon output of the i-th element of a laser array can be determined by considering the individual normalised drive currents, n_{oi}, and the array geometry.

6.3.2 Maximised Photon Output Calculations..

Table 6.3.2.1 details the power distribution in an array as a function of individual drive currents. The current distribution is chosen to be uniform so that a simple, single contact array can be modelled. The drive currents are increased from 20mA to 50mA and the lateral light output distribution calculated. It is seen that, for a uniform input, the maximised output distribution is uniform (as predicted by equation 6.3.1.6). The individual element powers increase linearly from 2.7mW to 13.4mW as the

drive in each element increases from 20mA to 50mA. Furthermore note that as the normalised power density goes towards zero (the threshold condition), the normalised current densities converge on $1/C^2$ (i.e. a constant) and all current and carrier densities are the same.

TABLE 6.3.2.1

OUTPUT POWERS FOR A 5-ELEMENT, UNIFORM ARRAY ARRAY WITH 2μm RIDGES ON A 4μm PITCH WITH A UNIFORM CURRENT PROFILE INPUT

$I_1=I_2=I_3=I_4=I_5$ (mA)	Power in 1st, 5th Element, $P_1 = P_5$ (mW)	Power in 2nd, 4th Element, $P_2 = P_4$ (mW)	Power in 3rd Element, P_3 (mW)
20	2.74	2.74	2.74
30	6.26	6.26	6.26
40	9.84	9.84	9.84
50	13.43	13.43	13.43

Now, the photon powers can be converted into supermode weighting factors relating to the relative proportion of each supermode present in the total output. If the power in the i-th element is Φ_i and the amount of supermode k present is a_k then:

$$\Phi_i = \sum_{k=1}^{n} \Gamma_{r_i}^{k} \, a_k \qquad \text{.....(6.3.2.1)}$$

In matrix terms $\bar{\Phi} = \bar{\Gamma}\bar{a}$, where $\bar{\Phi}$ represents an nx1 matrix of elements Φ_j, $\bar{\Gamma}$ is an nxn matrix of confinement factors and $\bar{a}$ is the column matrix of supermode weighting factors. By inverting Γ, $\bar{a}$ may be found:

$$\bar{a} = \bar{\Gamma}^{-1}\bar{\Phi} \qquad \text{.....(6.3.2.2)}$$

Since the values of Φ_j and Γ^k_{rj} are known, then the supermode weighting factors can be derived. Table 6.3.2.2 shows the different weighting factors associated with different lateral current profiles. It is seen that weighting factors are both negative and positive. However, a negative weighting factor for photons is clearly not realisable in practice. Thus, these solutions cannot be supported by the array. An alternative to the approach of Katz et al. is needed to remove the anomaly. What is needed instead is to calculate the nett modal gains corresponding to a specified current profile and determine the dominant mode at threshold. The mode which then lases is then the one with the highest nett gain. Table 6.3.2.3 shows the normalised gain of each mode for various current profiles. In each case, the mode with the highest gain will lase above threshold for that specified current profile - if the array lases in a single supermode

TABLE 6.3.2.2

OUTPUT POWERS AND NORMALISED SUPERMODE WEIGHTING FACTORS FOR A 5 ELEMENT UNIFORM ARRAY WITH 2μm RIDGES ON A 4μm PITCH WITH VARYING CURRENT PROFILES BUT THE TOTAL INPUT CURRENT STAYING CONSTANT

Stripe Currents (mA)					Powers in Elements (mW)					Normalised Weighting Factors				
I_1	I_2	I_3	I_4	I_5	P_1	P_2	P_3	P_4	P_5	a_1	a_2	a_3	a_4	a_5
30	30	30	30	30	6.3	6.3	6.3	6.3	6.3	-0.98	0.60	0.01	-0.62	1.00
22	32	42	32	22	4.5	6.9	8.7	6.9	4.5	-0.99	0.61	0.01	-0.64	1.00
38	28	18	28	38	8.1	6.1	3.2	6.1	8.1	-0.98	0.59	0.01	-0.62	1.00

Note: The normalised supermode weighting factor is defined by the ratio of the actual weighting factor to the modulus of the maximum weighting factor

TABLE 6.3.2.3

NORMALISED GAIN DISTRIBUTION FOR SUPERMODES

ACCORDING TO THE CONDITIONS OF TABLE 6.3.2.2

Stripe Currents (mA)					Normalised Gain				
I_1	I_2	I_3	I_4	I_5	P_1	P_2	P_3	P_4	P_5
30	30	30	30	30	0.98	0.97	0.95	0.98	1
22	32	42	32	22	0.98	0.95	0.95	0.96	1
38	28	18	28	38	0.98	0.98	0.98	0.99	1

6.3.3 Calculating the Required Current for a Given Supermode Power Distribution.

By inverting equation 6.3.1.5, the individual drive currents for a given photon distribution at the output can be found; that is, by specifying a supermode distribution for a given power output, the s_i's are calculated and the p_i's can be found:

$$p_i = (1+s_i)^2 \frac{(\lambda-1)}{\lambda} \qquad \text{.....(6.3.3.1)}$$

Using this equation in 6.3.1.3 yields:

$$\sum_{i=1}^{n}\left((1+s_i)\ A - 1\right)s_i r_i = 0$$

where $A = (\lambda-1)/\lambda$.

Hence, $A = \sum_{i=1}^{n} s_i r_i \ / \ \sum (1+s_i) s_i r_i$

and $$p_i = (1+s_i)^2 \sum_{i=1}^{n} s_i r_i \Big/ \sum_{i=1}^{n} (1+s_i) s_i r_i \qquad \text{.....(6.3.3.2)}$$

This equation relates the currents required to support a given output power distribution. For a pure supermode to be supported, 6.3.3.2 must be solved for the required mode and output power. The resulting currents can then be substituted back into 6.3.1.6 and the lateral power distribution checked for single-mode stability. When considering threshold operation $s_i \to 0$ and 6.3.3.2 gives $p_i \to 1$. Alternatively, if $s_i \gg 1$, $p_i \to \dfrac{s_i \sum s_i r_i}{\sum s_i^2 r_i}$.

Plots of the drive currents required to support the pure modes of a 5-element, uniform array with ridge widths of 2μm and ridge separations of 2μm are shown in fig.6.3.3.1 whilst the table beneath the graph shows the drive currents required for threshold and 100mW output corresponding to the graphs. Since the discrimination between the modes is so low, the drive current values for each mode are almost identical. The individual drive currents versus output powers in each element are also shown in figs. 6.3.3.2 Due to symmetry, only elements 1, 2 and 3 are displayed in the latter graphs since the output of elements 5 and 4 are the same as those for elements 1 and 2 respectively. From the graphs, the following points are noted:

(i) the drive current required for 100mW of mode 3 is lower than all other modes. This is in agreement with the normalised equations since, after denormalisation, it is found that, for an output power of 100mW, then:

$$\sum p_i r_i \approx 4.46\text{x}10^{-4} \left(1 + \frac{18.4\text{x}10^{-3}}{\Sigma \Gamma_{r_i}^2} \right)$$

Now, Σf_{ri}^2 is smallest for the mode with the lowest number of

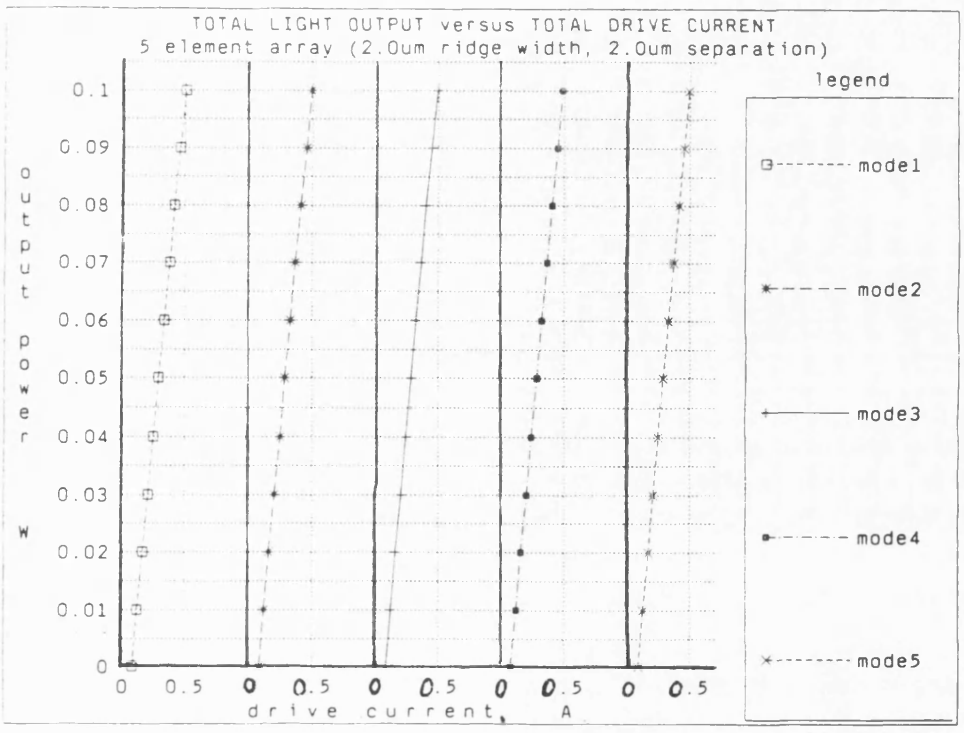

MODE	THRESHOLD CURRENT (mA)	DRIVE CURRENT FOR 100mW (mA)
1	84.23	502.1
2	84.17	495.9
3	84.07	487.2
4	83.96	490.1
5	83.87	493.7

FIGURE 6.3.3.1 Total Light Output versus Total Drive Current
For a 5 Element Array with 2um Ridges Separated by 2um
According To the Method of Section 6.3.2

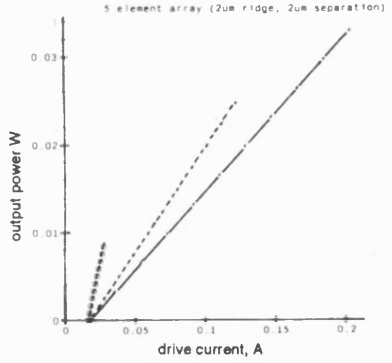

a) fundamental mode, n=1

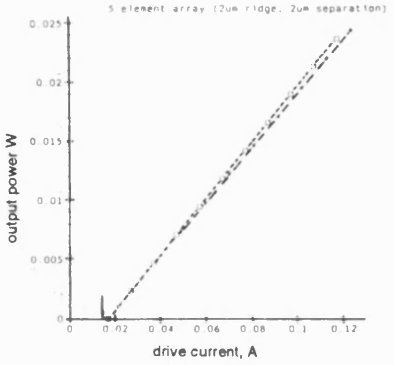

b) First order mode, n=2

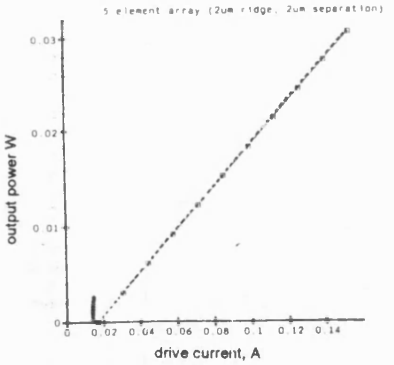

c) Second order mode, n=3

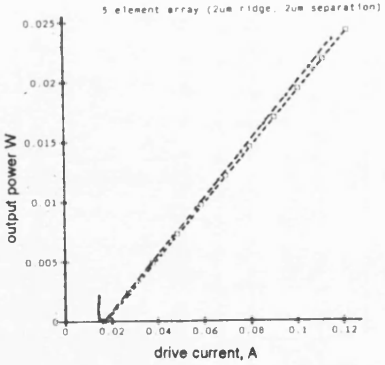

d) Third order mode, n=4

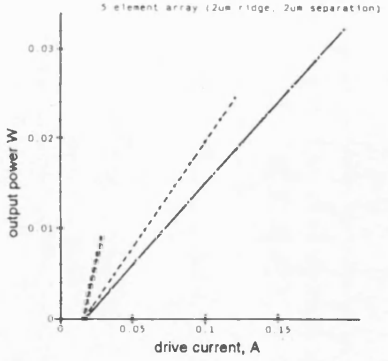

e) Highest order mode, n=5

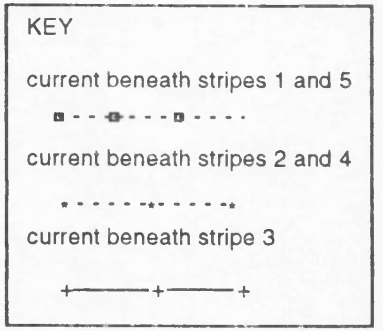

Figure 6.3.3.2 Drive Currents of Each Ridge Laser Corresponding to the Characteristics Shown in Figure 6.3.3.1 - Corresponding to Method 6.3.2

eigenvectors - mode 3; this then requires the lowest drive current for a given output power.

(ii) the total threshold current decreases as the order of the mode increases since higher order modes experience lower modal losses.

(iii) some stripes exhibit a decrease in their drive currents for increasing total ouput .power. This anomaly is offset by the fact that the "missing" drive current is diverted to stripes where the mode confinement is highest.

If the carrier densities are computed corresponding to these drive currents, then, from 6.3. .6:

$$n_i = \frac{n_{oi}+n_{om}s_i}{1+s_i} = \frac{p_i}{1+s_i} + n_{om}$$

Therefore,

$$n_i = n_{om} + (1+s_i) \sum_{i=1}^{n} s_i r_i \Big/ \sum_{i=1}^{n} (1+s_i) s_i r_i$$

By replacing the normalised parameters with their principle values then:

$$N_i = N_0 + \frac{1}{\bar{a}\tau_{ph}} \frac{\left(1 + \frac{\bar{a}\tau_s \Gamma_v \Gamma_{r_i} \Psi}{r_i d}\right)}{\sum \left(1 + \frac{\bar{a}\tau_s \Gamma_v \Gamma_{r_i} \Psi}{r_i d}\right) \Gamma_{r_i}} \qquad \text{.....(6.3.3.3)}$$

since $\sum \Gamma_{r_i} = 1$ and $S_i = \frac{\Gamma_v \Gamma_{r_i} \Psi}{r_i d}$

Equation 6.3.3.3 shows that N_i is not clamped at its threshold value as is frequently observed in single element lasers, but depends on the output power via Ψ. This is a feature of the method used here - for low powers

(Ψ->0), n_i->$1+n_{om_i}$ - the carrier density at threshold is constant across the array and independent of i. As Ψ increases, then the carriers are to be injected to optimise the modal gain (i.e. where the mode confinement to the ridge is highest). Figure 6.3.3.3 demonstrates this variation for the uniform array of fig.6.3.1.1. From 6.3.3.9, as s_i ->0, n_i ->$n_{om_i}+1$ whilst for s_i>>1, n_i->$n_{om_i}+s_i\Sigma s_i r_i / \Sigma s_i^2 r_i$ .This latter equation can be shown to be independent of Ψ.

$$n_i = n_{om_i} + \frac{\Gamma_{r_i} / r_i}{\sum \Gamma_r^2 / r_i}$$

If Γ_{ri}->0 then n_i->n_{om_i} as the output power increases. This corresponds to a decrease in the carrier density in the i-th element if the mode confinement is low and approaching zero. In order to optimise the modal gain, the carriers are then injected where the mode confinement is tightest - if $\Gamma_{r_i}/r_i > \sum \Gamma_{r_i}^2/r_i$, then the carrier density will increase as Ψ increases. This behaviour is not typical of single element lasers where gain saturation and carrier clamping at the threshold value occurs for low power densities. Figure 6.3.3.3 displays this non-uniform variation of the denormalised carrier density, N_i, as the output power of each element increases. It should be borne in mind that both sets of graphs represent the current or carrier density for given modal outputs. In practice if the current predicted by 6.3.3.3 was injected into the array, the first supermode to lase would be the one which had the best modal overlap with this injected carrier distribution. This may not necessarily be the same supermode used initially in the calculation of the stripe currents. For example if one considers the current distributions required to excite the fundamental and highest order supermodes, it is obvious that the current corresponding to threshold for the fundamental mode is capable of stimulating the highest order supermode to operate above threshold since the higher order mode requires

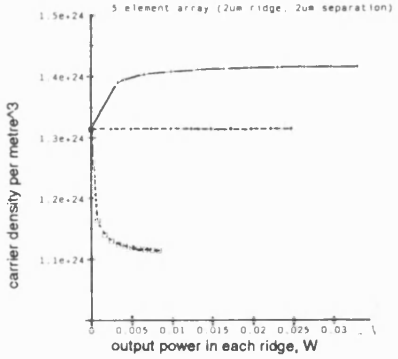

a) fundamental mode, n=1

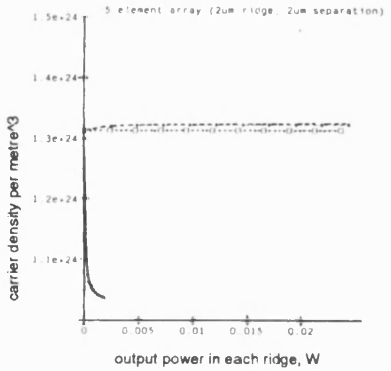

b) First order mode, n=2

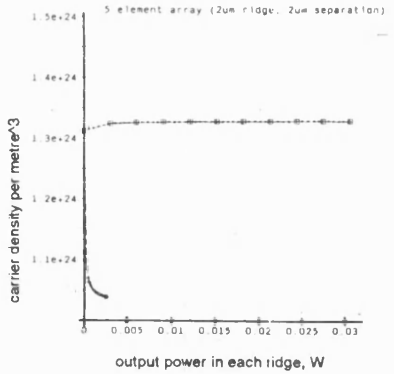

c) Second order mode, n=3

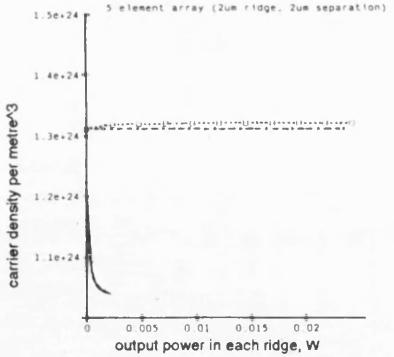

d) Third order mode, n=4

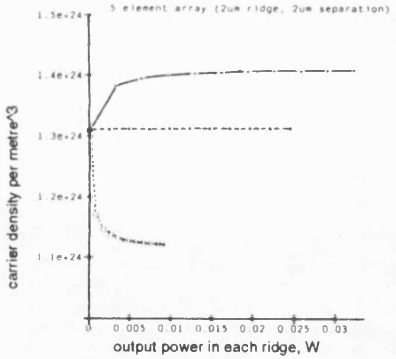

e) Highest order mode, n=5

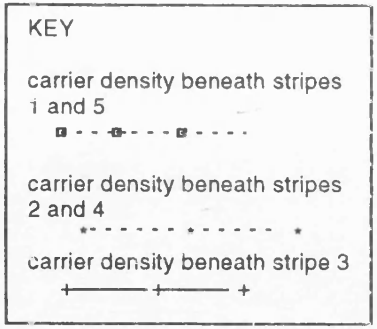

Figure 6.3.3.3 Carrier Densities of Each Ridge Laser Corresponding to the Characteristics Shown in Figure 6.3.3.1 - Corresponding to Method 6.3.2

a similar envelope of current but lower absolute values.

Due to the uncharacteristic nature of the variation of the carrier density, N_i, as the output power is increased, an alternative physical quantity for optimisation is considered in the next section in order to gain insight into the array's behaviour.

6.3.4 Method 2 - Minimising the Lateral Gain Distribution.

Since the previous equations predict anomalous behaviour in the laser array, an alternative representation is sought to analyse the behaviour of a laser array under current injection. An initial attempt was made by considering the maximisation of the lateral modal gain as a function of injected carrier concentration. However, this yielded trivial solutions. Thus, instead, it is proposed that another way of expressing the maximisation of the lateral gain and achieving non-trivial solutions is to maximise the square of the gain. The lateral gain profile is related to $\sum(n_i-n_{om})r_i$. However, if one was to consider maxima of this function with respect to changes in n_i, it is apparent that n_i can be large and negative such that the nett modal gain constraint may be satisfied whilst the overall carrier concentration ($\sum n_i r_i$) is low. However, large negative values of n_i are not considered since one is modelling a laser under forward or zero bias. Thus, to correct this, the function to be minimised is redefined as $\sum\left((n_i-n_{om})r_i\right)^2$ - in this way all values of n_i, including negative ones have a positive contribution to the function. Thus, a maximum value of the function may be found and all values of n_i can be defined as positive simply by taking the positive square root.

Using 6.3.7, a new function, G, is defined:

$$G = \sum_{i=1}^{n}\left((n_i - n_{om})r_i\right)^2 + \mu \sum_{i=1}^{n}\left(n_i - n_{om} - 1\right)s_i r_i \qquad \text{.....(6.3.4.1)}$$

where μ is the new Lagrange multiplier.

A minimum of G occurs when $dG/dn_i=0$:

$$\frac{dG}{dn_i} = 2\left(n_i - n_{om}\right)r_i^2 + \mu s_i r_i = 0$$

$$\Rightarrow n_i = n_{om} - \frac{\mu s_i}{2r_i} \qquad \text{.....(6.3.4.2)}$$

Substituting this in 6.3.7 gives an equation for μ:

$$\mu = -2\frac{\sum s_i r_i}{\sum s_i^2}$$

whence $$n_i = n_{om} + \frac{s_i}{r_i}\frac{\sum s_i r_i}{\sum s_i^2} \qquad \text{.....(6.3.4.3)}$$

and $$p_i = (1+s_i)\frac{s_i}{r_i}\frac{\sum s_i r_i}{\sum s_i^2} \qquad \text{.....(6.3.4.4)}$$

Once again, by re-writing the normalised parameters in their denormalised form, it is found that:

$$N_i = N_{om} + \frac{\Gamma_{r_i}}{\bar{a}\tau_p}\frac{1}{\sum\left(\Gamma_{r_i}/r_i\right)^2} \qquad \text{.....(6.3.4.5)}$$

It is important to note that N_i is now independent of Ψ, whilst the normalised current density, p_i contains a linear dependence on Ψ:

$$p_i = \left(1 + \frac{\bar{a}\tau_s\Gamma_v\Gamma_{r_i}}{r_i d}\Psi\right)\frac{\Gamma_{r_i}}{\bar{a}\tau_p}\frac{1}{\sum\left(\Gamma_{r_i}/r_i\right)^2} \qquad \text{.....(6.3.4.6)}$$

Figures 6.3.4.1 and 6.3.4.2 illustrate the variation of the currents and carrier densities as the output power is increased. Note now the linear

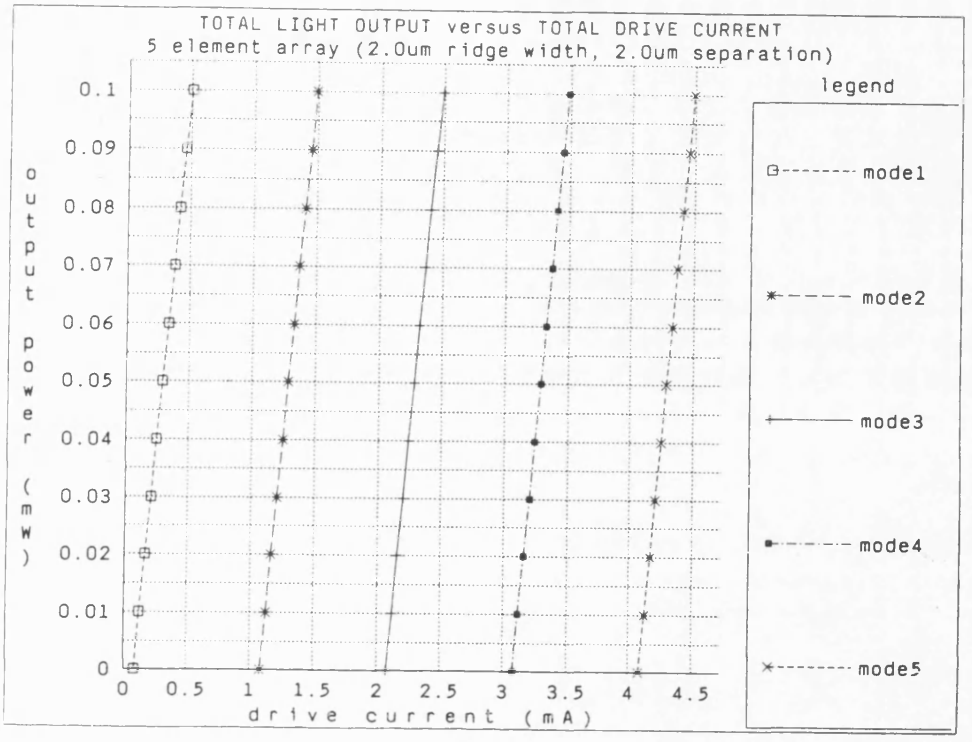

MODE	THRESHOLD CURRENT (mA)	DRIVE CURRENT FOR 100mW (mA)
1	80.27	501.90
2	80.77	495.80
3	77.46	487.00
4	80.67	490.00
5	80.28	493.60

FIGURE 6.3.4.1 Total Light Output versus Total Drive Current
For a 5 Element Array with 2um Ridges Separated by 2um
According To the Method of Section 6.3.4

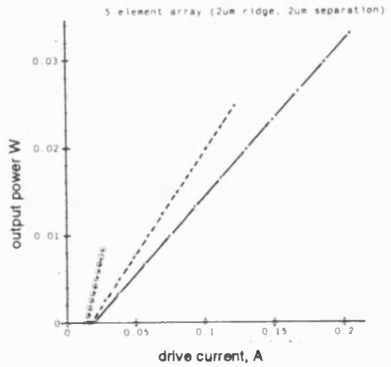

a) fundamental mode, n=1

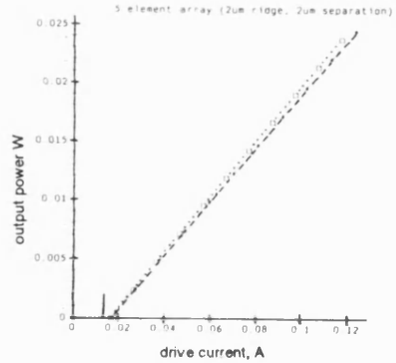

b) First order mode, n=2

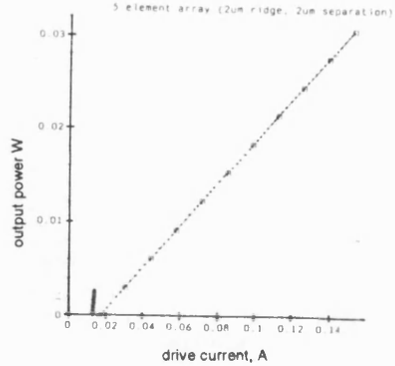

c) Second order mode, n=3

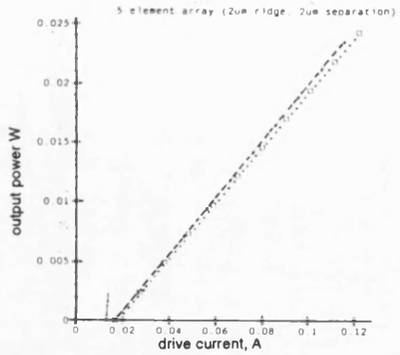

d) Third order mode, n=4

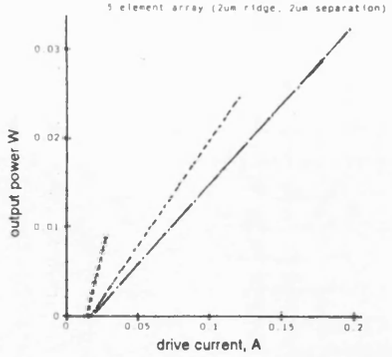

e) Highest order mode, n=5

KEY

current beneath stripes 1 and 5

current beneath stripes 2 and 4

current beneath stripe 3

Figure 6.3.4.2 Drive Currents of Each Ridge Laser Corresponding to the Characteristics Shown in Figure 6.3.4.1 - Corresponding to Method 6.3.4

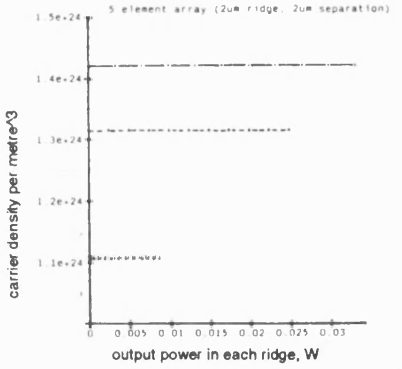

a) fundamental mode, n=1

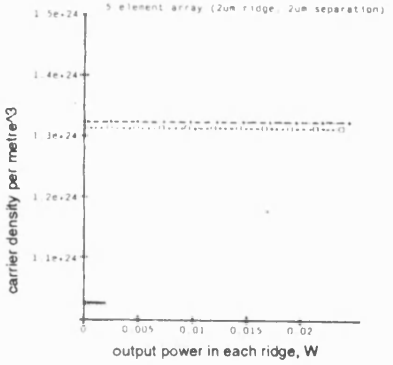

b) First order mode, n=2

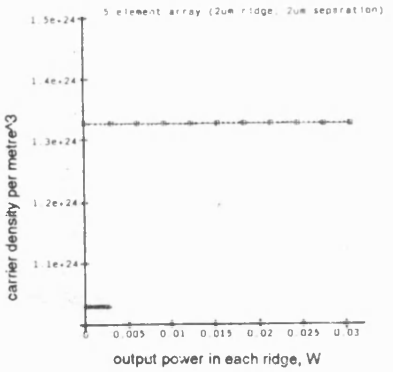

c) Second order mode, n=3

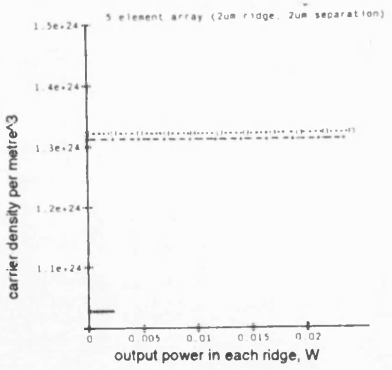

d) Third order mode, n=4

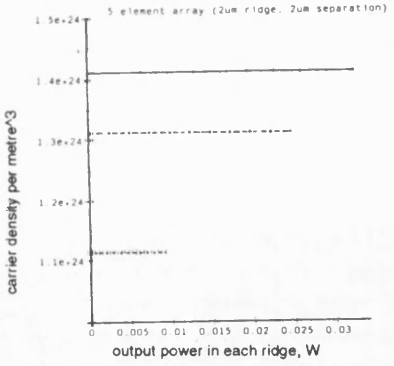

e) Highest order mode, n=5

KEY

carrier density beneath stripes 1 and 5

carrier density beneath stripes 2 and 4

carrier density beneath stripe 3

Figure 6.3.4.3 Carrier Densities of Each Ridge Laser Corresponding to the Characteristics Shown in Figure 6.3.4.1 - Corresponding to Method 6.3.4

increase in output with drive current of each element and the "clamping" of the carrier distribution at its threshold value. However, as with the 1st method, supermode 3 still requires the least amount of drive current to reach 100mW output per facet.

6.4 Comparison of Methods One and Two.

The results obtained using the analyses of sections 6.3.2 and 6.3.4 are now compared directly. Figures 6.4.1(a)-(e) reveal a slight difference between the L/I characteristics for the individual stripes using the different methods. In order to explain this observation it is necessary to investigate the variation in carrier density as a function of drive current (figures 6.4.2(a)-(e)). As mentioned earlier, method 1 does not predict the clamping of the carrier density at its threshold value as is common in single element lasers. However, as the drive current is increased the carrier densities of method 1 assymptotically approach the values of method 2. However, to achieve this, the carrier density in some stripes reduces whilst in others it increases. This manifests itself as a reduction in the drive current of one stripe despite the increase in the overall total output power. In all cases, since method 2 proposes the maximisation of the overlap of the photon distribution with the lateral gain profile, it is anticipated that this method will predict lower drive currents for a given mode output power. Figure 6.4.3 presents the difference between the total drive currents calculated by methods 1 and 2 as a function of increasing output power. The difference in drive currents is small but most noticeable at threshold - mode 3 exhibits the greatest difference in currents. Bearing in mind the comments made in section 6.3.3 pertaining to

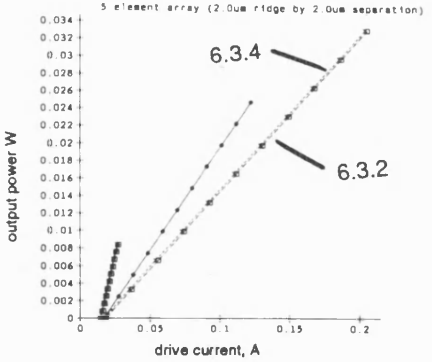

a) fundamental mode, n=1

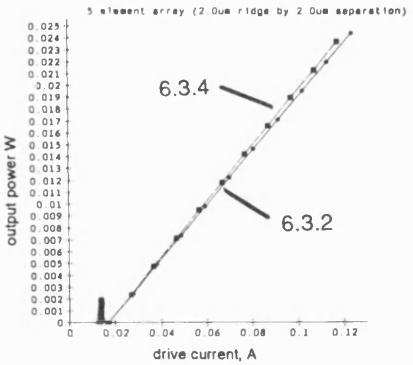

b) First order mode, n=2

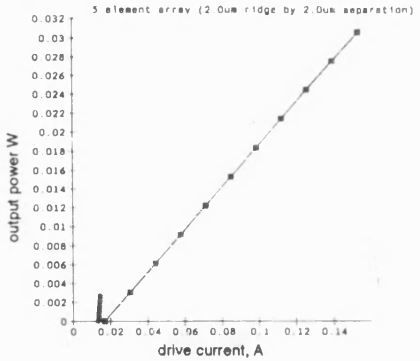

c) Second order mode, n=3

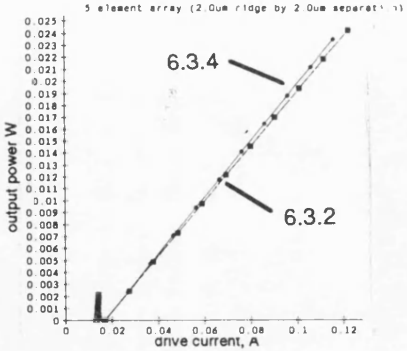

d) Third order mode, n=4

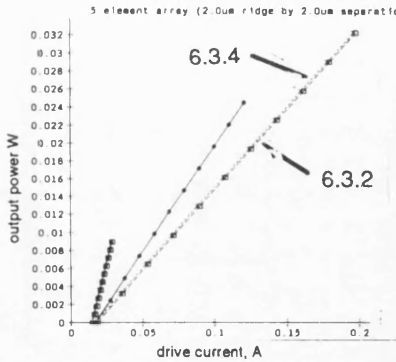

e) Highest order mode, n=5

NOTE:

"6.3.2" denotes method of section 6.3.2

Figure 6.4.1 Comparison of the Drive Currents of Each Ridge Laser Corresponding to the Characteristics Shown in Figure 6.3.3.1 and 6.3.4.1 - Corresponding to the Methods of Sections 6.3.2 and 6.3.4

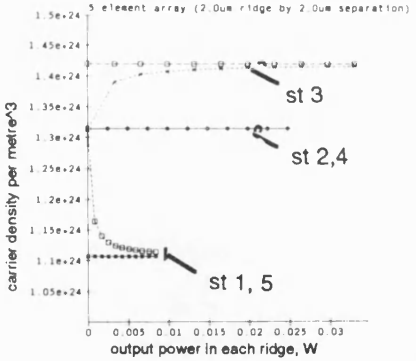

a) fundamental mode, n=1

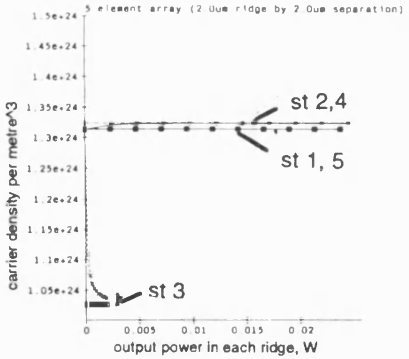

b) First order mode, n=2

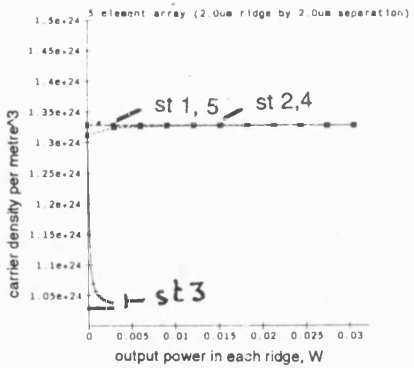

c) Second order mode, n=3

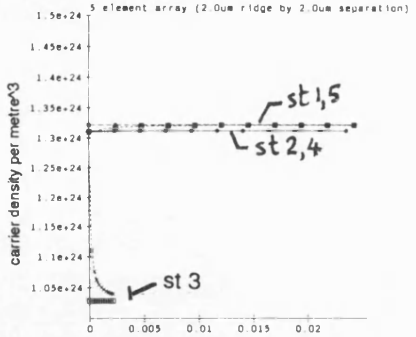

d) Third order mode, n=4

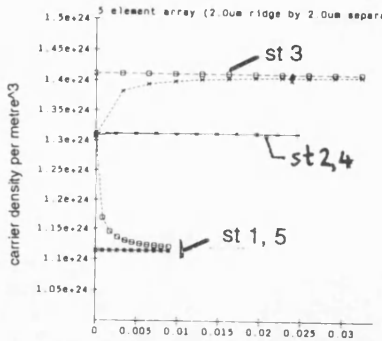

e) Highest order mode, n=5

NOTE:

"st1" denotes stripe 1

Figure 6.4.2 Comparison of the Carrier Densities of Each Ridge Laser Corresponding to the Characteristics Shown in Figure 6.3.3.1 and 6.3.4.1 - Corresponding to the Methods of Sections 6.3.2 and 6.3.4

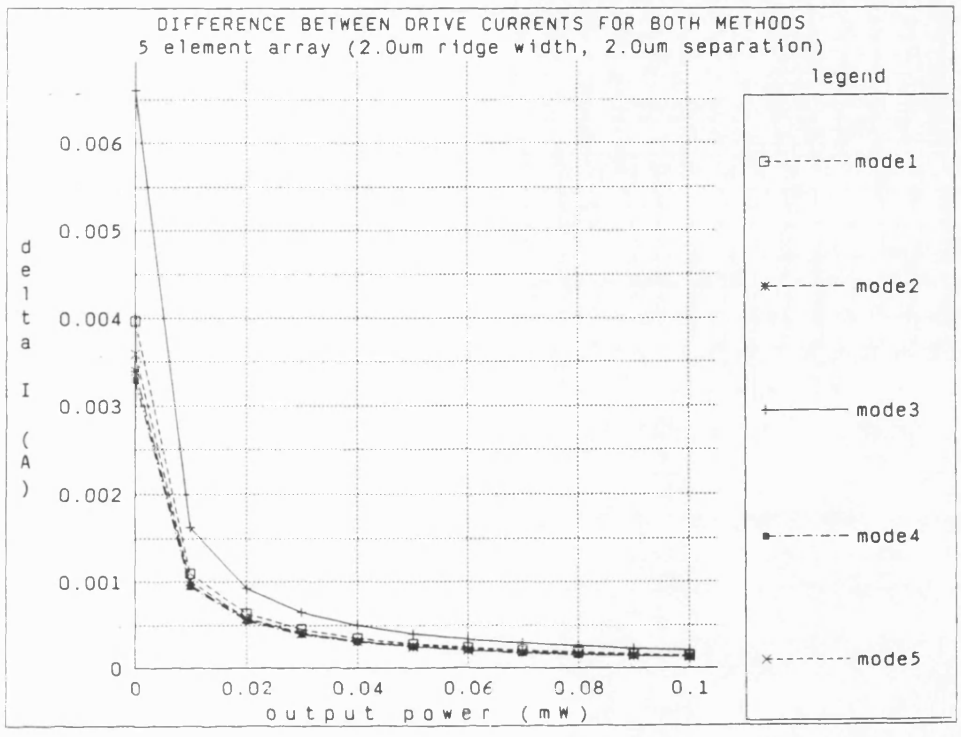

Figure 6.4.3 Difference Between the Total Drive Currents Calculated by the Methods of Sections 6.2 and 6.4 as a Function of Output Power

the function $\sum \Gamma_{rl}^{2}$, it is not unexpected that this mode displays the greatest difference in drive currents.

6.5 The Uniform Intensity Array.

The uniform intensity array was first proposed by Buus (ref.15,16) . It consists of an array in which all elements are the same except the two outer ones - these two are more strongly coupled to their neighbours. The effect of this is that the field distribution is "pulled out" to form a uniform distribution. This array was discussed briefly in section 4.3.3 in terms of the overall mode structure and mode gain. Here, the L/I characteristics and carrier density variations are computed as a function of increasing total output power for the "Buus" array.

Figure 6.5.1 shows the variation of the total drive current versus total output power using the two methods of section 6.3. Method 1 predicts that all modes have (approximately) the same threshold current whilst method 2 predicts that the lowest order mode requires the highest drive current for threshold. On further investigation, it is seen that the variation of carrier density is similar to that of the uniform element arrays - the carrier densities of method 1 approach those of method 2 as the total output power increases (figure 6.5.2). However, it is apparent that the fundamental mode requires lower carrier densities in the end elements. This is cause for concern if one is to consider the effects of carrier-induced dielectric constant changes and spatial hole burning , -the nonuniform variation of carrier density across the array will lead to a nonuniform (active) dielectric constant profile, which, in turn, will cause the array to propagate a nonuniform mode intensity. This is explained in

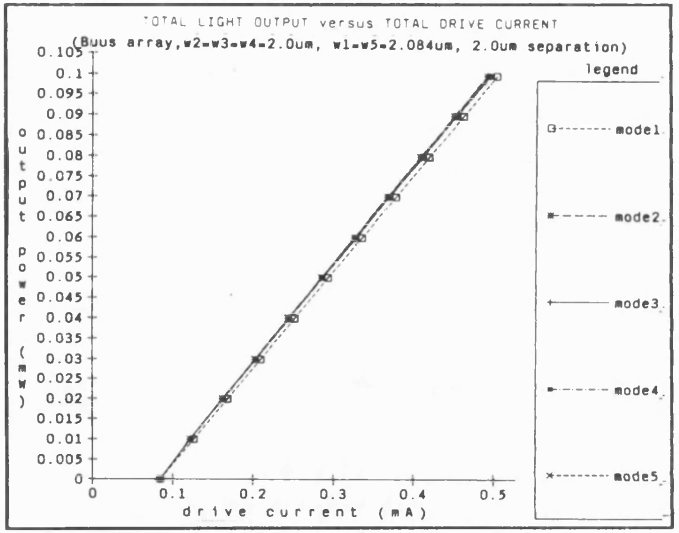

a) Method of Section 6.3.2

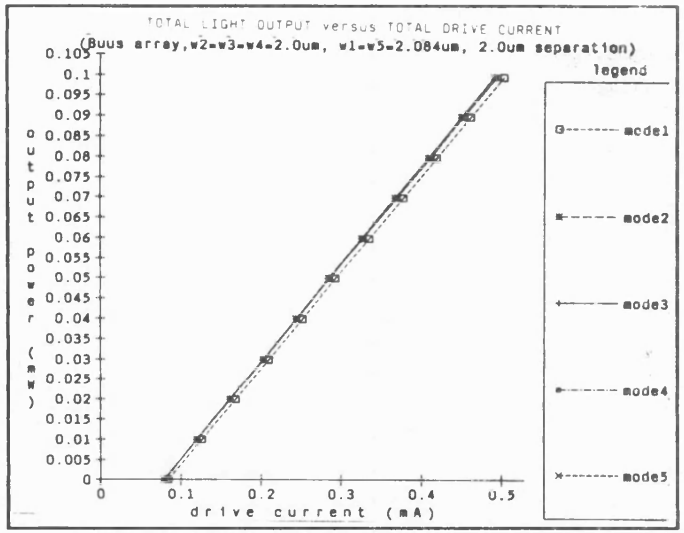

a) Method of Section 6.3.4

Figure 6.5.1 Output Power versus Total Drive Currents For the Uniform Intensity Array According to the Methods of Sections 6.3.2 and 6.3.4

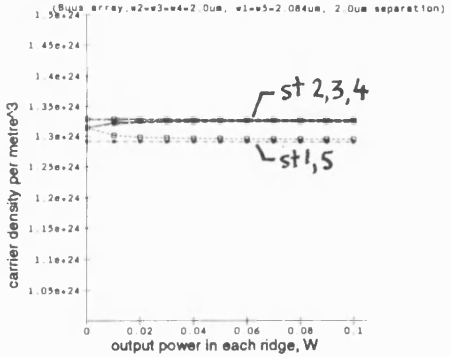

a) fundamental mode, n=1

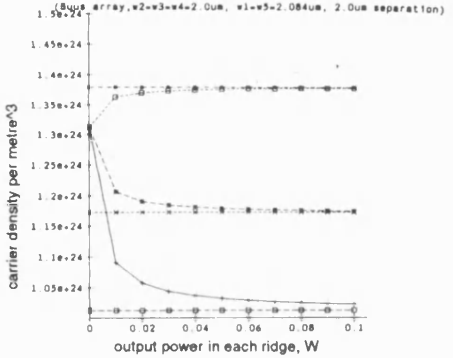

b) First order mode, n=2

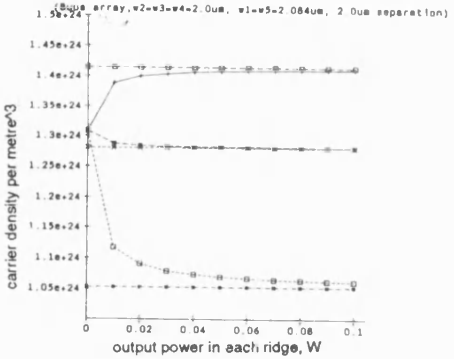

c) Second order mode, n=3

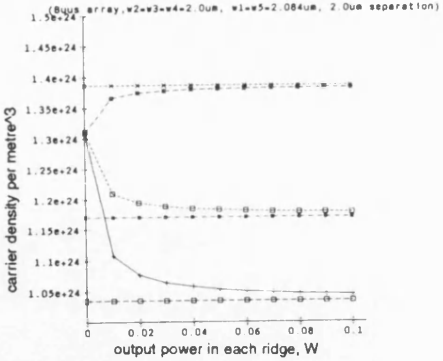

d) Third order mode, n=4

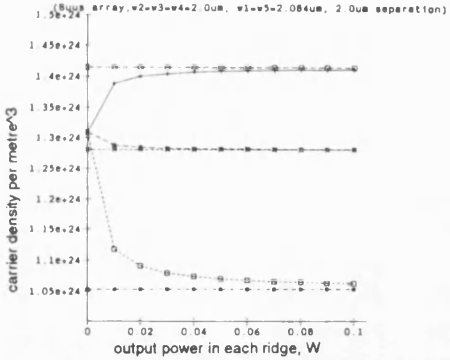

e) Highest order mode, n=5

NOTE:

"str1" denotes stripe 1

"6.3.2" denotes method of section 6.3.2

etc.

Figure 6.5.2 Comparison of the Carrier Densities of Each Ridge Laser Corresponding to the Characteristics Shown in Figure 6.5.1 - Corresponding to the Methods of Sections 6.3.2 and 6.3.4

the next section.

6.6 Carrier-Induced Dielectric Constant Changes.

So far, the laser array has been dealt with passively despite the calculation of carrier concentrations and current densities. The effects of free-carriers on the array performance have only been modelled in terms of their effects on the lateral gain profile. In order that one may investigate the effects of carriers on the lateral dielectric constant profile (caused by the plasma effect and the dependence between the real and imaginary components of the complex dielectric constant via the Kramers Kronig relationship), this section investigates the effects of the individual element carrier densities on the coupled mode performance. The modes are computed for a passive array and then the threshold condition is used to calculate the element carrier densities. The new lateral dielectric constant profile is computed and an iteration procedure begins. Stable solutions are sought.

Before considering the array's behaviour, consider a single ridge laser under uniform carrier injection with current density J_1

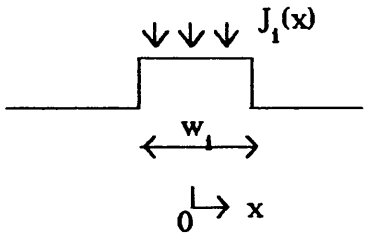

An analytic form for the carrier density has been derived (ref 119):

$$N_i(x) = N_o\left(1 - \frac{\cosh(|x|/L_d)}{\exp(w/2L_d)}\right) \quad \text{beneath ridge (over } w_i\text{)}$$

$$= N \sinh(w/2L_d)\exp\left(-\frac{|x|}{L_d}\right) \quad \text{outside ridge.}$$

Consider now the i-th ridge in an array and its nearest neighbours:

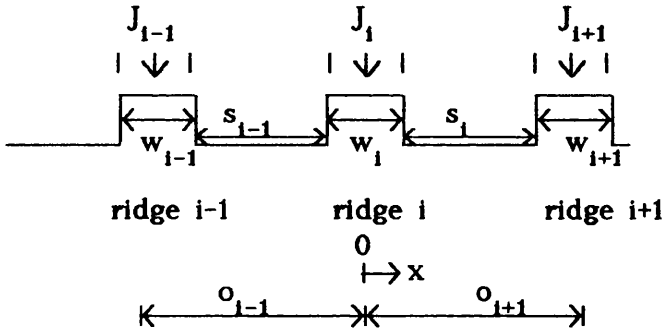

Let the approximate carrier densities in each region be:

$$N_{CHN_i}(x) = N_{i+1}\sinh\left(\frac{w_{i+1}}{2l_d}\right)\exp\left(\frac{|x - o_{i+1}|}{L_d}\right)$$

$$+ \; N_{i+1}\sinh\left(\frac{w_i}{2l_d}\right)\exp\left(-\frac{|x|}{L_d}\right)$$

and $$N_{RWG_i}(x) = N_i\left(1 - \frac{\cosh(|x|/L_d)}{\exp(w_i/2L_d)}\right)$$

$$+ \; N_{i-1}\sinh(w_{i-1}/2L_d)\exp(-|x+o_{i-1}|/L_d)$$

$$+ \; N_{i+1}\sinh(w_{i+1}/2L_d)\exp(-|x-o_{i+1}|/L_d)$$

where :

$N_{CHN_i}(x)$ denotes the carrier density at point x beneath channel i,

$N_{RWG_i}(x)$ denotes the carrier density at point x beneath ridge i,

N_{i-1} is the carrier density amplitude beneath ridge i-1,

N_{i+1} is the carrier density amplitude beneath ridge i+1,

N_i is the carrier density amplitude beneath ridge i,

w_{i-1} is the width of ridge i-1,

w_{i+1} is the width of ridge i+1,

w_i is the width of ridge i,

o_{i-1} is the distance between the centre of ridges i and i-1,

o_{i+1} is the distance between the centre of ridges i and i+1,

and L_d is the diffusion length of holes in n-type material (as the laser structure is assumed to be grown on an n-type substrate).

An approximate expression for the carrier density in the ridge and channel regions may now be obtained using the above equations as long as the injected carrier amplitudes are known.

Let the average value of $N_{RWG_i}(x)$ and $N_{CHN_i}(x)$ be denoted by $\bar{N}_{RWG_i}$ and $\bar{N}_{CHN_i}$ respectively. Then:

$$\bar{N}_{RWG_i} = \frac{1}{w_i} \int_{-w_i/2}^{+w_i/2} N_{RWG_i}(x)\, dx.$$

$$\bar{N}_{CHN_i} = \frac{1}{s_i} \int_{w_i/2}^{w_i/2+s_i} N_{CHN_i}(x)\, dx.$$

Using the previous equations, the above expressions become:

$$\bar{N}_{RWG_i} = N_{i-1}\left(\frac{L_d}{w_i}\right)\sinh\left(\frac{w_{i-1}}{2L_d}\right)2\sinh\left(\frac{w_i}{2L_d}\right)\exp-\left(\frac{s_{i-1}+w_{i-1}/2+w_i/2}{L_d}\right)$$

$$+ N_i\left(\frac{1}{w_i}\right)\left\{w_i - \frac{2L_d\sinh\left(w_i/2L_d\right)}{\exp\left(w_i/2L_d\right)}\right\}$$

$$+ N_{i+1}\left(\frac{L_d}{w_i}\right)\sinh\left(\frac{w_{i+1}}{2L_d}\right)2\sinh\left(\frac{w_i}{2L_d}\right)\exp-\left(\frac{s_i+w_{i+1}/2+w_i/2}{L_d}\right)$$

$$\bar{N}_{CHN_i} = L_d \frac{\left(1 - \exp(s_i/L_d)\right)}{s_i} \left\{ N_{i+1} \sinh(w_{i+1}/2L_d) \exp(w_{i+1}/2L_d) + N_i \sinh(w_i/2L_d) \exp(w_i/2L_d) \right\}$$

Thus, average values of carrier density for the channel and ridge regions may be computed if N_i, N_{i-1} and N_{i+1} are known. However, these have not yet been calculated - instead, the average values of carrier density over the whole element width, r_i, may be found using the method of section 6.3.. These are denoted $\overline{N_i}$ and may be linked to the values of $\overline{N_{CHN_i}}$ and $\overline{N_{RWG_i}}$ as follows.

Denote the gain corresponding to $\bar{N}_{RWG_i}$ and $\bar{N}_{CHN_i}$ as $\bar{g}_{RWG_i}$ and $\bar{g}_{CHN_i}$

$$\bar{g}_{RWG_i} = a\frac{c}{n}\left(\bar{N}_{RWG_i} - N_o \right)$$

$$\bar{g}_{CHN_i} = a\frac{c}{n}\left(\bar{N}_{CHN_i} - N_o \right)$$

Let the average values of photon densities over the channel and ridge regions be denoted by $\bar{S}_{CHN_i}$, $\bar{S}_{RWG_i}$ respectively - these may be derived from the eigenvector distributions directly.

Let

$$\bar{g}_{RWG_i} \bar{S}_{RWG_i} = \frac{1}{w_i} \int_{-w_i/2}^{+w_i/2} g(x)\, S(x)\, dx.$$

$$\bar{g}_{CHN_i} \bar{S}_{RWG_i} = \frac{1}{s_i} \int_{w_i/2}^{w_i/2+s_i} g(x)\, S(x)\, dx.$$

$$\bar{g}_{CHN_{i-1}} \bar{S}_{RWG_{i-1}} = \frac{1}{s_{i-1}} \int_{-w_i/2}^{-w_i/2 - s_{i-1}} g(x)\, S(x)\, dx.$$

If the gain corresponding to $\bar{N}_i$ is $\bar{g}_i$, then

$$\bar{g}_i = a\frac{c}{n}\left(\bar{N}_i - N_o\right)$$

and

$$\bar{g}_i \bar{S}_i r_i = \int_{-w_i/2 - s_{i-1}/2}^{w_i/2 + s_i/2} g(x)\, S(x)\, dx.$$

$$\approx \bar{g}_{RWG_i} \bar{S}_{RWG_i} w_i + \bar{g}_{CHN_{i-1}} \bar{S}_{CHN_{i-1}} s_{i-1}/2$$

$$+ \bar{g}_{CHN_i} \bar{S}_{CHN_i} w_i/2$$

Now, define the following parameters

$$\bar{S}_{RWG_i} = k\, \Gamma_{w_i} \Gamma_v S_{tot} / L dw_i$$

$$\bar{S}_{CHN_i} = k\, \Gamma_{s_i} \Gamma_v S_{tot} / L ds_i$$

$$\bar{S}_{CHN_{i-1}} = k\, \Gamma_{s_{i-1}} \Gamma_v S_{tot} / L ds_{i-1}$$

and $\bar{S}_i = k\, \Gamma_{r_i} \Gamma_v S_{tot} / L dr_i$

where k is a constant

Thus,

$$\bar{g}_i \Gamma_{r_i} \approx \bar{g}_{RWG_i} \Gamma_{w_i} + \bar{g}_{CHN_{i-1}} \Gamma_{s_{i-1}}/2 + \bar{g}_{CHN_i} \Gamma_{s_i}/2$$

Substituting for the values of $\bar{N}_i$, $\bar{N}_{RWG_i}$, $\bar{N}_{CHN_i}$ and $\bar{N}_{CHN_{i-1}}$ and simplifying:

$$\bar{N}_i \Gamma_{r_i} = \bar{N}_{RWG_i} \Gamma_{w_i} + \bar{N}_{CHN_{i-1}} \Gamma_{s_{i-1}}/2 + \bar{N}_{CHN_i} \Gamma_{s_i}/2$$

Now $\bar{N}_i$, Γ_{r_i}, Γ_{w_i}, $\Gamma_{s_{i-1}}$ and Γ_{s_i} are known. If the following parameters

are defined:

$$a_i = \frac{L_d}{s_{i-1}} \left(1-\exp(-s_{i-1}/L_d)\right)\sinh\left(\frac{w_{i-1}}{2L_d}\right)$$

$$a_{i-1} = \frac{L_d}{s_{i-1}} \left(1-\exp(-s_{i-1}/L_d)\right)\sinh\left(\frac{w_i}{2L_d}\right)$$

$$b_{i-1} = \frac{2L_d}{w_i} \sinh\left(\frac{w_{i-1}}{2L_d}\right)\sinh\left(\frac{w_i}{2L_d}\right)\exp\left(-\left(\frac{w_i}{2}+s_{i-1}\right)/L_d\right)$$

$$b_i = \frac{1}{w_i}\left(w_i - 2L_d\exp\left(-\frac{w_i}{2L_d}\right)\sinh\left(\frac{w_i}{2L_d}\right)\right)$$

$$b_{i+1} = \frac{2L_d}{w_i} \sinh\left(\frac{w_{i+1}}{2L_d}\right)\sinh\left(\frac{w_i}{2L_d}\right)\exp\left(-\left(\frac{w_i}{2}+s_i\right)/L_d\right)$$

$$c_i = \frac{L_d}{s_i} \left(1-\exp(-s_i/L_d)\right) \sinh\left(\frac{w_i}{2L_d}\right)$$

$$c_{i+1} = \frac{L_d}{s_i} \left(1-\exp(-s_i/L_d)\right) \sinh\left(\frac{w_{i+1}}{2L_d}\right)$$

whence:

$$\Gamma_{r_i}\bar{N}_i = \Gamma_{w_i}\left(b_{i-1}N_{i-1} + b_iN_i + b_{i+1}N_{i+1}\right)$$

$$+ \Gamma_{s_{i-1}}/2\left(a_{i-1}N_{i-1} + a_iN_i\right)$$

$$+ \Gamma_{s_i}/2\left(c_iN_i + c_{i+1}N_{i+1}\right)$$

In matrix form, the above equation becomes:

$$\begin{bmatrix} \Gamma_{r_1} & & \underline{0} \\ & \ddots & \\ \underline{0} & & \Gamma_{r_n} \end{bmatrix} \begin{bmatrix} \bar{N}_1 \\ \vdots \\ \bar{N}_n \end{bmatrix} = \begin{bmatrix} \alpha_{11}\alpha_{12} & \underline{0} & \\ \alpha_{21}\alpha_{22}\alpha_{23} & & \\ & \ddots & \\ \underline{0} & \alpha_{nn-1}\alpha_{nn} & \end{bmatrix} \begin{bmatrix} N_1 \\ \vdots \\ N_n \end{bmatrix}$$

where $\alpha_{jj} = \Gamma_{w_j} b_j + \frac{\Gamma_{s_{j-1}}}{2} a_j + \frac{\Gamma_{s_j}}{2} c_j$

$$\alpha_{jj+1} = \Gamma_{w_j} b_{j+1} + \frac{\Gamma_{s_j}}{2} c_{j+1}$$

$$\alpha_{jj-1} = \Gamma_{w_j} b_{j-1} + \frac{\Gamma_{s_{j-1}}}{2} a_{j+1}$$

Since all α's and $\overline{N_i}$'s are known, the N_i's can be determined using

$$\underline{N} = \underline{\alpha}^{-1} \underline{\Gamma} \underline{\bar{N}}$$

where all underscored values denote matrices of the respective variables. Thus, since the average values of carrier density in each element can be found, the average values of carrier density in the ridge and channel regions can be determined. The effective dielectric values of the channel and ridge regions can now be modified to accommodate carrier-induced dielectric changes. The effective dielectric value of a multi-layer dielectric slab waveguide under carrier injection is now given by:

$$\varepsilon_{RWG_{act_i}} = \varepsilon_{RWG_i} - \Gamma_v N_{RWG_i} \frac{d\varepsilon}{dN}$$

$$\varepsilon_{CHN_{act_i}} = \varepsilon_{CHN_i} - \Gamma_v N_{CHN_i} \frac{d\varepsilon}{dN}$$

where $\varepsilon_{RWG_{act_i}}$ denotes the effective dielectric beneath the i-th ridge under carrier injection

$\varepsilon_{CHN_{act_i}}$ denotes the effective dielectric beneath the i-th channel under carrier injection

and $\frac{d\varepsilon}{dN}$ denotes the change in dielectric with free carrier density.

The solution of the eigenmodes of a semiconductor laser array under

carrier injection is now simply an iterative process. The eigenmodes of the passive modes of the array are found for the required drive level. The desired mode is then selected for the iterative procedure. The corresponding carrier distribution for the selected mode is then calculated and the new lateral effective dielectric profile is used to re-calculate the modes under the drive conditions. This process is repeated until the eigenmode solution repeats itself. If the eigenmode solution is not self-stabilising, the mode is deemed to be unstable.

Using this method, iterated mode solutions are found. Figure 6.6.1 shows the iterated solutions for a 5 element, uniform array with 3μm ridges on a 6μm pitch with an assumed carrier diffusion length of 1.5μm and dn/dN = 10^{-10} cm^{-3}. Two solutions are presented for comparison - the first is the result of seven iterations, the second the result of 20 iterations. It is seen that fundamental, first and second order modes establish stable solutions, whilst the two highest order modes do not. This is in contrast to the self-stabilising mode scenario proposed by Thompson and Whiteaway (ref. 100). However, it should be remembered that this iteration procedure assumes the presence of the starting mode only and looks for self-stabilisation of that mode; the model of Thompson and Whiteaway looks for the highest gain mode for each iteration. Thus, the model proposed here is useful for looking for self-consistency of a particular mode and does not generate consistent solutions for a given carrier profile. In this way the conditions for, say, the fundamental mode to be stable are identified. From figures 6.6.1(a) to 6.6.1(e), it is seen that large perturbations occur to the eigenvector profile due to the changes in the dielectric constant.

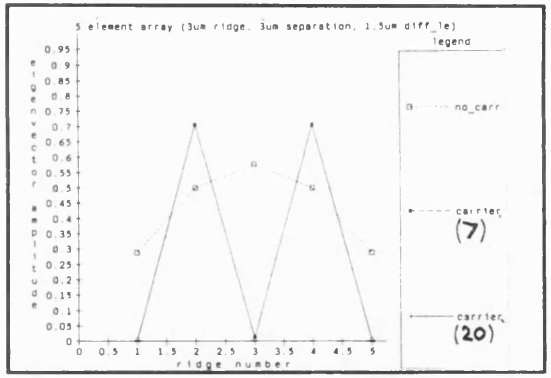

a) fundamental mode, n=1

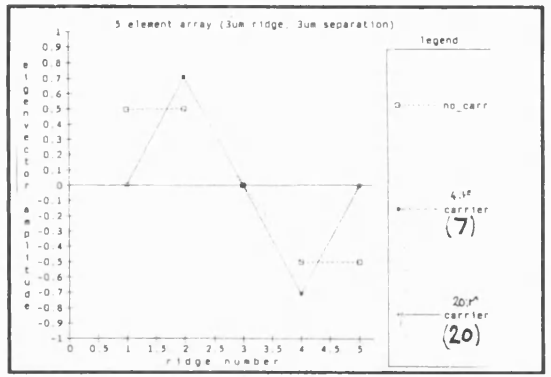

b) First order mode, n=2

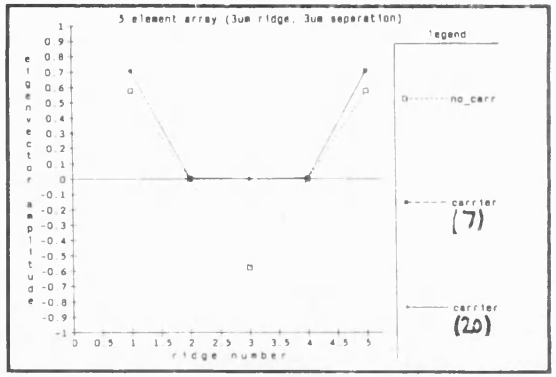

c) Second order mode, n=3

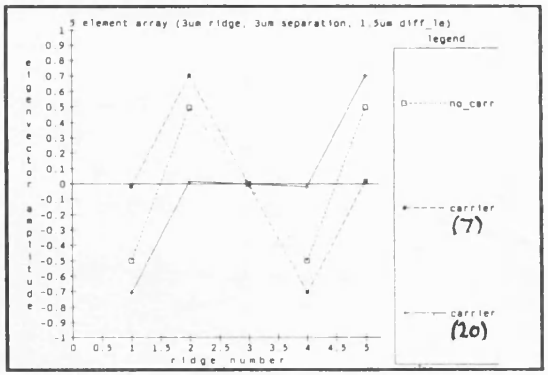

d) Third order mode, n=4

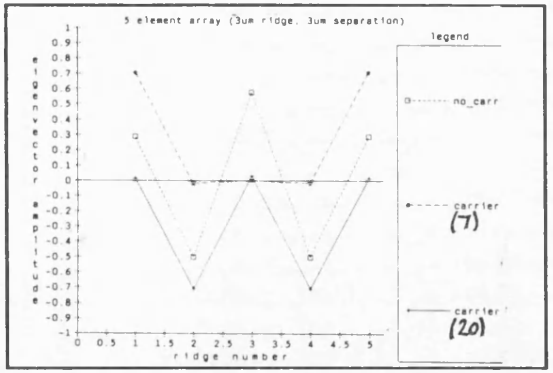

e) Highest order mode, n=5

Figure 6.6.1 Eigenvector Distribution Before and After Considering the Effects of Carrier-Induced Dielectric Changes - the Uniform Array

Another array of special interest is the uniform 'Buus' array. The iterated solutions for all modes of a 5-element and the fundamental and highest order mode of a 10-element, uniform-intensity array are given in figures 6.6.2 and 6.6.3. Once again, it is seen from figure 6.6.2 that the first three modes appear to be self-stabilising whilst the highest order modes are not - the same is true of the 10-element array. Also observe how non-uniform the eigenvectors become - in the case of the 5-element array, the distributions are similar to those obtained for the uniform array; the weak lateral guiding of the outer ridges is swamped by the effect of carrier-induced dielectric changes. In all cases, it is seen that the mode profiles are greatly affected by the dielectric perturbation caused by carrier injection demonstarting that the arrays cannot be treated effectively by a passive-component mode.

6.7 Conclusions

This chapter has presented a number of models of an active laser array accounting for the interacrtions of carriers and photons. In this way threshold and drive conditions have been calculated for given output powers. The basic model of Katz, Kapon, Margalit and Yariv (ref, 53) has been used and expanded upon to provide a laser model capable of accounting for the behaviour of non-uniform array structures. In the last section, the most favourable of these models was linked into a simple self-consistent model to account for changes in the dielectric constant as a result of the perturbation caused by carrier injection. It was demonstrated that passive models of laser arrays may be very inaccurate - the mode profiles obtained by the self-consistent model were very different from the ' passive' predictions. As a result, when designing laser arravs. a self-consistent model should be used.

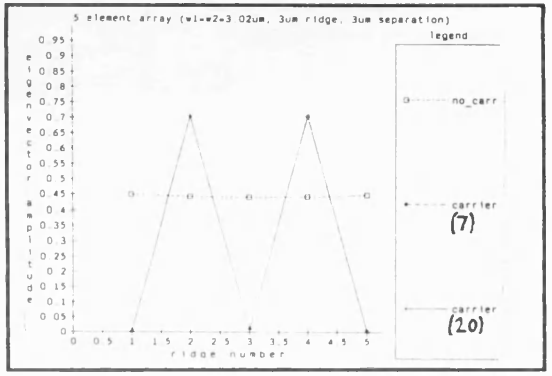

a) fundamental mode, n=1

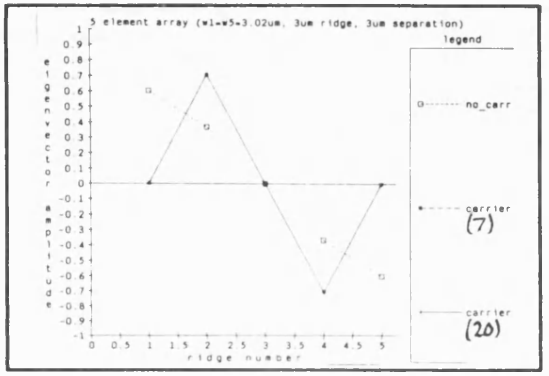

b) First order mode, n=2

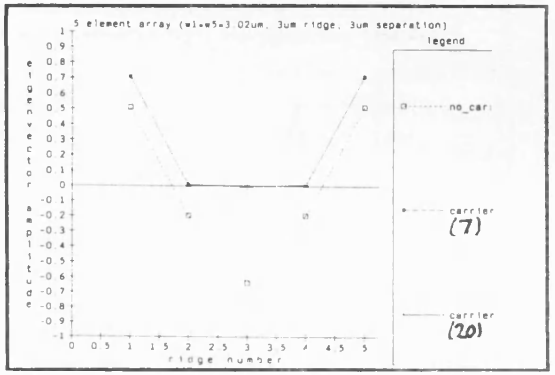

c) Second order mode, n=3

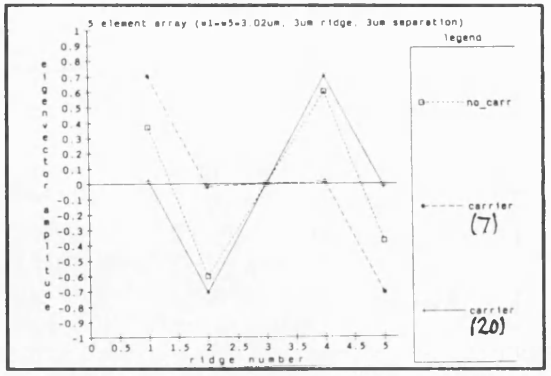

d) Third order mode, n=4

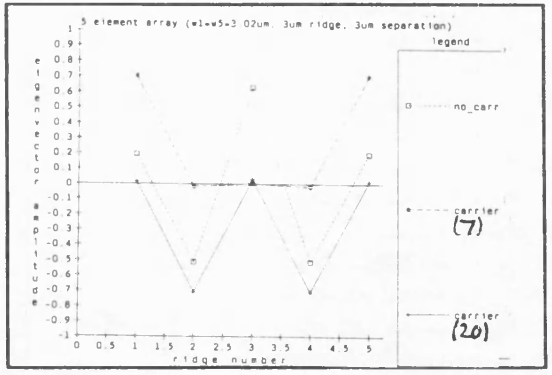

e) Highest order mode, n=5

Figure 6.6.2 Eigenvector Distribution Before and After Considering the Effects of Carrier-Induced Dielectric Changes - the High Uniformity Intensity Array

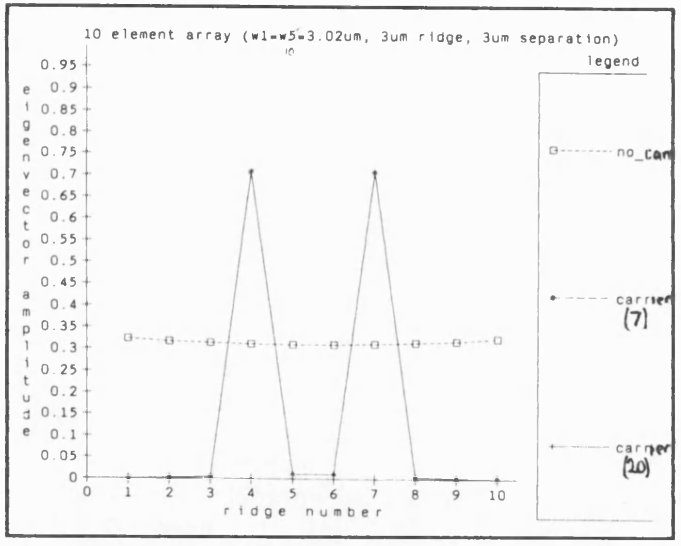

a) Fundamental Mode

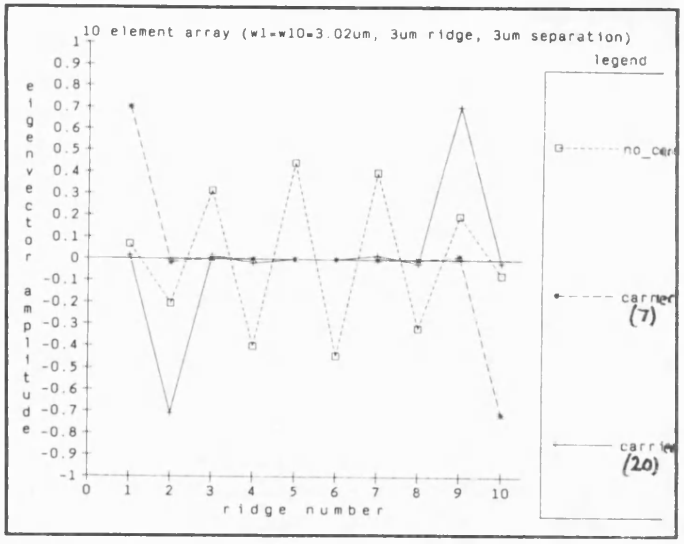

a) Highest Order Mode

Figure 6.6.3 Eigenvector Distribution Before and After Considering the Effects of Carrier-Induced Dielectric Changes - the 10 Element, High Uniformity Intensity Array

CHAPTER 7

CONCLUSIONS

The requirement for high power, single-mode laser arrays has led to the development of phase-locked laser arrays. These structures rely upon the single-mode stability of individual structures to be coupled together to form coherent, high power, single-mode output. Early structures consisting of multi-element emitters operated incoherently, the output being the incoherent sum of the individual emitters. Later devices utilised increasingly complex coupling schemes - starting with evanescently-coupled, uniform arrays, progressing onto chirped arrays and developing onto anti-guided arrays.

This thesis has concentrated on the design of a multiple ridge waveguide laser array for high power, single mode output. Starting with the behaviour of individual ridges, the lateral and transverse guiding structures have been discussed. The mode sets of this structure are divided into Transverse Electric and Transverse Magnetic modes. The transverse waveguide dominates the properties of the structure - the TE modes of this guide are dominant. A simple effective index method is used to reduce the two-dimensional waveguide into an effective one-dimensional waveguide. The modes of this structure have been investigated. Of particular importance in determining the threshold of the laser waveguide is a property known as the confinement factor or power-filling factor. This parameter determines the relative proportion of the optical energy within

the active region of the laser. In turn, it influences the threshold of the laser since the threshold is shown to be proportional to the overlap of the gain distribution with the photon distribution.

Following the review of the single-element ridge waveguide laser, the coupled mode formalism of Yariv (ref 127) and Hardy and Streifer (ref 36, 37) was used to derive coupled equations pertaining to the waveguiding properties of evanescently-coupled multiple ridge waveguides. The formalism, in its simplest form, describes the performance of an array of guides in terms of the propagation constants and distributions of the individual waveguides and two modifiers - the coupling constant and the induced phase-change parameter. These are seen to depend on the guide strength and separation. The general formalism is used to investigate the behaviour of many array types - uniform arrays, chirped arrays and, of much interest, the high-uniformity intensity array proposed by Buus (refs 15, 16). The latter is a tailored array in which the coupling of the outer elements of the array is used to pull the intensity distribution close to uniformity. Unfortunately, this design is very susceptible to very small changes in guide strength and, even when the guides are correctly dimensioned to achieve uniform intensity, the highest order mode is preferred due to its lower modal loss (i.e. it requires less gain to reach threshold). In general, the array designs investigated will either operate in a higher order mode or the light distribution is so non-uniform that the performance would be no better than that of a single element device.

In order to overcome the difficulties of the various design instabilities, two alternative design arrays were proposed utilising another form of mode selection. The first involves the angling of the facet of a laser array

to induce phase-changes beneath the ridges converting the preferred highest order mode to the fundamental mode; the second design involved attaching a broad area laser to the end of a multi-element ridge structure to act as a mode conversion filter. Unfortunately, the angled facet laser array was shown to produce degenerate modes at the point of most interest (180° phase-change). On the other hand the array with broad area mode filter was shown to promote the fundamental mode. However, the limiting factor inhibiting its performance is the belief that the structure could break down into random filamentary oscillation since, due to its extrended width, it is capable of supporting many modes.

Having investigated the mode properties of laser arrays, the lasing behaviour of the array was considered. A model of the lasing action of the array was formulated based upon a model by Kapon, Katz, Margalit and Yariv (ref. 53). Two models were derived from the same basic formulae - the first involved calculating the maximised photon output for a given current distribution, inverting this result to yield the currents for a given photon output power; the second model was based on minimising the lateral gain distribution for a given output power. The two results were seen to differ at thereshold but converge for high output powers. Of note was the fact that the first model suggested that to maximise the output power, carriers were diverted to the ridge with the greatest photon density. This in turn suggests that the carrier density should not be clamped at its threshold value but that carriers should be injected where they are needed most once lasing has begun.

The second model, however, fixes the carrier density at its threshold value; it also calculates slightly lower drive currents for a given output power. These calculations are shown to be consistent with the models used.

Having derived an active model of the laser, the last step explored was to tie the calculated carrier profiles into a simple self-consistent model by iterating the mode solutions as the effective index profile changed under carrier injection. One important assumption made for the model was that the mode solution was known (e.g. the fundamental mode was selected) and the resulting distribution calculated. It was shown that the effects of carriers dominated the laser array designs under consideration - the carrier-induced dielectric changes caused the eigenvector distributions to vary significantly from the 'passive' solutions and, in some cases, stable mode solutions could not be obtained.

In conclusion, this thesis has investigated several ridge waveguide laser array designs and has suggested models for use in analysing these structures. However, simple solutions providing a stable, single-mode, high power laser output were not obtained.

REFERENCES

1. Ackley, D.E. and Engelman, R.W.H. "High-Powered Leaky-Mode Multiple Stripe Lasers". Appl. Phys. Lett., 39 (1), 27, 1981.

2. Ackley, D.E., Butler, J.K. and Ettenberg, M. "Phase-Locked Injection Laser Arrays with Variable Stripe Spacing". IEEE J. Quantum Electron., Vol. QE-22, No. 12, December 1986. pp. 2204-2211.

3. Adams, M.J. "Introduction to Optical Waveguides", Wiley, 1981

4. Agrawal, G.P. "Lateral-Mode Analysis of Gain-Guided and Index-Guided Semiconductor-Laser Arrays". J. Appl. Phys. **58** (8), 15 October 1985. pp. 2922-2931.

5. Amann, M.-C. and Kappeler, F. "Analytical Solution for the Lateral Current Distribution in Multiple Stripe Laser Diodes". Appl. Phys. Lett. **48** (25), 23 June 1986. pp. 1710-1712.

6. Botez, D. and Connolly, J.C. "High-Power Phase-Locked Arrays of Index-Guided Diode Lasers". Appl. Phys Lett. **43** (12), 15 December 1983. pp. 1096-1098

7. Botez, D., Hayashida, P., Mawst, L.J. and Roth, T.J. "Diffraction-Limited-Beam, High-Power Operation From X-Junction Coupled Phase-Locked Arrays of AlGaAs/GaAs Diode Lasers". Appl. Phys. Lett. **53** (15), 10 October 1988. pp. 1366-1368.

8. Botez, D., Mawst, L., Hayashida, P., Peterson, G. and Roth, T.J. "High-Power, Diffraction-Limited-Beam Operation From Phase-Locked Diode-Laser Arrays of Closely Spaced "Leaky" Waveguides (Antiguides)". Appl. Phys. Lett. **53** (6), 8 August 1988. pp. 464-466.

9. Botez, D., Mawst, L., Hayashida, P., Roth, T.J. and Anderson, E. "Stable, Single-(Array)-Mode Operation From Phase-Locked, Interferometric Arrays of Index-Guided AlGaAs/GaAs Diode Lasers". Appl. Phys. Lett **52** (4), 25

January 1988. pp. 266-268.

10. Buckley, D. and Shore, K.A. "Supermode Discrimination in Current-Tailored, Phase-Locked Laser Arrays", SIOE, Cardiff, 1986

11. Buckley, D. and Shore, K.A. "Current Tailoring in Phase-Locked Semiconductor Laser Arrays". IEE Proc., Vol. 134, Pt. J, No. 1, February 1987. pp. 65-68.

12. Butler, J.K., Ackley, D.E. and Botez, D. "Coupled-Mode Analysis of Phase-Locked Injection Laser Arrays". Appl. Phys. Lett. **44** (3), 1 February 1984. pp. 293-295.

13. Butler, J.K., Ackley, D.E. and Ettenberg, M. "Coupled-Mode Analysis of Gain and Wavelength Oscillation Characteristics of Diode Laser Phased Arrays". IEEE J. Quantum Electron., Vol QE-21, No. 5, May 1985. pp. 458-463.

14. Buus, J. "'Excess' Modes in Gain-Guided Laser Arrays". Electron. Lett., Vol. 22, No. 24, 20 November 1986. pp. 1296-1297.

15. Buus, J. "Semiconductor Laser Arrays with Enhanced Mode Stability". IEEE J. Quantum Electron., Vol. QE-23, No. 6, June 1987.

16. Buus, J. "Analysis of Semiconductor Laser Arrays with High-Intensity Uniformity". IEEE J. Quantum Electron, Vol. QE-24, No. 1, January 1988. pp. 22-28.

17. Buus, J., Williams, P.J., Goodridge, I., Robbins, D.J., Urquhart, J., Webb, A.P., Reid, T., Nicklin, R., Charles, P., Reid, D.C.J. and Carter, A.C. "Surface-Emitting Two-Dimensional Coherent Semiconductor Laser Array". Appl. Phys. Lett. 55 (4), 24 July 1989, pp.331-333.

18. Carlin, D.B., Goldstein, B., Bednarz, J.P., Harvey, M.G. and Dinkel, N.A. "A Ten-Element Array of Individually Addressable Channeled-Substrate-Planar AlGaAs Diode Lasers". IEEE J. Quantum Electron., Vol. QE-23, No. 5, May 1987. pp. 476-477.

19. Casey, H.C., jnr. and Panish, M.B., "Heterostructure Lasers" (Parts a and b), Academic Press Inc.,

20. Chen, K.-L. and Wang, S. "Effect of Mirror Imperfections on Phase-Locked Semiconductor Laser Arrays". IEEE J. Quantum Electron., Vol QE-21, No. 3, March 1985. pp. 264-270.

21. Chen, K.-L., and Wang, S. "Single-Lobe Symmetric Coupled Laser Arrays". Electron. Lett., Vol. 21, No. 8, 11 April 1985. pp. 347-349.

22. Chen, K.-L. and Wang, S. "Spatial Hole Burning Problems in Evanescently Coupled Semiconductor Laser Arrays". Appl. Phys. Lett. **47** (6), 15 September 1985. pp. 555-557.

23. Chen, K.-L. and Wang, S. "Analysis of Symmetric Y-Junction Laser Arrays with Uniform Near-Field Distribution". Electron. Lett. , Vol. 22, No. 12, 5 June 1986. pp. 644-645.

24. Daniel, D.R., Buckley, D., Garrett, B. "Quantum Well Ridge Lasers Optimised For High Power Single-mode Applications. Proc. Conf. SPIE, Los Angeles, 1989

25. Dutta, N.K., Cella, T., Napholtz, S.G. and Craft, D.C. "1.3μm InGaAsP Index-Guided Multirib Waveguide Laser Array". Electron. Lett., Vol. 21, No. 8, 11 April 1985. pp.326-327

26. Dutta, N.K., Koszi, L.A., Segner, B.P., Craft, D.C. and Napholtz, S.G. "High-Power Index-Guided Multiridge Waveguide Laser Array". Appl. Phys. Lett., **46** (9), 1 May 1985. pp. 803-805.

27. Dutta, N.K., Koszi, L.A., Segner, B.P. and Napholtz, S.G. "InGaAsP Ridge Waveguide Laser Array with Nonuniform Spacing". Appl. Phys. Lett., **48** (5), 3 February 1986. pp. 312-314.

28. Frateschi, N.C. and De Castro, A.R. "Perturbation Theory for the Wave Equation and the "Effective Refractive Index" Approach". IEEE J. Quantum Electron., Vol. QE-22, No. 1, January 1986. pp. 12-15.

29. Fuhr, P.L. "Wavelength Fluctuations in Pulsed Variable Spacing Phase-Locked Laser Diode Arrays". Electron. Lett., Vol. 21, No. 16, 1 August 1985. pp. 697-699.

30. Fujii, H., Suemune, I. and Yamanishi, M. "Analysis of Transverse Modes of Phase-Locked Multi-Stripe Lasers". Electron. Lett., Vol. 21, No. 16, 1 August 1985. pp. 713-714.

31. Hadley, G.R. "Cavity Supermodes for Gain-Saturated Diode Laser Arrays". J. Appl. Phys. **58** (1), 1 July 1985. pp. 97-100.

32. Hadley, G., Hohimer, J.P. and Owyoung, A. "High Order (ν>10) Eigenmodes in Ten-Stripe Gain-Guided Laser Arrays". Appl. Phys. Lett., **49** (12), 22 September 1986. pp. 684-686.

33. Hadley, G.R., Hohimer, J.P. and Owyoung, A. "Free-Running Modes for Gain-Guided Diode Laser Arrays". IEEE J. Quantum Electron., Vol. QE-23, No. 6, June 1987. pp. 765-773.

34. Hadley, G.R., Hohimer, J.P. and Owyoung, A. "Comprehensive Modelling of Diode Arrays and Broad-Area Devices with Applications to Lateral Index Tailoring". IEEE J. Quantum Electron., Vol. QE- , No. , November 1988. pp.

35. Hamada, K., Wada, M., Kume, M., Shimizu, H., Itoh, K., Kano, G. and Teramoto, I. "A New High Power Semiconductor Laser Array of Phase-Locking Free Structure". Solid State Electron., Vol. 30, No. 1, 1987. pp. 33-37

36. Hardy, A. and Streifer, W. "Analysis of Phased-Array Diode Lasers". Optics Lett., Vol. 10, No. 7, July 1987. pp. 335-337.

37. Hardy, A. and Streifer, W. "Coupled Modes of Multiwaveguide Systems and Phased Arrays". IEEE J. Lightwave Technology, Vol. LT-4, No. 1, January 1986. pp. 90-99.

38. Harnagel, G.L. , Cross, P.S., Lennon, C.R., Devito, M. and Scifres, D.R. "Ultra-High-Power Quasi-CW Monolithic Laser Diode Arrays With High

Power Conversion Efficiency". Electron. Lett., Vol. 23, No. 14, 2 July 1987. pp. 743-744.

39. Harnagel, G.L., Cross, P.S., Scifres, D.R. and Worland, D.P. "11W Quasi-CW Monolithic Laser Diode Arrays". Electron. Lett., Vol. 22, No. 5, 27 February 1986. pp. 231-232.

40. Heidel, J.R., Rice, R.R. and Appleman, H.R. "Use of a Phase-corrector Plate to Generate a Single-Lobed Phased Array Far Field Pattern". IEEE J, Quantum Electron., Vol. QE-22, No. 6, June 1986, pp.749-752

41. Kajimura, T., Kazutoshi, S., Noriyuki, S. and Ryoichi, I. "Leaky-Mode Buried Heterostructure AlGaAs Injection Lasers". Appl. Phys. Lett., Vol. 30, No. 11, 1 June 1977. pp. 590-591.

42. Kapon. E. "The Supermode Structure of Phase-Locked Diode Laser Arrays with Variable Channel Spacing". IEEE J. Quantum Electron., Vol. QE-23, No. 1, January, 1987. pp. 89-93.

43. Kapon, E. "Nonuniform Phased Arrays od Diode Lasers For Fundamental Supermode Operation". Electron. Lett., Vol. 23, No. 17, 13 August 1987. pp. 879-881.

44. Kapon, E., Katz., Margalit, S. and Yariv, A. "Longitudinal-Mode Control in Integrated Semiconductor Laser Phased Arrays by Phase Velocity Matching". Appl. Phys. Lett., **44** (2), 15 January 1984. pp. 157-159.

45. Kapon, E., Katz, J. and Yariv, A. "Supermode Analysis of Phase-Locked Arrays of Semiconductor Lasers". Optics Letters, Vol. 10, No. 4, April 1984. pp. 125-127.

46. Kapon, E., Katz, J., Margalit, S. and Yariv, A. "Controlled Fundamental Supermode Operation of Phase-Locked Arrays of Gain-Guided Lasers". Appl. Phys. Lett., **45** (6), 15 September 1984. pp. 600-602.

47. Kapon. E., Lindsey, C., Katz, J., Margalit, S. and Yariv, A. "Coupling Mechanism of Gain-Guided Integrated Semiconductor Laser Arrays". Appl.

Phys. Lett., **44** (4), 15 February 1984. pp. 389-391.

48. Kapon, E., Lindsey, C., Katz, J., Margalit, S. and Yariv, A. "Chirped Arrays of Diode Lasers for Supermode Control". Appl. Phys. Lett., **45** (3), 1 August 1984. pp. 200-202.

49. Kapon, E., Lindsey, C.P., Smith, J.S., Margalit, S. and Yariv, A. "Inverted-V Chirped Phased Arrays of Gain-Guided GaAs/GaAlAs Diode Lasers". Appl. Phys. Lett., **45** (12), 15 December 1984. pp. 1257-1259.

50. Kapon, E., Lu, L.T., Rav-Noy, Z., Yi, M., Margalit, S. and Yariv, A. "Phased Arrays of Buried-Ridge InP/InGaAsP Diode Lasers". Appl. Phys. Lett., **46** (2), 15 January 1985. pp. 136-138.

51. Katz., J. "Power Conversion Effeciency of Semiconductor Injection Lasers And Laser Arrays in CW Operation". IEEE J. Quantum Electron., Vol. QE-21, No. 12, December 1985. pp. 1854-1857.

52. Katz, J., Kapon, E., Lindsey, C., Margalit, S., Shreter, U. and Yariv, A. "Phase-Locked Semiconductor Laser Array with Separate Contacts". Appl. Phys. Lett., **43** (6), 15 September 1983. pp. 521-523.

53. Katz, J., Kapon, E., Margalit, S. and Yariv, A. "Rate Equations Analysis of Phase-Locked Semiconductor Laser Arrays Under Steady State Conditions". IEEE J. Quantum Electron., Vol. QE-20, No. 8, August 1984. pp. 875-879.

54. Katz, J., Margalit, S. and Yariv, A. "Diffraction Coupled Phase-Locked Semiconductor Laser Array". Appl. Phys. Lett., **42** (7), 1 April 1983. pp. 554-556

55. Katz, J. and Marshall, W.K. "Gain Saturation Effects in Supermodes of Phase-Locked Semiconductor Laser Arrays". Electron. Lett., Vol. 21, No. 21, 10 October 1985. pp. 974-975.

56. Kendall, P.C., McIlroy, P.W.A. and Stern, M.S. "Spectral Index Method for Rib Waveguide Analysis". Electron. Lett., Vol. 25, No. 2, 19 January

1989, pp.107-108.

57. Koshiba, M. and Suzuki, M. "Equivalent Network Analysis of Dielectric Thin-Film Waveguides for Optical Integrated Circuits". Trans. of the IECE of Japan, Vol. E64, No. 4, April 1981. pp. 266-267.

58. Kumar, T. "Steady-State Self-Consistent Analysis of Diode Laser Arrays". Appl. Phys. Lett. **50** (14), 6 April 1987. pp. 877-879.

59. Lang, R.J., Salzman, J. and Yariv, A. "Modal Analysis of Semiconductor Lasers with Nonplanar Mirrors". IEEE J. Quantum Electron., Vol. QE-22, No. 3, March 1986. pp. 463-470.

60. Lay, T-S, Lee, S-C and Lin, H-H. "Y-junction and Misaligned-Stripe Diode Laser Arrays with Nonuniform Reflective Diffraction Coupler". IEEE J. Quantum Electron., Vol. 25, No. 4, April 1989, pp. 689-695.

61. Leger, J.R., Swanson, G.J. and Holz, M. "Efficient Side Lobe Suppression of Laser Diode Arrays". Appl. Phys. Lett., **50** (16), 20 April 1987. pp. 1044-1046.

62. Liau, Z.L. and Walpole, J.N. "Large Monolithic Two-Dimensional Arrays of GaInAsP/InP Surface-Emitting Lasers". Appl. Phys. Lett., **50** (9), 2 March 1987. pp. 528-530.

63. Lindsey, C., Derry, P. and Yariv, A. "Tailored-gain Broad-Area Semiconductor Laser with Single-Lobed Diffraction-Limited Far-Field Pattern". Electron. Lett., Vol. 21, No. 16, 1 August 1985. pp. 671-673.

64. Lindsey, C.P., Kapon, E., Katz, J., Margalit, S. and Yariv, A. "Single Contact Tailored Gain Phased Array of Semiconductor Lasers". Appl. Phys. Lett., **45** (7), 1 October 1984. pp. 722-724.

65. Marshall, W.K. and Katz, J. "Direct Analysis of Gain-Guided Phase-Locked Semiconductor Laser Arrays". IEEE J. Quantum Electron., Vol. QE-22, No. 6, June 1986. pp. 827-832.

66. Mawst, L.J., Botez, D. and Roth, T.J. "High-Power,

Diffraction-Limited-Beam Operation from Diode-Laser Phase-Locked Arrays Operating in Coupled First-Order Modes". Appl. Phys. Lett., **53** (14), 3 October 1988. pp. 1236-1238.

67. Mawst, L.J., Botez, D., Roth, T.J. and Peterson, G. "High-Power, in-phase-mode Operation from Resonant Phase-Locked Arrays of Antiguided Diode Lasers". Appl. Phys. Lett., 55 (1), 3 July 1989, pp. 10-12.

68. Matsumoto, M., Taneya, M., Matsui, S., Yano, S. and Hijikata, T. "Single-Lobed Far-Field Pattern Operation in a Phased Array with an Integrated Phase Shifter". Appl. Phys. Lett., **50** (22), 1 June 1987. pp. 1541-1543.

69. Mehuys, D., Mitsunaga, K., Eng, L., Marshall, W.K. and Yariv, A. "Supermode Control In Diffraction-Coupled Semiconductor Laser Arrays". Appl. Phys. Lett., **53** (13), 26 September 1988. pp. 1165-1167.

70. Mukai, S., Lindsey, C., Katz, J., Kapon, E., Rav-Noy, Z., Margalit, S. and Yariv, A. "Fundamental Mode Oscillation of a Buried Ridge Waveguide Laser Array". Appl. Phys. Lett., **45** (8), 15 October 1984. pp. 834-835.

71. Paiss, I and Hardy, A. "A Coupled-Mode Analysis of Twin-Stripe Index-Guided Lasers". IEEE J. Quantum Electron., Vol. 25, No. 7, July 1989, pp.1609-1615

72. Palfrey, S.L., Hammer, J.M., Longeway, P.A., Carlson, N.W., Evans, G.A., Andrews, J.T., Jaklik, J., Kirk, J.B., Stolzenberger, R. and Triano, A.R. "Phase-Locked Operation of a Three-Element InGaAsP/InP Grating-Surface-Emitting Diode Laser Array". Appl. Phys. Lett., **54** (14), 3 April 1989. pp. 1296-1298.

73. Payne, F.P. "A New Theory of Rectangular Optical Waveguides". Optical and Quantum Electronics, **14** (1982). pp. 525-537.

74. Puretz, J., DeFreez, R.K., Elliott, R.A. and Orloff, J. "300mW Operation of a Surface-Emitting Phase-Locked Array of Diode Lasers". Electron. Lett.,

Vol. 23, No. 3, 29 January 1987. pp. 130-131.

75. Salzman, J., Lang, R., Margalit, S. and Yariv, A. "Tilted-Mirror Semiconductor Lasers". Appl. Phys. Lett., **47** (1), 1 July 1985. pp. 9-11.

76. Salzman, J., Larsson, A. and Yariv, A. "Phase-Locked Controlled Filament Laser". Appl. Phys. Lett., **49** (11), 15 September 1986. pp. 611-613.

77. Salzman, J. and Yariv, A. "Phase-Locked Arrays of Unstable Resonator Semiconductor Lasers". Appl. Phys. Lett., **49** (8), 25 August 1986. pp.440-442.

78. Scifres, D.R., Burnham, R.D., Streifer, W. and Burnstein, M. "Lateral Beam Collimation of a Phased Array Semiconductor Laser ". Appl. Phys. Lett., 41(7), pp614, 1982

79 . Scifres, D.R., Burnham, R.D., Streifer, W., and Paoli, T.L. "Phase-Locked (GaAl)As Laser Emitting 1.5W cw per Mirror". Appl. Phys. Lett. 42(8), pp645, 1983.

80. Scifres, D.R., Burnham, R.D. and Streifer, W. "Phase-Locked Semiconductor Laser Array". Appl. Phys. Lett., 33(12), pp1015, 1978

81 . Scifres, D.R., Burnham, R.D., Streifer, W. and Burnstein "High Power Coupled Multiple Stripe Quantum Well Injection Lasers". Appl. Phys. Lett., 41(2) pp118, 1982

82. Scifres, D.R., Lindstrom, C., Burnham, R.D., Streifer, W. and Paoli, T.L. "Phase-Locked (GaAl)As Laser Diode Emitting 2.6W cw froma Single Mirror ". Electron. Lett., 19 (5), 169, 1983

83. Scifres, D.R., Streifer, W. and Burnham, R.D. "GaAs/GaAlAs Diode Lasers with Angled Pumping Stripes". IEEE J. Quantum Electron., Vol. QE-14, No. 4, April 1978. pp. 223-227.

84. Scifres, D.R., Streifer, W. and Burnham. "High-Powered Coupled Multiple Stripe, Phase-Locked Injection Laser". Appl. Phys. Lett., 34(4), 259, 1979.

85. Scifres, D.R., Streifer, W. and Burnham, R.D. "Experimental and Analytic Studies of Coupled Multiple Stripe Diode Lasers". IEEE J. Quantum Electron., Vol. QE-15, No. 9, September 1979. pp. 917-922.

86. Scifres, D.R., Streifer, W., Burnham, R.D., Paoli, T.L. and Lindstrom, C. . Appl. Phys. Lett., 42(6) pp495, 1983

87. Shore, K.A. "Analysis of Closely-Spaced Index-Guided Semiconductor Lasers. I. Multistripe Devices". Optical and Quantum Electronics, 1984. pp. 235-242.

88. Streifer, W., Cross, P.S., Welch, D.F. and Scifres, D.R. "Analysis of a Y-Junction Semiconductor Laser Array". Appl. Phys. Lett., **49** (2), 14 July 1986. pp. 58-60.

89. Streifer, W., Hardy, A., Burnham, R.D. and Scifres, D.R. "Single-Lobe Phased-Array Diode Lasers". Electron. Lett., Vol. 21, No. 3, 31 January 1985. pp. 118-119

90. Streifer, W., Osinski, M., Scifres, D.R., Welch, D.F. and Cross, P.S. "Phased-Array Lasers with a Uniform, Stable Supermode". Appl. Phys. Lett., **49** (22), 1 December 1986. pp. 1496-1498.

91. Streifer, W., Welch, D.F., Berger, J. and Scifres, D.R. "Nonlinear Analysis of Y-Junction Laser Arrays", IEEE J. Quantum Electron., Vol. 25, No.7, July 1989, pp. 1617-1624.

92. Streifer, W., Welch, D.F., Cross, P.S. and Scifres, D.R. "Y-junction Semiconductor Laser Arrays: Part I - Theory". IEEE J. Quantum Electron., Vol. QE-23, No. 6, June 1987. pp 744-751.

93. Streifer, W., Welch, D.F., Berger, J., Cross, P.S. and Scifres, D.R. "Losses in Y-Junction Semiconductor Laser Arrays". Appl. Phys. Lett., **52** (16), 18 April 1988. pp. 1297-1299.

94. Streifer, W., Welch, D.F., Berger, J. and Scifres, D.R. "Above-Threshold Analysis of Ideal Y–Junction Semiconductor Laser Arrays". Appl. Phys.

Lett., **54** (5), 30 January 1989. pp. 409-411.

95. Suemune, I., Terashige, T. and Yamanishi, M. "Phase-Locked, Index-Guided Multiple-Stripe Lasers with Large Refractive Index Differences". Appl. Phys. Lett., **45** (10), 15 November 1984. pp. 1011-1013.

96. Syms, R.A. "Multiple-Waveguide Distributed Feedback Lasers". IEEE J. Quantum Electron., Vol. QE-22, No.3, March 1986. pp. 411-418.

97 . Taneya, M., Matsumoto, M., Matsui, S., Yano, S. and Hijikata, T. "0° Phase Mode Operation in Phased-Array Laser Diode With Symmetrically Branching Waveguide". Appl. Phys. Lett., **47** (4), 15 August 1985. pp. 341-343.

98. Temkin, H., Dupuis, R.D., Logan, R.A. and Van Der Ziel, J.P., Appl. Phys. Lett., 44(5), p473, 1984

99. Thompson, G.H.B. "Physics of Semiconductor Laser Devices", Wiley

100 . Thompson, G.H.B. and Whiteaway, J.E.A. "Analysis of the Stability of the Highest-Order Supermode In Semiconductor Laser Arrays". Electron. Lett., Vol. 23, No. 9, 23 April 1987. pp. 444-446.

101. Thornton, R.L., Burnham, R.D., Paoli, T.L., Holonyak, jnr., N. and Deppe, D.G. "Highly Efficient Multiple Emitter Index Guided Array Lasers Fabricated by Silicon Impurity Induced Disordering". Appl. Phys. Lett., **48** (1), 6 January 1986. pp. 7-9.

102. Thornton, R.L., Welch, D.F., Burnham, R.D., Paoli, T.L. and Cross, P.S. "High Power (2.1W) 10-Stripe AlGaAs Laser Arrays with Si Disordered Facet Windows". Appl. Phys. Lett., **49** (23), 8 December 1986. pp. 1572-1574.

103. Twu, Y., Chen, K.-L., Dienes, A., Wang, S. and Whinnery, J.R. "High-Performance Index-Guided Semiconductor Laser Arrays". Electron. Lett., Vol. 21, No. 8, 11 April 1985. pp. 324-325.

104 . Twu, Y., Dienes, A., Wang, S. and Whinnery, J.R. "High Power Coupled Ridge Waveguide Semiconductor Laser Arrays". Appl. Phys. Lett.,

45 (7), 1 October 1984. pp. 709-711.

105 . Twu, Y., Chen, K.-L., Wang, S., Whinnery, J.R. and Dienes, A. "Eigenmode Analysis of Phase-Locked Semiconductor Laser Arrays". Appl. Phys. Lett., **48** (1), 6 January 1986. pp. 16-18.

106. Twu, Y., Wang, S., Whinnery, J.R. and Dienes, A. "Mode Characteristics of Phase-Locked Semiconductor Laser Arrays At and Above Threshold". IEEE J. Quantum Electron, Vol. QE-23, No. 6, June 1987. pp. 788-795.

107. Uchiyama, S. and Iga, K. "Two-Dimensional Array of GaInAsP/InP Surface -Emitting Lasers". Electron. Lett., Vol. 21, No. 4, 14 February 1985. pp. 162-163.

108. Wang, S., Wilcox, J.Z., Jansen, M. and Yang, J.J. "In-Phase Locking in Diffraction-Coupled Phased-Array Diode Lasers". Appl. Phys. Lett., **48** (26), 30 June 1986. pp. 1770-1772.

109. Wang, S.S. and Winful, H.G. "Dynamics of Phase-Locked Semiconductor Laser Arrays", Appl. Phys. Lett., 52 (21), 23 May 1988. pp. 1774-1776.

110 . Welch, D.F., Cardinal, M., Streifer, W., Scifres, D.R. and Cross, P.S. "High-Brightness, High-Efficiency, Single-Quantum-Well Laser Diode Array". Electron. Lett., Vol. 23, No. 23, 5 November 1987. pp. 40-41.

111. Welch, D.F., Cross, P., Scifres, D., Streifer, W. and Burnham, R.D. "In-Phase Emission From Index-Guided Laser Array up to 400mW". Electron. Lett., Vol. 22, No. 6, 13 March 1986. pp. 293-294.

112. Welch, D.F., Cross, P., Scifres, D.R., Harnagel, G., Cardinal, M., Streifer, W. and Burnham, R.D. "High-Power and High Efficiency Phased Array Lasers Grown By a Two-Step Metalorganic Chemical Vapour Deposition". Electron. Lett., Vol. 22, No. 9, 24 April 1986. pp. 464-466.

113. Welch, D.F., Cross, P.S., Scifres, D.R. and Streifer, W. "Single-Lobe 'Y'

Coupled Laser Diode Arrays". Electron. Lett., Vol. 23, No.6, 12 March 1987. pp. 270-271.

114. Welch, D.F., Cross, P.S., Scifres, D.R., Streifer, W. and Burnham, R.D. "High-Power (CW) In-Phase Locked "Y" Coupled Laser Arrays". Appl. Phys. Lett., **49** (24), 15 December 1986. pp. 1632-1634.

115. Welch, D.F., Scifres, D., Cross, P., Kung, H., Streifer, W., Burnham, R.D. and Yaeli, J. "High-Power (575mW) Single-Lobed Emission From a Phased-Array Laser". Electron. Lett., Vol. 21, No. 14, 4 July 1985. pp. 603-605.

116. Welch, D.F., Scifres, D., Cross, P., Kung, H., Streifer, W., Burnham, R.D. Yaeli, J. and Paoli, T.L. "High Power CW Operation of Phased Array Diode Lasers with Diffraction Limited Output Beam". Appl. Phys. Lett., **47** (11), 1 December 1985. pp. 1134-1136.

117. Welch, D.F., Streifer, W., Cross, P.S. and Scifres, D.R., "Y-Junction Semiconductor Laser Arrays: Part II - Experiments", IEEE J. Quantum Electron., Vol. QE-23, No. 6, June 1987, pp752-756

118. Welch, D.F., Streifer, W., Thornton, R.L. and Paoli, T. "2.4W CW, 770nm Laser Arrays With Nonabsorbing Mirrors". Electron. Lett., Vol. 23, No. 10, 7 May 1987. pp. 525-527.

119. Westbrook, L.D. "Measurements of dg/dN and dn/dN and Their Dependence on Photon Energy in λ=1.5μm InGaAsP Laser Diodes". IEE Proc., Vol. 133, Pt. J, No. 2, April 1986. pp. 135-142.

120. Whiteaway, J.E.A. "Zero-Order Supermode Discrimination in Semiconductor Laser Arrays". Electron. Lett., Vol. 22, No. 10, 8 May 1986. pp. 560-562.

121 . Wilcox, J.Z., Jansen, M., Yang, J.J., Ou, S.S., Sergant, M. and Simmons, W.W. "Supermode Selection in Diffraction-Coupled Semiconductor Laser Arrays". Appl. Phys. Lett., **50** (19), 11 May 1987. pp. 1319-1321.

122 . Wilcox, J.Z., Jansen, M., Yang, J., Peterson, G., Silver, A., Simmons, W., Ou, S.S. and Sergant, M. "Supermode Discrimination in Diffraction-Coupled Laser Arrays with Separate Contacts". Appl. Phys. Lett., **51** (9), 31 August 1987. pp. 631-633.

123 . Winful, H.G. and Wang, S.S. "Stability of Phase Locking in Coupled Semiconductor Laser Arrays". Appl. Phys. Lett., **53** (20), 14 November 1988. pp. 1894-1896.

124.. Yaeli, J., Streifer, W., Scifres, D.R., Cross, P.S., Thornton, R.L. and Burnham, R.D. "Array Mode Selection Utilizing an External Cavity Configuration". Appl. Phys. Lett., **47** (2), 15 July 1985. pp. 89-91.

125. Yaeli, J. "Phase Measurement of Laser Diode Array Radiation". Appl. Phys. Lett., **49** (8), 25 August 1986. pp. 427-429.

126 . Yang, J.J. and Jansen, M. "Single-Lobed Emission from Phase-Locked Array Lasers". Electron. Lett., Vol. 22, No. 1, 2 January 1986. pp. 2-4.

127 . Yariv, A. "Coupled-Mode Theory For Guided-Wave Optics". IEEE J. Quantum Electron., Vol. QE-9, No. 9, September 1973. pp. 919-933.

128. Zmudzinski, C.A., Mawst, L.J., Givens, M.E., Emanuel, M.A. and Coleman, J.J. "Phase Locked Narrow Zinc Diffused Stripe Laser Arrays". Appl. Phys. Lett., **48** (21), 26 May 1986. pp. 1424-1426.

129 . Zmudzinski, C.A., Givens, M.E., Bryan, R.P. and Coleman, J.J. "Nonplanar Index-Guided Quantum Well Heterostructure Periodic Laser Array". Appl. Phys. Lett., **53** (5), 1 August 1988. pp. 350-352.